ABSTRACT

Title of Dissertation: COMMUNITY- AND POPULATION-LEVEL EFFECTS OF CHYTRIDIOMYCOSIS IN A NEOTROPICAL AMPHIBIAN COMMUNITY

Graziella Vittoria DiRenzo, Doctor of Philosophy, 2016

Dissertation directed by: Dr. Karen R. Lips, Department of Biology

As the number of fungal pathogen outbreaks become more frequent worldwide across taxa, so have the number of species extirpations and communities persisting with the pathogen. This phenomenon raises questions, such as: "what leads to host extinction during an outbreak?" and "how are hosts persisting once the pathogen establishes?." But the data on host populations and communities across life stages before and after pathogen arrival rarely exist to answer these questions. Over the past three to four decades, the amphibian-killing fungus *Batrachochytrim dendrobatidis* (*Bd*) spread in a wave-like manner across Central America, leading to rapid species extirpations and population declines. I collected data on tadpole and adult amphibians in El Copé, Panama before, during, and after the *Bd* outbreak to answer these questions. I used Bayesian statistical approaches to account for imperfect host and pathogen detection of marked and unmarked individuals. In the tadpole community, within 11 months of *Bd*s arrival, density and occupancy rapidly declined. Species losses were

phylogenetically correlated, with glass frogs disappearing first, and tree frogs and poison-dart frogs remaining. I found that tadpole communities resembled one another more strongly after the outbreak than they did before *Bd* invasion. I found no tadpoles within 22 months of the outbreak and limited signs of recovery within 10 years. In contrast, at the same site, for a population of male glass frogs, *Espadarana prosopleon*, I found that 10 years post-outbreak, the population was consistently half its historic abundance, and that the lack of recruits to the population explained why the population had not rebounded, rather than high pathogen-induced mortality. And finally, examining the entire amphibian community, I found high pathogen prevalence, low infection intensities, and high survival rates of uninfected and infected hosts. *Bd* transmission risk, *i.e.*, the probability a susceptible host becomes infected, did not relate to host density, pathogen prevalence, or infection intensity– *Bd* transmission risk was uniform across the study area. My results are especially relevant to conservation biologists aiming to predict the future impacts of *Bd* outbreaks, those trying to manage persisting populations, and those interested in reintroducing species back into wild amphibian communities.

COMMUNITY- AND POPULATION-LEVEL EFFECTS OF CHYTRIDIOMYCOSIS IN A NEOTROPICAL AMPHIBIAN COMMUNITY

by

Graziella Vittoria DiRenzo

Dissertation submitted to the Faculty of the Graduate School of the
University of Maryland, College Park, in partial fulfillment
of the requirements for the degree of
Doctor of Philosophy
2016

Advisory Committee:
Professor Karen R. Lips, Chair
Dr. William Fagan
Dr. Daniel Gruner, Dean's Representative
Dr. Nathan Kraft
Dr. Kennedy Paynter

Preface

This dissertation contains an overview chapter (Chapter I), three research chapters (Chapters II-IV), a synthesis chapter (Chapter V), an appendix, and a supplement. The research chapters (II-IV) represent primary work, the appendix provides additional support to each chapter in terms of figures and tables, and the supplement provides the explanation for additional analyses and R code. All chapters are presented in manuscript form and formatted depending on the journal in which they are intended to be published. A single reference section occurs at the end for the literature cited throughout the dissertation.

Dedication

Para mamá y papá

Per mamma e papà

To mom and dad

"Begin at the beginning," the King said, very gravely, "and go on till you come to the end: then stop."

- Lewis Carrol, Alice in Wonderland

Acknowledgements

Karen Lips− I cannot thank you enough for giving me the opportunity to learn and grow as a scientist, and not giving up on me my first day of field work when I dropped the infrared temperature gun, that is not waterproof, into the stream when I was trying to go over a boulder [June 2011]. I thought for sure I was out of graduate school that moment. Thank you for your kindness, patience, and support throughout these five years.

Mamá y Papà − No les puedo decir cuanto orgullo yo siento por ustedes. Son las personas mas fuerte que conozco y sin ustedes, yo no pudiera llevar la vida que tengo. Mis palabras no pueden explicar lo que yo siento por ustedes. Los quiero mucho, desde aquí hasta la luna. Y aunque papa no puede estar aquí, yo se que me acompaña.

Luke Browne− You are amazing, and I couldn't have asked for anyone more compassionate, patient, and loving to help and support me through my dissertation. Thank you for the encouragement, the meditations, and the thoughtful reminders of the large picture− always bringing it back to the "why?".

Joseph, John Paul, Emily, & Erika− My beautiful loving family. Thank you for your support and loving embraces. And no, I was not on vacation when I was collecting this data in Panama.

Carly Muletz-Wolz− My lab sister!! I hold a special place in my heart for you. And thank you for your endless hours of counseling and support. I couldn't have asked for anyone more wonderful to be my lab sister.

Tate Tunstall− "what now? between you and me", "We face each other as God intended… sportmanlike. No tricks, no weapons, skill against skill alone." But, "this is not Nam. This is bowling. There are rules."

Christian Che-Castaldo− I couldn't have completed my first chapter without your tremendous guidance, support, patience, pranks, and mentoring. It was always great to talk to you about Bayesian stats, even when you did spray me with water bottles and left fake notes on my desk so that I would email Bill Fagan asking when he wants to meet with me. After all, "Success is an accumulation of successful days."

I am grateful to my wonderful committee: Bill Fagan, Dan Gruner, Nathan Kraft, and Ken Paynter. Thank you for all of your advice in improving the quality of my work.

I owe a huge debt of gratitude to all of my field assistance [Nicole Angeli, Alexander Cunha, and Edward Kabay], the Zamudio Lab, the Fagan Lab, BEES Graduate students [Alex, Novarro, Jessica Goodheart, Daniel Escobar, Maria Natalia Umana, Andy Simpson, Nick Caruso], the Parque Omar Torrijos Herrera guarda-parques [Andres Gonzales, Donaciano Sanchez, and Lazaro], The Disorbo Family [Linda, Luigi, Lena, Joe, and Steve], and The Browne Family.

Gracias a Macedonio Perez, Julie Ray, and Maya de Vries por su hospitalidad en Panama.

I am tremendously grateful to have worked with and talked to the following statistical gurus: Andy Royle, Marc Kéry, Elise Zipkin, and Evan Grant. I admire each of you.

This work was generously supported by an NSF GRFP, NSF grant to Karen Lips and Kelly Zamudio, BISI-BEES graduate program, STRI, an NSF REU, and an NSF RET.

Table of Contents

List of Tables

List of Figures

Chapter I: OVERVIEW

At the first World Congress of Herpetology in 1989, scientists realized that many once abundant, common amphibian species had started to disappear for no obvious reason, even in remote or protected areas (Blaustein and Wake 1990). It was well known that temperate pond breeding amphibian populations experienced large population fluctuations throughout the year, and at the time, many herpetologists assumed that the population declines were just part of natural population cycles (Alford and Richards 1999). This assumption was fuelled by the lack of long-term demographic data that was needed to assess whether the unnaturally low amphibian populations were part of natural cycles, or part of a bigger problem. Combined, these assumptions and lack of data hampered the early detection of a worldwide amphibian crisis.

In Central America, enigmatic amphibian declines were first noticed with the disappearance of the golden toad, *Incilius periglenes*, in Monteverde, Costa Rica in 1986 (Crump et al. 1992). These amphibian disappearances became even more apparent when biologists went back to survey historic sites in Mexico and failed to find once-common species (Lips et al. 2004). Throughout the 1990s and 2000s, herpetologists reported additional declines particularly concentrated in upland forests of southern Costa Rica and Panama (Lips 1998, 1999; Lips et al. 2006, 2008). The declines appeared to be spreading from Northern Costa Rica towards the southeast into Panama, which gave rise to the "spreading pathogen hypothesis" (Lips et al. 2008).

The pathogen that was spreading was *Batrachochytrium dendrobatidis* (*Bd*), first described in 1999 (Longcore et al. 1999). *Bd* is a basal fungal lineage in the phylum Chytridiomycota, which is distinct from other fungi in that they have motile, flagellate zoospores (Fisher et al. 2009). *Bd* has a free-living flagellated zoospore that acts as the infective stage, and upon encountering keratinized epidermal amphibian skin, the zoospore encysts (Pessier et al. 1999, Longcore et al. 1999). The encysted zoospores develop into thalli, and once mature, are referred to as zoosporangia. The zoosporangium produces zoospores asexually, and grows a germ tube towards the skin surface of the infected individual. Within two to seven days, the zoospores inside the zoosporangium are released onto the skin surface. There, the zoospores can reinfect the same individual or infect others.

Amphibians are the only known hosts of *Bd*. Once a host is infected, its symptoms and the effects of *Bd* are highly variable across and within amphibian species, but symptoms include: lethargy, excessive skin shedding, skin thickening, vasodilation, hyperkeratosis, and abnormal feeding behavior (Pessier et al. 1999). It is hypothesized that osmotic and electrolyte imbalance across the skin leads to cardiac arrest of an infected host and is the cause of death (Voyles et al. 2009).

Fungal pathogens are unlike any other infectious bacteria or viral pathogens. Fungal pathogens are unique because they have both macro- and micro-parasite attributes− where they reproduce within the host, like a microparasite, but lack an effective way to transmit zoospores from cell-to-cell so the infectious propagule is shed onto the skin surface, like a macroparasite (Briggs et al. 2010). Fungal pathogens are also unique in that they may also have a resting or saprophytic stage

external to the host, that allows them to drive their host to extinction more easily (Mitchell et al. 2008).

Bd caused severe population declines and species extirpation of hundreds amphibians in highland Central and South America (Lips et al. 2008, Cheng et al. 2011). The combination of *Bd* and amphibian ecologies contributes to the pronounced impacts. First, *Bd* grows best under environmental conditions typical of cloud forests found in the Neotropics: i.e., year-round high humidity and temperatures between 15−25°C (Collins & Crump 2009). Second, many Neotropical amphibian species have small population sizes, narrow distributional ranges, and are habitat specialists, which contribute to their susceptibility to external threats (Lips et al. 2003, Whitfield et al. *in press*). And finally, high amphibian diversity and endemism in this region contributes to high rates of amphibian loss, with over 50% of all newly described species stemming from this area (Duellman 1999).

Herein, I review our current knowledge of amphibian declines in Central America, focusing on how we predict amphibian declines, the impacts of *Bd* on amphibian populations and community structure, and highlight knowledge gaps in relation to amphibian and *Bd* interactions.

I. How did Bd spread in Central America?

Starting in the late 1980s, amphibian declines spread from Monteverde, Costa Rica toward the southeast (Whitfield et al. *in press*). This spatiotemporal pattern of decline gave rise to the novel pathogen hypothesis (NPH), arguing that *Bd* was a novel pathogen spreading throughout Central America. These studies speculated that

a recent change in pathogen virulence occurred, leading to rapid spread of the pathogen across the regional landscape. Early genetic studies of *Bd* isolates supported this hypothesis, showing that *Bd* had low global variation at both microsatellite and sequenced loci, with both types of markers having only two alleles (James et al. 2009).

The systematic, directional spread of *Bd* from Costa Rica into Panama was likely the result of human facilitation of pathogen movement (Dobson 2000), effects of small-scale geography, or effects of population dynamics (Lips et al. 2008). Landscape geography influences both amphibian and pathogen gene flow and movement, where certain habitats promote pathogen survival and spread (e.g., mountain chains and river valleys) while others slow spread (e.g., desert and lowlands). Alternatively, anthropogenic facilitation of *Bd* spread is also likely, perhaps along highways, seasonal routes of livestock herding, or other travel routes that might produce a patter of nonlinear declines (Lips et al. 2008).

On the local scale, *Bd* is transmitted via an aquatic flagellated zoospore (Longcore et al. 1999) either via direct frog-to-frog or indirect frog-to-environment contact. But little is known about *Bd* transmission rates (Rachowicz & Briggs, 2007) and *Bd* persistence outside of the host (Fisher et al. 2012) because it is difficult to track, monitor, and follow. *Bd* has been detected on waterfowl feet (Garmyn et al. 2012), lizards (Kilburn et al. 2011), and surface waters (Chestnut et al. 2014). But none of these studies quantified the viability of zoospores or reproduction external to their amphibian host, leaving many questions about the transmissibility of *Bd* zoospores.

II. How do we predict species declines?

In Central America, the species that are the most vulnerable to extirpations and declining share similar traits (Lips et al. 2003). Declining populations tend to be associated with riparian habitats, have small geographic ranges, restricted elevational ranges, and are large-bodied (Lips et al. 2003). In addition, endemic species are at greater risk because of small populations and habitat specialization, which tend to concentrate in highland areas (Lips et al. 2003, Smith et al. 2009). These traits can be used to predict species susceptibility to *Bd* infection and population declines.

III. What are the impacts of Bd on amphibian population demography?

In general, we know very little about Neotropical amphibian population demography (i.e., survival rates, recruitment rates, and population size) because it is logistically challenging to capture, mark, and track individuals over appropriate time periods, also known as capture-mark-recapture surveys (McCaffery and Lips 2013); We know even less about the impacts of *Bd* on Neotropical amphibian population demography because the species that survive the outbreak have low population densities and are challenging to find, making it more difficult to obtain sufficient data for analyses. There have been attempts to compare before and after estimates of host survivorship (*Craugastor punctariolus*, Ryan et al. 2008; *Atelopus zeteki, Atelopus varius*: McCaffery et al. 2015), but long-term analyses were generally not possible because these species populations declined too rapidly and in all cases were extirpated within 12 months of *Bd* arrival.

In other cases, capture-mark-recapture has been done at locations post-*Bd* outbreak, when data before *Bd* arrival is not available. These studies tend to quantify amphibian survivorship and recruitment but they fail to account for disease status of hosts (*Atelopus cruciger*; Lampo et al. 2011), or these studies set out with the goal to quantify *Bd* impacts, but find no *Bd* infected hosts (*Atelopus spumarius*: Tarvin et al. 2014).

IV. How does Bd change amphibian community structure?

In Central America, *Bd* has reshaped patterns of amphibian biodiversity across the region and dissolved historical biogreographical patterns, such that larger distances between sites is not correlated with community composition dissimilarity even at 500 km distance (Smith et al. 2009). *Bd* outbreaks throughout the region eliminated the endemic species, resulting in regional homogenization of amphibian fauna and ecology, where particular reproductive modes and habitats experienced greater declines. These historic and current biogreographical patterns are essential in understanding why species are in their present locations, which informs conservation efforts.

Despite the severity of the crisis, quantitative data on the effects of a *Bd* outbreak on amphibian communities are rare because I lack equivalent data collected before and after a disease outbreak. Crawford et al. (2010) is among one of the only studies that has collected these data, where they found that 41% of species extirpated in El Copé, Panama (30 of 74 species), 11 of which were undescribed cryptic species, and abundance declines were random with respect to community phylogeny. This is

among one of the only quantifications of amphibian losses, and represents important information for amphibian biodiversity conservation demonstrating the direct impact of an infectious disease on amphibian diversity and community phylogeny. Despite large abundance and species richness declines, amphibians persist at sites where *Bd* is present.

V. What are we still missing? And what does this dissertation contribute?

Despite substantial advances in our understanding in community and population level effects of this novel pathogen on amphibians within the last couple decades, there remain a substantial number of unresolved questions. A major roadblock to improving our understanding of *Bd*'s impact is the lack the data on amphibian populations and communities before and after *Bd* invasion, which would provide a direct assessment of *Bd*'s impact. By the time many sites in Central America were surveyed, it was too late to collect the before and after data needed because amphibians were already infected with *Bd*.

One of our largest knowledge gaps pertains to what happens to tadpoles when *Bd* arrives. Clearly though, if adult amphibians decline, then tadpoles will decline, but their patterns of decline may be fundamentally different because adults and tadpoles differ in habitat and resource use, mortality rates, and interactions with other species. The impact of disease on the juveniles sets the stage with respect what happens to adult population abundances. In chapter II, I use historic data on tadpole communities collected directly before and after *Bd* arrival to determine what factors (i.e.,

phylogeny, rarity, habitat or resource use overlap) correlate to the magnitude and order of species declines.

The lack of population recoveries indicates that *Bd* must still be causing unobserved mortality or there is a lack of recruitment. To effectively manage amphibian species populations and understand what is limiting natural population recovery, we need to know how *Bd* has altered survivorship and recruitment of species. In chapter III, I use capture-mark-recapture data collected before and after *Bd* arrival for a population of male *Espadarana prosoblepon* to determine how host survivorship, recruitment, and population size is affected by pathogen presence.

In terms of the amphibian community, we largely do not know how individuals are persisting in the presence *Bd* because amphibian species that have been affected by *Bd* tend to have extremely low abundances, making them difficult to study. Many Neotropical amphibian species had small population sizes before *Bd* arrival, and *Bd*-related population declines have made it virtually impossible to understand population dynamics. In chapter IV, to handle this sparse amphibian dataset, I created a novel multi-state disease-structured Dail-Madsen model for unmarked individuals that corrects for imperfect host and pathogen detection, allowing me to estimate the same parameters of a capture-mark-recapture analysis, i.e., host survivorship, recruitment, and population size, without the intensive effort of marking individuals. Here, I examine what processes are contributing to the persistence of the few remaining sparse amphibians following a *Bd* outbreak by estimating disease state-specific survivorship, arrival rates, detection probability,

recovery and infection probabilities, community abundance, and the change in abundance across years.

In the recorded history of infectious diseases, there are no comparable examples that have caused catastrophic declines in any single group of animals (Collins & Crump 2009) and have such low host specificity that it infects all members of an entire class of vertebrates (Pasmans et al. 2004). However, it seems as though *Bd* is the first of many infectious diseases of this type, with the recent emergence of white-nose syndrome in bats, snake fungal disease in snakes, and *Batrachochytrium salamandrivorans* in salamanders, making it more critical to learn from *Bd* to be able to apply our knowledge in controlling the spread of other fatally infectious fungal pathogens and conserving biodiversity.

Therefore, in an effort to build on our basic understanding of amphibian population biology and *Bd* disease ecology, and answering the questions "what leads to host extinction during a *Bd* outbreak?" to "how are hosts persisting once *Bd* becomes established?," I designed a three part study that involved field research, lab work, and statistical modeling to determine the population and community level effects of *Bd* arrival, and I developed new statistical models that improve inference on difficult to find hosts at low abundances following pathogen invasion.

VI. The study site: El Copé, Panama

In 1998, a long-term amphibian-monitoring project was established in El Copé, Panama. This monitoring project created the opportunity to collect critically needed data on amphibian adult and tadpole populations for multiple species before

Bd arrival. The chapters to follow all use these datasets from before, during, and after the 2004 *Bd* outbreak in El Copé. For several species, capture-mark-recapture projects were started, and seven total permanent transects were created in both riparian and trail habitats. This is one of the only sites in the Central America with this type of amphibian data collected before and after *Bd* arrival, providing the opportunity to answer many unresolved questions.

Chapter II: COMMUNITY DISASSEMBLY OF A TADPOLE COMMUNITY BY A MULTI-HOST FUNGAL PATHOGEN WITH LIMITED EVIDENCE OF COMMUNITY RECOVERY

Coauthors: CHRISTIAN CHE-CASTALDO, AMANDA RUGENSKI, ROBERTO BRENES, MATT R. WHILES, CATHERINE M. PRINGLE, SUSAN S. KILHAM, AND KAREN R. LIPS

Abstract

Emerging infectious diseases can cause host community disassembly, but the mechanisms driving the order of species declines and extirpations following a disease outbreak are unclear. I documented the community disassembly of a Neotropical tadpole community during a chytridiomycosis outbreak, triggered by the generalist fungal pathogen, *Batrachochytrium dendrobatidis* (*Bd*). Within the first 11 months of *Bd* arrival, tadpole density and occupancy rapidly declined. Species rarity and habitat or food resource use overlap among species did not predict the magnitude of declines. But species losses were taxonomically selective, with glass frogs (Family: Centrolenidae) disappearing the fastest and tree frogs (Family: Hylidae) and dart-poison frogs (Family: Dendrobatidae) remaining. I found biotic homogenization of tadpole communities, with post-decline communities resembling one another more strongly than pre-decline communities. The entire tadpole community was extirpated within 22 months following *Bd* arrival, and I found limited signs of recovery 10 years post-outbreak. Because of detection issues inherent in sampling tadpoles, I used simulations in conjunction with our detection estimates to provide recommendations

for future surveys to insure adequate sampling of diverse Neotropical tadpole communities. Our unique dataset on tadpole community composition before and after *Bd* arrival is a valuable baseline for assessing Neotropical amphibian recovery. Our results are of direct interest to conservation managers and community ecologists trying to better understand the timing, magnitude, and consequences of disease outbreaks as emerging infectious diseases spread globally.

Introduction

Emerging infectious diseases can cause community disassembly (Zavaleta et al. 2009; Fisher et al. 2012), defined as the predictable loss of species and population declines. During community disassembly, the first species extirpated are generally rare species− species with small geographic ranges, small population size, or a narrow habitat tolerance (Rabinowitz, 1981; Larsen, Williams, & Kremen 2005; Gehring et al. 2014; Rader et al. 2014). Subsequent losses tend to include common, generalist species that have declined since the initial disturbance (e.g., Wright, Gonzalez, & Coleman 2007; Larsen, Lopera, & Forsyth 2008). The last remaining species may reduce patterns of community turnover across the site, increasing biotic homogenization (McKinney and Lockwood 1999).

In the case of tropical amphibian declines and extirpations caused by the fungal pathogen *Batrachochytrium dendrobatidis* (hereafter *Bd*), many amphibian communities experience rapid, widespread declines and species extirpations following pathogen arrival (Berger et al. 1998; Lips et al. 1998, 1999, 2006). Species declines and extirpations are best predicted by infection intensity (Vredenburg et al.

2010, Savage and Zamudio 2011, Grogan et al. 2016), where high pathogen burdens compromise the host's skin function, killing the host (Voyles et al. 2009). Host mortality and subsequent species declines are, therefore, largely dependent on pathogen exposure, pathogen growth rates, and pathogen re-exposure.

Bd exposure, re-exposure, and susceptibility are related to several species-level characteristics. First, species identity and taxonomy can predict species susceptibility to *Bd*. For example, family-level amphibian phylogenies suggest that families with similar traits share the same vulnerabilities to threats (Corey and Waite 2008, Smith et al. 2009), but a species-level phylogeny showed no evidence that species with similar traits were equally susceptible to *Bd* (Crawford et al. 2010). The discrepancy between these results could be an artifact of taxonomic, spatial, or temporal scales− where rapid, widespread amphibian losses produce an illusion of no phylogenetic variation to *Bd* susceptibility. Second, habitat and food resource use overlap among species may affect pathogen exposure and re-exposure, where host aggregations increase the likelihood of gaining infection (Longo et al. 2010, Venesky et al. 2011). For example, when species converge on common resources or refugia, like *Eleutherodactylus coqui* during severe droughts, clumping behavior increases contact rates and pathogen transmission. Finally, host ecology, abundance, and distribution affect both host susceptibility and pathogen transmission rates (Lips et al. 2003, Rachowicz and Briggs 2007, Briggs et al. 2010). To illustrate, the host-pathogen interactions of *Rana muscosa-Bd* largely depend on density-dependent processes regulating pathogen exposure and re-infection (Briggs et al. 2010), where higher densities rapidly increase host infections and mortality rates. Similarly,

geographically rare species tend to experience greater *Bd*-related declines than widespread species (Smith et al. 2009)− driven by high pathogen re-infection rates and host susceptibility.

But the inability to distinguish between species rarity (i.e., low density, low occupancy, habitat specialization) and difficult to detect species (i.e., cryptic, fossorial, secretive) is largely overlooked in community disassembly studies− where difficult to detect species tend to appear rare. For instance, cryptic amphibian species, like those in the families Craugastoridae or Strabomantidae, tend to be hard to find, but are actually widespread and abundant. This illusion of species rarity is produced by imperfect detection (i.e., MacKenzie et al. 2006; Kéry 2010). By underestimating species occupancy pre- and post- outbreaks, population declines will tend to be overestimated and extirpations will be biased towards difficult to find species, leading to false inference regarding the cause of declines.

Here, I describe the community disassembly of a stream-dwelling tadpole community in response to a *Bd* outbreak, while taking into account imperfect species detection. In this system, stream tadpoles occupy semi-isolated microhabitats (e.g., leaf packs, isolated pools, and in-stream pools and riffles) that allow for the consistent quantification of tadpole occupancy, density, and species richness. Prior to the introduction of *Bd*, these tadpole assemblages were diverse (McDiarmid & Altig 1999; Crawford, Lips, & Bermingham 2010), abundant (McDiarmid & Altig 1999) and structured spatially (Inger, Voris, & Frogner 1986) and temporally (Heyer 1976), creating an opportunity to compare several species characteristics simultaneously that can contribute to the order of species losses caused by disease outbreaks. I address the

following specific questions in this study: (1) What are the patterns of community disassembly following an outbreak? (2) What factors correlate to the order of species losses? (3) And how can we improve tadpole community sampling given imperfect detection?

I expected that tadpole occupancy would decline following the mass mortality of adult amphibians at the site (Lips et al. 2006), and that the magnitude of tadpole occupancy declines would depend on their microhabitat use and season. Like most other multi-host pathogens, I predicted that specialist species and their relatives that share similar traits would be extirpated first, where the time since species divergence would correlate to species disappearance date, because more closely related species will share similar traits and pathogen susceptibility. I fit several evolutionary time models that each represents different rates of trait divergence, and a white noise model that predicts no correlation between relatedness and species disappearance date. I predicted that as habitat or food resource use overlap increases among tadpole species, the likelihood a species declines will also increase. I predicted that the tadpole communities that remain following the *Bd* outbreak will be more similar in species composition, mainly comprised of common, generalist species. And finally, I expected that *Bd* arrival would cause rapid changes to the tadpole community that would persist several years post-invasion. My results are useful to conservation and restoration practices considering the species vulnerability and taxonomic uniqueness alongside setting species action, especially as generalist fungal pathogens spread globally.

Methods

STUDY SITE

The study site was located within Parque Nacional G. D. Omar Torríjos Herrera in Coclé Province, approximately 8 km north of the town of El Copé, Panama (8° 40' N, 80° 37' 17'' W, Lips, Reeve, & Witters 2003). The park spans elevations between 500 and 1000 m, and our study sites are located at ~775 m elevation. This site experiences both a dry (December to April) and wet (May to November) season. Mean annual air temperature at the park during 2003–2005 ranged from 16−23°C, and mean annual rainfall was ~3709 mm (McCaffrey & Lips 2013; *unpublished data*).

STUDY SYSTEM

Starting in 1998, KRL started monitoring adult amphibian populations in El Copé, Panama (Lips et al. 2006) and was consistently capturing amphibians until September 2004 when *Bd* was first detected at the site. Tadpole populations were monitored starting 15 months prior to the adult die-off (July 2003). The system experienced rapid species losses and declines. I, therefore, expect minimal compensatory or evolutionary dynamics interfering with community disassembly inference. This project is part of the larger Tropical Amphibians Declines in Streams (TADS) project to quantify what the consequences of amphibian loss are to ecosystem structure and function.

The original El Copé amphibian community consisted of 74 species (Lips, Reeve, & Witters 2003; Crawford, Lips, & Bermingham 2010), of which ~22 had

stream-dwelling tadpoles. The amphibian community was diverse with respect to life history (e.g., habitat use, reproductive mode), demography (e.g., survivorship, longevity), and ecology (e.g., clutch size, body size, dispersal distance). By 2008, only 44 species remained at low population densities (Crawford, Lips, & Bermingham 2010).

FIELD SURVEYS

RB surveyed tadpole communities in four 200 m stream transects: Loop, Silenciosa, Cascada, and Guabal. RB mapped and measured the area covered by each of four microhabitats (riffle, pool, isolated pool, and leaf pack) at the beginning of the wet and dry seasons. Riffles were defined as fast-flowing, shallow sections with gravel and cobble substrates, pools as areas of calm water deeper than 20 cm in the main channel, isolated pools as small, shallow pools spatially separated from the main stream channel, and leaf packs as detritus accumulations at the bottom of pools.

I used a *k*-means clustering analysis to divide streams into segments that were repeatedly visited each month throughout the study. The *k*-means analysis divided each stream transect into four segments for a total of 16 stream sites per microhabitat. Each segment was sampled either once, twice, or three times per month using the random sampling method described below.

To sample riffles, RB used 250 μm D-nets and disturbed substrate with our feet while holding nets immediately downstream (Barbour et al. 1999). To sample leaf packs, RB used a modified stovepipe benthic corer (22 cm diameter) with a base of rubberized flaps that kept the sampler sealed against rough and uneven substrates.

RB drove the corer into the substrate and removed searched through the contents for tadpoles (Colón-Gaud et al. 2010). RB used a dip net to exhaustively sample pools and isolated pools until three consecutive scoops produced no tadpoles (Heyer et al. 1994; Ranvestel et al. 2004). RB also measured the length, width, and depths of all microhabitats across each 200 m transect to account for variability in survey area.

For leaf packs, isolated pools, and riffles, RB randomly sampled three sites per microhabitat per stream each month for 15 months before (June 2003–August 2004) and 11 months following (October 2004–August 2005) *Bd* arrival in September 2004. For pools, RB randomly sampled between four and eight sites per stream each month before *Bd* arrived. AR re-sampled all microhabitats in at least one stream annually between 2006 and 2011 and again in 2014 (Table A2.1). All analyses are based on the first two years of intensive sampling (2003–2005) of leaf pack, isolated pools, and riffles because no individuals were found in the majority of subsequent annual surveys.

I excluded pools from all analyses because logistical difficulties prevented the sampling of pools post-decline (2004–2005) and the sampling of leaf packs from September to December 2003. I report data of pools pre-decline to provide baseline data of these understudied communities. I also did not include September 2004 in analyses to limit biases between pre- and post- *Bd* samples because *Bd* arrived mid-September 2004 (Lips et al. 2006).

STATISTICAL ANALYSES

I. Patterns of community disassembly

Tadpole density

To determine if the magnitude of tadpole declines differed among microhabitats or between seasons, I calculated tadpole habitat-weighted density (HWD) before and after *Bd* arrival in each microhabitat and stream by pooling monthly tadpole abundances across species. I used HWD to adjust for spatiotemporal variations in microhabitat availability caused by differences among streams and between seasons. HWD was calculated by dividing total tadpole abundance per microhabitat in each stream each month by the total area sampled and multiplying by the percent area each microhabitat covered in each stream that season. I reformatted data consisted of tadpole HWD per microhabitat per stream per month from 2003−2005.

To determine if tadpole HWD differed among microhabitats or between seasons following *Bd* arrival, I used a generalized linear mixed effects model, with monthly tadpole HWD as the response variable and microhabitat, season, disease state (*Bd* present or absent), all two-way interactions, and the three-way interaction as the explanatory variables. I included month as a fixed effect to account for repeated measures of density across months and included stream as a random effect (Gillies et al. 2006) to account for pseudo-replication of microhabitats within streams. I used a negative binomial distribution to account for over dispersion of the response variable, and I accessed model fit by visually inspecting the residuals. I fit this model using

package glmmADMB (Fournier et al. 2012, Skaug et al. 2014) in R version 3.2.1 (R Core Team 2015).

To account for biases in tadpole abundance caused by detection probability, I fit species-specific hierarchical *N*-mixture models to estimate true tadpole densities using stream segments as the sites and monthly repeated visits to different microhabitat samples within stream segments as replicate surveys, but model fits were extremely poor. Poor model fit was probably due to large jumps in tadpole densities between replicate surveys at each site. The large jumps in tadpole densities were likely caused by clustered microhabitat use within stream segments and not necessarily a violation of the population closure assumption (i.e., no births, deaths, immigration, or emigration). Density estimates that are not adjusted for imperfect detection are often underestimates of the true abundance, but can still be useful to quantify the strength and direction of an ecological effect (i.e., Banks-Leite et al. 2014).

Species occupancy

To determine if species occupancy differed before and after *Bd* arrival, I used a hierarchical occupancy model to quantify changes in species-specific occupancy. In this analysis, I was able to account for imperfect detection, by estimating microhabitat specific detection rates. I define the probability of occupancy as the probability a species occupied a stream segment, and I define detection probability as the probability I detect a species in a given stream segment, given that the species is present. I included data for all species that were detected in three or more

microhabitat samples within a season (Ferraz et al. 2007, Ruiz-Guiterrez et al. 2010; see Table A2.2). I had sufficient data to estimate occupancy for eight of the 13 species identified to species level.

I used microhabitat samples as repeated surveys at a stream site (Hines et al. 2010). Since I did not know *a priori* species microhabitat use or breeding season, I ran each species occupancy model with the full set of microhabitat and season covariates.

For a selected species, I estimated the true occurrence of tadpoles as,

$$z_{i,m} \sim Bernoulli(\psi_{i,m}),$$

where $z = 1$ when the m_{th} species occupies the i_{th} site, and z = 0 otherwise. I investigated the association between species tadpole occupancy and the covariates microhabitat, season, disease state, and their interactions using an effects-parameterized generalized linear mixed model where,

$$logit(\psi_{i,m}) = \alpha_{0,n,m} + \beta_{0,m}Wet_i + \beta_{1,m}LeafPack_i + \beta_{2,m}Riffle_i + \beta_{3,m}Wet_iLeafPack_i + \beta_{4,m}Wet_iRiffle_i + \beta_{5,m}Post_i + \beta_{6,m}Post_iWet_i + \beta_{7,m}Post_iLeafPack_i + \beta_{8,m}Post_iRiffle_i + \beta_{9,m}Post_iWet_iLeafPack_i + \beta_{10,m}Post_iWet_iRiffle_i + \gamma_{i,m}.$$

I included $\alpha_{0,n,m}$ to account for spatial variations of the n_{th} stream for the m_{th} species, and where $\gamma_{i,m} \sim Normal(0, \sigma^2)$ was included as a random effect to account for variation among sites for the m_{th} species.

I estimated detection probability as,

$$y_{i,j,m} \sim Bernoulli(p_i z_{i,m}),$$

where,

$$logit(p_i) = \alpha 1 + \beta Hab_i.$$

When tadpoles of the m_{th} species were observed during the j_{th} survey at the i_{th} site then $y = 1$, and $y = 0$, otherwise. Detection was modeled as the product of p_i, the probability of detecting a species, given that it is present at the i_{th} site (i.e., $z = 1$).

To reduce the number of parameters estimated and to increase precision, I combined the detection probability of leaf packs and isolated pools as the intercept of the model and riffles as the covariate *Hab*, since previous runs of the model showed very similar detection probability estimates between leaf packs and isolated pools (*unpublished*). I assumed that tadpole detection probability was constant between seasons and years because sparse data post-decline prevented us from estimating detection probability.

I fit all models using Bayesian methods and estimated the posterior distributions for all parameters using Markov chain Monte Carlo (MCMC) methods implemented in JAGS 3.4.0 in R version 3.2.1 (R Core Team 2015) using the rjags package (Plummer, 2015). For all parameters, I used non-informative priors (i.e., normal(0, 0.368), gamma(0.01, 0.01), uniform(0, 1)). I ran three chains for each parameter, and ran each chain for 100,000 iterations with a burn-in period of 5,000 iterations. I evaluated convergence of chains by visual inspecting trace plots, and using the diagnostics of Gelman (Brooks & Gelman 1998). I also assessed model fits using posterior predictive checks (Gelman et al. 2014).

To determine how much more likely a species was to successfully occupy a microhabitat before *Bd* than after *Bd* arrival, I calculated the odds ratio (i.e., OR = $odds_{post}/odds_{pre}$) by dividing the post-*Bd* logit output of the occupancy model by the pre-*Bd* logit output of the occupancy model. If the OR is close to one, then it suggests

that there was no change in occupancy. If the OR is below one, then it suggests that the odds of occupancy are greater pre-*Bd* than post-*Bd* then occupancy has declined. And if the OR is above one, then the odds of occupancy are lower pre-*Bd* than post-*Bd*, indicating an increase in occupancy. I considered the effect of *Bd* biologically meaningful if the 95% credible interval fell below or above one− interpreted as a 95% probability that the OR significantly changed.

Community composition

To determine if tadpole communities post-*Bd* invasion were more similar to one another than tadpole communities before *Bd* arrival, I used a permutational analysis of multivariate dispersion (PERMDISP2; Anderson et al. 2006) in R version 3.2.1 (R Core Team 2015). I used the Bray-Curtis metric, which allows dispersion distance to reflect variability in community structure. I visualized the data using non-metric multidimensional scaling (NMDS). I defined communities as the tadpole assemblages sampled in each microhabitat-stream-season-year combination, for a total of 48 communities (3 microhabitats x 4 streams x 2 seasons x 2 years). I only included data between 2003 and 2005.

II. The order of species losses

Species relatedness

To determine if the order of species disappearances was correlated with their phylogenetic relationship, I fit several macro-evolutionary likelihood models to the last Julian day a species was seen at the site. I fit Brownian, Ornstein-Uhlenbeck,

Lambda, and white noise models using the package 'geiger' in the R version 3.2.1 (Harmon et al. 2008; R Core Team 2015). I used our observational field data to determine the last Julian Day each species was detected at the site. I did not interpret results as the true date of species extirpations because our data likely reflect the date of last species detection.

I set 01 January 2003 as Julian Day 0, and 31 December 2005 as Julian Day 1095. *Bd* likely arrived between Julian Day 609 and 638 in September 2004 (Lips et al. 2006). I used a rooted, time-calibrated El Copé amphibian tree (Crawford, Lips, & Bermingham 2010). All species differed from sister lineages by a genetic distance at the COI gene or 16S gene by at least eight or two percent, respectively. The length of basal branches may be underestimated because of the use of the relatively fast-evolving mitochondrial DNA markers used to infer evolutionary history. Crawford et al. (2010) used several temporal constraints to calibrate evolutionary time on the entire amphibian phylogeny using the MPL algorithm. First, the age of the most recent common ancestor (MRCA) of Lissamphibia was placed at 332.6 million years ago (Ma). And, they added the minimum and maximum ages of three nested nodes: the MRCA of *Craugastor* + *Lithobates* (Phtanobatrachia) to the interval 143.3 to 179.9 Ma, the MRCA of *Lithobates* + *Nelsonophyrne* (Ranoidea) to the interval 106.2 to 130.9 Ma, and the MRCA of *Craugastor* + *Rhinella* (Nobleobatrachia minus *Rhinoderma*) to the interval 50.9 to 75.5 Ma.

I excluded any individuals that were not classified to species level (e.g., *Centrolene* spp. and *Colostethus* spp.). I also did not include any pool samples or pool habitat specialist (i.e., *Atelopus zeteki*) because the last Julian Day those species were

seen would have reflected the last day pools were sampled. I included all species that were found pre-*Bd* arrival for a total of 11 species, representing four families (i.e., Ranidae, Centrolenidae, Hylidae, Dendrobatidae), and I compared the fit of each model using AICc and model weights. I considered the model with the lowest AICc as the model of best fit, unless within 2 units (Schwarz, 2011).

Rarity

To determine if species rarity was a predictor of occupancy decline, I used two metrics: (1) tadpole seasonal microhabitat occupancy from the species occupancy model outlined above and (2) raw field data from transects of adult densities (Crawford et al. 2010). I used both tadpole occupancy and adult density to reflect species' variations in rarity across life stages. I calculated the species-specific habitat-weighted OR as the product of the odds ratios for each microhabitat in each season from the occupancy model outlined above and the average percent habitat available to adjust for variations in microhabitat cover among streams. To quantify the strength of the relationships between adult density and OR and between tadpole pre-*Bd* occupancy versus OR, I tested for an association between paired samples by calculating Pearson's correlation coefficient using the function cor.test() in R.

Habitat and resource use overlap

To determine if habitat overlap, defined as the average proportion of habitat shared by a species with all other species, affected the odds of decline for the m_{th} species, I averaged the occupancy probability for all other species, except the m_{th}

species, in each microhabitat and season from the model outlined above. Then, to quantify the strength of the correlation between habitat overlap and OR, I calculated Pearson's correlation coefficient.

To determine if resource use overlap, defined as the average proportion of habitat shared by a species with all other species in the same feeding guild, affected the odds of decline for the m_{th} species, I averaged the occupancy probability of all other species in the same feeding guild, following Verburg et al. (2007), in each microhabitat and season from the model outlined above. Again, I used Pearson's correlation coefficient to quantify the strength of the correlation between the m_{th} species resource use overlap and their OR.

III. Imperfect detection and sampling biases

Not adjusting for imperfect detection in occupancy models

I compared all the results from our detection-adjusted occupancy model (i.e., species occupancy declines, habitat and resource use overlap, and rarity analyses) to the results of a logistic regression, which does not adjust for detection probability, using a slightly modified dataset and the model outlined above. I modified the dataset by collapsing the site by visit matrix for each species, such that if a species was ever detected at a site it was considered present. I assigned the detection probability, p, for all microhabitat equal to one. I then used the same statistical approach using Markov chain Monte Carlo (MCMC) methods implemented in JAGS 3.4.0 in R version 3.2.1. (R Core Team 2015) using the "rjags" package (Plummer, 2015).

Optimizing species sampling

To determine how sampling effort affected occupancy estimates for a range of tadpole ecologies, I used a single-season single-species occupancy model to analyze simulated data under different scenarios (Supplement 2.1). I simulated occupancy data for a single species under scenarios spanning high to low detection and occupancy probabilities (range = 0.1 to 0.9) and varied the number of sites sampled (range: 5 to 200 sites by 20) and the number of surveys per site (range: 1 to 9 surveys per site by 2). I generated a total of 5,000 unique scenarios to test how variations in occupancy, detection, number of sites sampled, and number of surveys per site affected the precision of occupancy estimates.

I fit all models using Bayesian methods using the same procedure outlined above for species occupancy. For each unique combination of occupancy, detection, sites and surveys, I simulated 25 occupancy datasets and analyzed each dataset under a Bayesian framework. For each analysis, I ran three chains for each parameter, and ran each chain for 10,000 iterations with a burn-in period of 1,000 iterations.

To determine how well models performed under different sampling schemes, I calculated the root mean square error between true and recovered occupancy estimates for each of the 25 datasets per scenario. The root mean square error represents the sample standard deviation of the difference between predicted and true estimates. Based on occupancy and the degree of precision I wanted in model estimates, I decided *a priori* that my maximum acceptable root mean square error was 0.10 (i.e., Guillera-Arroita et al. 2010, Guillera-Arroita 2011).

Results

Field summary

We captured 2,021 individuals of 14 species across four microhabitats 15 months prior to *Bd*'s arrival. Of those, 1,123 individuals were found in pools. We found 11 species during the wet season and 12 species during the dry season, with 9 species common to both (Table A2.2). During the 11 months following *Bd*'s arrival, we captured 249 individuals of eight species across three microhabitats, representing a 72% decrease in captures and a 43% decrease in species richness.

Species that had >75% of captures during the dry season, included: *Atelopus varius*, *Colostethus panamensis*, *Lithobates warszewitschii*, *Espadarana prosoblepon*, *Sachatamia albomaculata*, *Hyloscirtus colymba,* and *Hyalinobatrachium colymbiphyllum.* Species with >75% of captures in the wet season included: *Colostethus spp.*, *Hyloscirtus palmeri*, *Sachatamia ilex* and *Teratohyla spinosa*. Species with >98% of captures in a single microhabitat included: *A. varius* (pools), *L. warszewitschii* (pools), most centrolenid species (leaf packs), and *Colostethus* spp. (isolated pools; Table A2.2).

Post-decline, the highest abundances of tadpoles were found in isolated pools, mostly of the families Dendrobatidae (*Silverstoneia flotator*, *C. panamensis*, *S. nubicola*, *A. talamancae, and Colostethus* spp.) or Hylidae (*H. palmeri, H. colymba*). Only two species had >75% of captures in the dry season: *Allobates talamancae* and *L. warszewitschii*, and only *Hyalinobatrachium colymbiphyllum* had >75% of captures during the wet season (Table A2.2). Five species were never seen post-decline (*A. varius, E. prosoblepon, S. albomaculata, S. ilex, T. spinosa*; Table A2.2).

I. Patterns of community disassembly

Tadpole density

Before *Bd* arrival, during the dry season, average monthly HWD per microhabitat ranged from 0.00 to 20.08 individuals m^{-2}, while during the wet season, average monthly HWD ranged from 0.00 to 6.69 individuals m^{-2} (Fig. 2.1). Within 11 months of *Bd* arrival, habitat-weighted density decreased from an average HWD of 4.53 ± 1.19 individuals m^{-2} (mean ± SE) to 0.34 ± 0.08 individuals m^{-2} after *Bd* (z = 4.12, $p < 0.001$; Fig. 1). The magnitude of declines did not differ between microhabitats or seasons ($p > 0.05$).

Idid not detect any tadpoles during any of the annual surveys conducted from 2006 to 2011, precluding further analyses. In April 2014, Ifound several pools and isolated pools with tadpoles of *Silverstoneia nubicola* and an unidentified species, ranging in HWD between 0.95 to 4.49 individuals m^{-2}.

Species occupancy

About half of the species in any microhabitat or season declined after *Bd* arrival (Fig. 2.2). Ialso found that detection probability was significantly higher for tadpoles in leaf packs and isolated pools (0.41±0.20), than for tadpoles found in riffles during the entire study (0.13±0.03; Table A3).

Community composition

Our evidence for biotic homogenization was that post-decline El Copé tadpole communities were more similar to one another than the pre-decline El Copé tadpole communities were to each other (Fig. 2.3; PERMDISP2, $F_{1,46} = 15.02$, $p < 0.001$). Pre-decline tadpole community dissimilarity among microhabitat and between seasons was 65% greater than their post-decline counterparts (Pre-decline average distance to median = 0.35; Post-decline average distance to median = 0.12).

II. The order of species losses

Species relatedness

Ifound that the Brownian model best fit the timing of species disappearance dates, indicating a taxonomic signal to the order of species losses and taxonomic homogenization (Fig. 2.4; Table A2.4), with centrolenids disappearing first− sometimes without ever being seen post-*Bd* arrival− and hylids, dendrobatids, and the ranids still seen several months post-*Bd* arrival. All other models increased the AICc score by at least 3 points (Table A2.4). No tadpoles were seen during the survey in 2006.

Rarity

Neither adult density nor tadpole occupancy predicted probability of decline among tadpole species (Fig. 2.2 & 2.5; Pearson's correlation coefficient = -0.13, $t = -0.33$, $df = 6$, $p = 0.75$; Pearson's correlation coefficient = -0.07, $t = -0.53$, $df = 46$, $p = 0.59$, respectively).

Habitat and resource use overlap

Ifound no trend in species decline odds by habitat overlap (Fig. 2.6; Pearson's correlation coefficient = 0.26, $t = 1.89$, $df = 46$, $p = 0.06$) or food resource overlap (Fig. 2.7; Pearson's correlation coefficient = -0.07, $t = -0.48$, $df = 46$, $p = 0.63$).

III. Imperfect detection and sampling biases

Not adjusting for imperfect detection in occupancy models

Using the logistic regression, Ifound that over half (~ 58%) of tadpole species, regardless of microhabitat or season, declined following *Bd* arrival (Table A2.5). Similar to the detection-adjusted model results, Ifound no relationship between food resource use overlap and the odds of species decline (Pearson's correlation coefficient = 16, $t = 1.16$, $df = 46$, $p = 0.24$) and no relationship between adult density and the odds of species decline (Pearson's correlation coefficient = -0.11, $t = -0.27$, $df = 6$, $p = 0.78$). But, in contrast to the detection-adjusted model, Ifound that as habitat overlap among species increased, then the likelihood a species declined also increased (Pearson's correlation coefficient = 0.39, $t = 2.93$, $df = 46$, $p = 0.005$) and that as tadpole pre-*Bd* occupancy increased, then the likelihood of species decline also increased (Pearson's correlation coefficient = 0.96, $t = 25.69$, $df = 46$, $p < 0.001$).

Optimizing species sampling

Our simulations showed that a biologist would need to survey at least 25 sites of each microhabitat at least three times each to obtain an occupancy estimate with a maximum error of 0.10 (Fig. A2.2; Table A2.6).

Discussion

Bd caused rapid, widespread declines in the tadpole community that were immediate and persistent. Tadpoles declined in abundance and occupancy rapidly within the first 11 months of the adult outbreak, and by the second year, all tadpoles had been extirpated. Sampling between 2006 and 2011 produced no tadpoles, even for species with adults that persisted post-*Bd* invasion. In 2014, the first tadpoles were detected but at very low densities and in few habitats.

Within 11 months of *Bd* invasion, tadpole community disassembly− the order of species declines and losses− was marked by taxonomic and ecologic homogenization with the disappearance of centrolenid habitat-specialists, resembling the regional pattern of adult community disassembly (Smith, Lips, & Chase 2009). Centrolenids were mainly found in leaf packs and were the first ones that disappeared, likely driving the homogenizing pattern across the site, whereas at the regional scale, geographically restricted endemic species drove the homogenizing pattern of adults (Smith, Lips, & Chase 2009). Homogenization in both adults and tadpoles resulted in higher than expected taxonomic and ecological similarity among communities post-*Bd*.

Species rarity, in terms of either adult density or tadpole occupancy, did not predict the magnitude of species declines caused by *Bd*, indicating that all naïve species were susceptibile to *Bd*. Both, rare and common species, experienced comparably large occupancy declines from *Bd* invasion. Rarity is a widely accepted indicator of species vulnerability for many taxa (Zavaleta et al. 2009), but the

mechanism (i.e., ecology versus rarity) driving species susceptibility can vary by disturbance. In this system, where *Bd* is highly virulent and hosts are naïve to infection, species rarity, of either tadpoles or adults, did not influence vulnerability to *Bd*. Host susceptibility to pathogen-related declines is more complicated than relating them to host population size, where aspects of host ecology may also contribute to species vulnerability (Lips et al. 2003). For example, riparian species are more vulnerable to declines than terrestrial species (Lips et al. 2003, Brem and Lips 2008). In our system, Ionly examined stream-dwelling tadpoles; if Ihad surveyed the entire landscape for tadpoles (i.e., bromeliads, canopy, refuges, etc.), Imay have detected more pronounced variations in susceptibility. Within a single habitat type though, Idid not find that species rarity predicted the magnitude of declines.

Ihypothesize that low adult abundance and low reproductive output during the disease outbreak may have contributed to the large tadpole declines− causing the rapid decline in abundance. Ifound little evidence that tadpole communities were recovering within the decade after *Bd* invasion, although Ilikely did not sample enough to detect all species of tadpoles. For tadpole abundance to increase, adult abundance and reproductive output needs to increase. It is possible that infected tadpoles have reduced growth rates (Parris and Cornelius 2004, Garner et al. 2009, Venesky et al. 2012) and higher disease-related mortality, or that metamorphs and subadults have high mortality rates (Berger et al. 1998, Rachowicz et al. 2006, Langhammer et al. 2014) but evidence for the latter is lacking. The few tadpoles detected in 2014 suggest that the amphibian community is starting to recover.

It seems that both isolated and heavily occupied communities had the same likelihood of declining, since habitat and food resource use overlap among species were not correlated with tadpole declines. If the presence of an infectious individual in a microhabitat increases the likelihood of pathogen exposure (e.g., Reeder et al. 2012, DiRenzo et al. 2014), then Iwould expect that tadpoles overlapping with infectious hosts would be more likely to decline (Lips 1998, Lips 1999). Likewise, if the probability of being exposed to *Bd* as a tadpole increases if infected individuals are sharing a food resource in the same habitat (e.g., Venesky et al. 2011), then species overlapping with an infectious species are more likely to decline. However, our results suggest that neither habitat or food resource overlap correlated with species declines, indicating that tadpole co-occurrence might not affect the likelihood of declining. A stronger predictor of declines might have been tadpole density, where as the proportion of infected tadpoles increases the likelihood of infection increases (Rachowicz and Briggs 2007), although Ihad no data to estimate infection intensity. Very little is known about how tadpole density affects the likelihood of contracting *Bd* (e.g., Rachowizc and Briggs 2007, Venesky et al. 2011). Yet, there are too many possible explanations for this scenario, where the lack of tadpoles could be because tadpole mortality increased, adults reproduction decreased, or post-metamorphosis survival decreased.

The magnitude of tadpole density declines reported here were much greater than the adult density declines described at this site (Crawford, Lips, & Bermingham 2010). The higher tadpole rate of loss is likely driven by both decreased recruitment and lower detection probability than adults. Tadpoles have naturally high mortality

rates (Calef 1973, Heyer et al. 1975) and when the additional chytrid-related mortality (Garner et al. 2009) is added to the system, the likelihood of tadpole survival is slim− explaining the discrepancy between the tadpole and adult magnitudes of decline. It may also be that tadpoles were still present but Idid not detect them− especially given that some centrolenid adults are present at the site and Idid not find their tadpoles (Crawford, Lips, & Bermingham 2010).

By not sampling pools after *Bd* arrival, Iwere unable to quantify the impact of *Bd* invasion on that microhabitat. However, our main conclusions would not have changed because amphibian adult mass mortality was widespread across the site (Lips et al. 2006). Iresampled pools in 2006, and Ifound no individuals, similar to the patterns in the other microhabitats.

Sampling recommendations

Iprovide the first estimates of Neotropical tadpole detection probabilities, which could replace vague priors traditionally used in Bayesian analyses to make more precise occupancy estimates. Most Neotropical regions have experienced widespread losses of amphibians from *Bd* (James et al. 2015), making it difficult to estimate unbiased tadpole detection probabilities. Tadpoles, like amphibian adults, are cryptic, secretive, and difficult to detect (Heard, Robertson, & Scroggie 2006; Smith et al. 2007), but monitoring tadpoles may provide a better solution to monitoring amphibian community dynamics post-*Bd* because stream-dwelling tadpoles are spatially constrained, whereas amphibian adults are not.

Our study was not designed with the intent of using *N*-mixture or occupancy models, but Iwere able to analyze the majority of species using occupancy models. If Ihad not accounted for imperfect species detection in this analysis, Iwould have overestimated occupancy declines and Iwould have incorrectly interpreted the correlations between tadpole declines and both rarity and habitat overlap. Observational error, in this case, can lead to misclassifying species as extirpated or having greater odds of decline. Irecommend for future studies to survey at least 25 sites of each microhabitat, three times each per season, to adequately sample a tadpole community for both rare and common species.

Occupancy studies should be designed carefully to ensure efficient use of available resources. To avoid wasted effort, biologists should anticipate the quality of their data (MacKenzie and Royle 2005, Guillera-Arroita et al. 2011). The precision and bias of occupancy estimates will also depend highly on the species biology and the system in general. For example, when working with rare species, the best sampling designs will tend to have more replication than in cases where only the precision of occupancy is of interest. Therefore, thought and care should be given to designing sampling schemes before collecting data to prevent loss of time, money, and resources.

Conclusions

Three traits associated with adult amphibian declines played no role in the declines of their tadpole counterparts. While the decline and extirpation of adult amphibians were predicted by (1) taxonomy (Corey and Waite 2008), (2) species

aggregation (Longo et al. 2010, Venesky et al. 2011), and (3) species abundance and distribution (Smith et al. 2009, Briggs et al. 2010), Idid not find evidence for two of these three for tadpoles, where closely related species did share their vulnerability to *Bd*. The discrepancy between order of extirpations and declines of adult and tadpoles may be attributed to when in the life cycle hosts are gaining infection and dying. If hosts are dying before reproduction, the patterns of species declines and extirpations will be greater than after they reproduce. For example, the mountain yellow-legged frog, *Rana muscosa*, develops fatal *Bd* infection post-metamorphosis, creating the illusion of healthy abundant tadpole populations but severely declined juvenile and adult populations (Briggs et al. 2010).

Ifound that tadpole communities were taxonomically and ecologically homogenized within 11 months of *Bd* invasion and communities collapsed within 22 months. *Bd* drove hosts to extirpation, and Ihave not seen signs or evidence of substantial tadpole community recovery within 10 years post outbreak. Our results are directly relevant to researchers interested in improving sampling methods of diverse communities, disease ecologists interested in understanding how multi-host fungal pathogens impact different life stages, community ecologists interested in pathogen-driven community disassembly of vertebrates, and conservation practitioners in charge of culling, vaccinating, and sterilizing wild populations experiencing declines and extirpations caused by multi-host fungal pathogens.

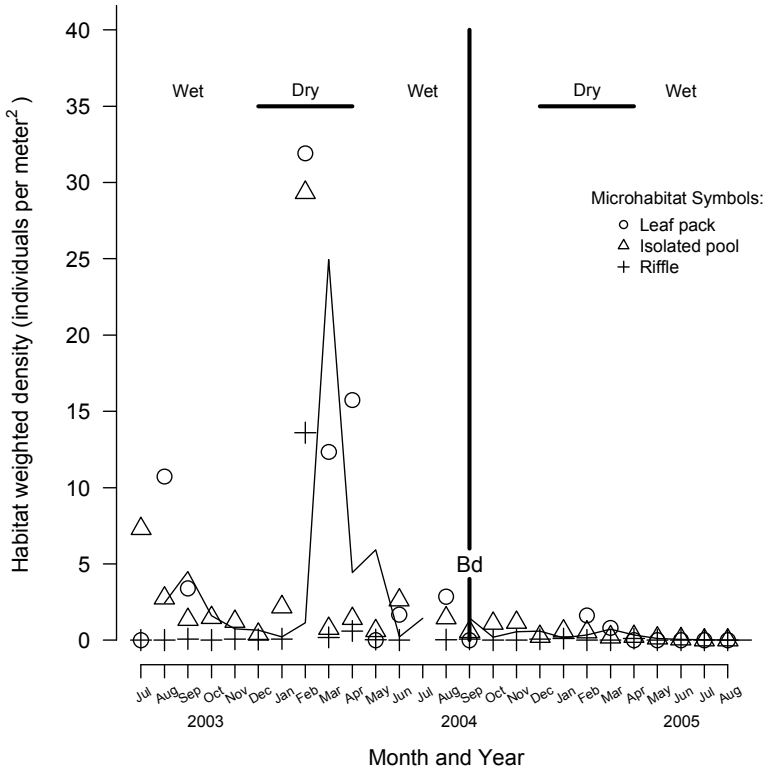

Figure 2.1 Effects of *Bd* arrival on habitat weighted density (individuals per meter^2) of tadpoles in each of three microhabitats (leaf pack, isolated pool, riffle) for 15 months before and 11 months after *Bd* arrival in September 2004 (Lips et al. 2006). The solid black line represents the rolling average of tadpole habitat weighted density for the entire tadpole community. The heavy black horizontal lines represent the dry season, and the heavy black vertical line represents the arrival of *Bd* in September 2004.

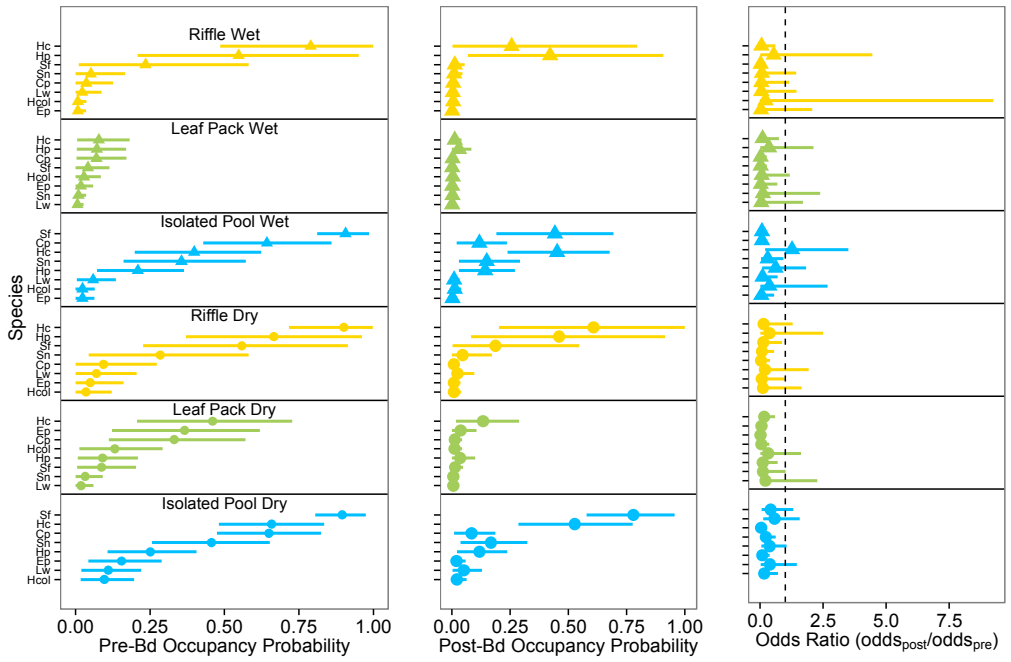

Figure 2.2 Patterns of occupancy by species, microhabitat, and season pre- (left) and post- (middle) *Bd* arrival with the odds ratio (i.e., OR = $odds_{post}/odds_{pre}$; right). All points represent the mean ± 95% credible interval. Tadpole pre-*Bd* occupancy rarity was not a significant predictor of decline (Pearson's correlation coefficient = -0.07, t = -0.53, df = 46, p = 0.59). Odds ratios less than one indicate occupancy declines post-*Bd*. Species codes: Hc = *H. colymba*; Hp = *H. palmeri*; Sf = *S. flotator*; Sn = *S. nubicola*; Cp = *C. panamensis*; Lw = *L. warszewitschii*; Hcol = *H. colymbiphyllum*; Ep = *E. prosoblepon.*

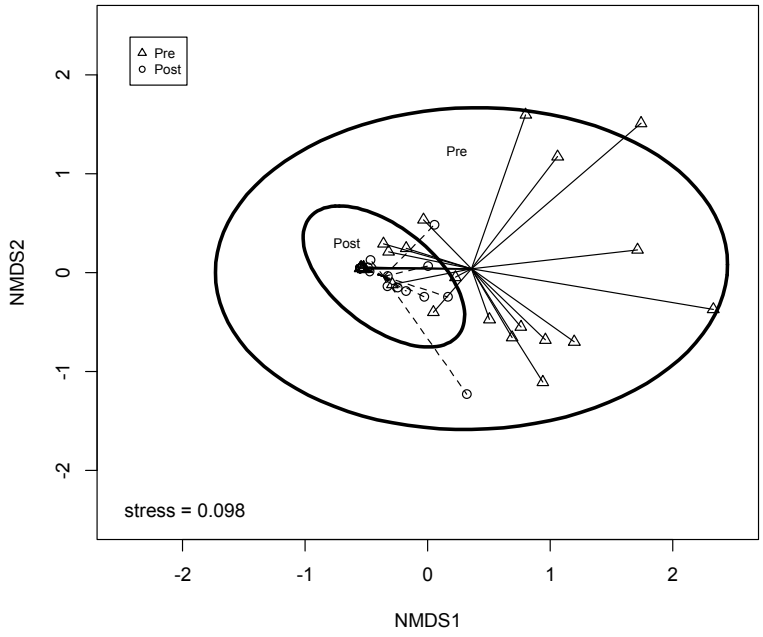

Figure 2.3 Non-metric multidimensional scaling (NMDS) ordination of tadpole communities− tadpole samples from each microhabitat-stream-season combination− pre- and post-*Bd* using Bray-Curtis dissimilarity. After *Bd* arrival, tadpole communities became more similar to one another, represented by the nested circles. Lines connect communities to the centroid of each group (i.e., pre- or post-*Bd*). Ellipses represent 95% confidence intervals around group centroids.

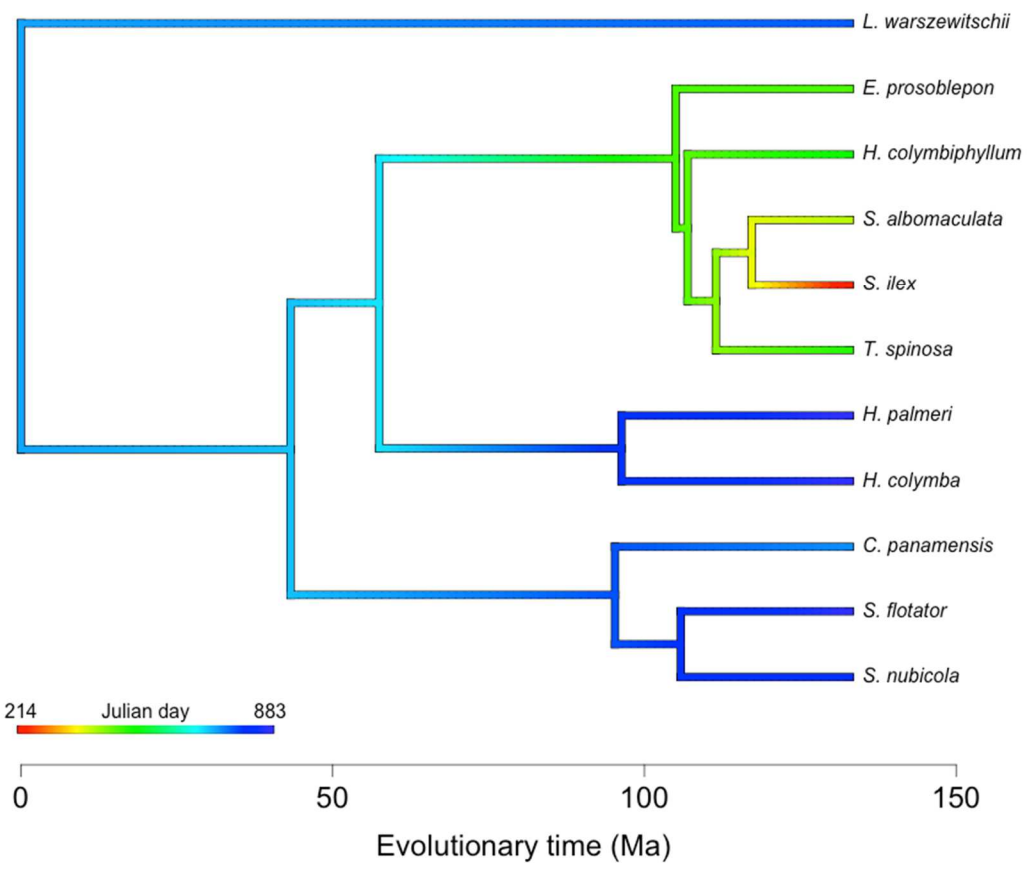

Figure 2.4 Phylogenetic patterns of order of species losses in stream-dwelling tadpoles with last Julian Day a species was seen mapped onto branches. Our rooted, time-calibrated, and trimmed phylogenetic tree was comes from the El Copé amphibian tree (Crawford, Lips, & Bermingham 2010). The x-axis represents divergence time in million of years ago (Ma). Julian Day zero corresponds to 01 January 2003, and Julian day 1095 corresponds to 31 December 2005. *Bd* arrived between Julian day 609 and 638. Most glass frog species were the first to disappear from the site− with many not seen post-*Bd* arrival; while treefrogs and poison-dart frogs remained detectable at the site after *Bd* arrival (model of best fit: Brownian; Table A4).

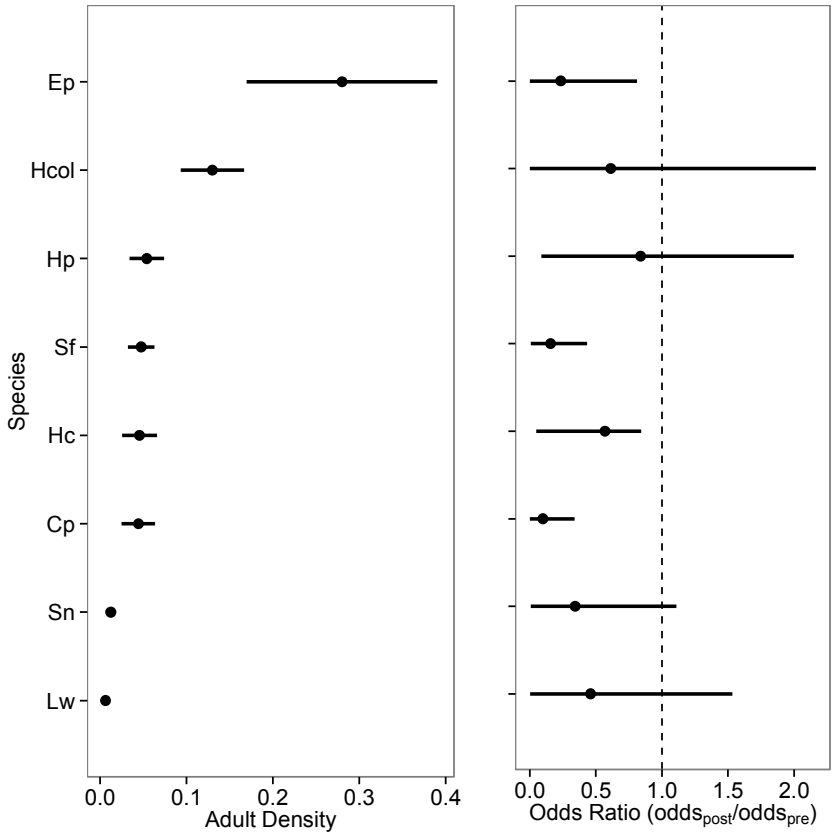

Figure 2.5 Mean adult species density pre-*Bd* arrival (left; 2000-2004; Crawford et al. 2010) by habitat-weighted odds ratio of tadpole declines (right). Adult rarity was not a significant predictor of the odds of tadpole decline (Pearson's correlation coefficient = -0.13, t = -0.33, df = 6, p = 0.75). Species codes: Hc = *H. colymba*; Hp = *H. palmeri*; Sf = *S. flotator*; Sn = *S. nubicola*; Cp = *C. panamensis*; Lw = *L. warszewitschii*; Hcol = *H. colymbiphyllum*; Ep = *E. prosoblepon*.

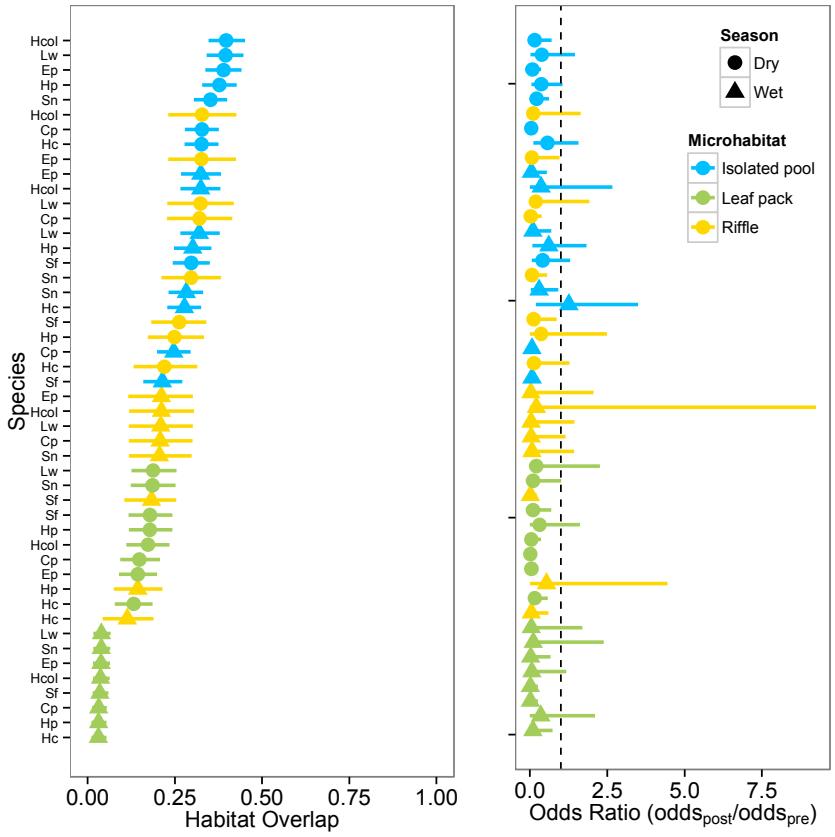

Figure 2.6 Habitat use overlap among species in each season and microhabitat (left) did not predict the odds of decline (right; Pearson's correlation coefficient = 0.26, t = 1.89, df = 46, p = 0.06). Habitat use overlap close to zero indicates less habitat overlap with other species, while values close to one represent more habitat overlap with other species. Species codes: Hc = *H. colymba*; Hp = *H. palmeri*; Sf = *S. flotator*; Sn = *S. nubicola*; Cp = *C. panamensis*; Lw = *L. warszewitschii*; Hcol = *H. colymbiphyllum*; Ep = *E. prosoblepon*.

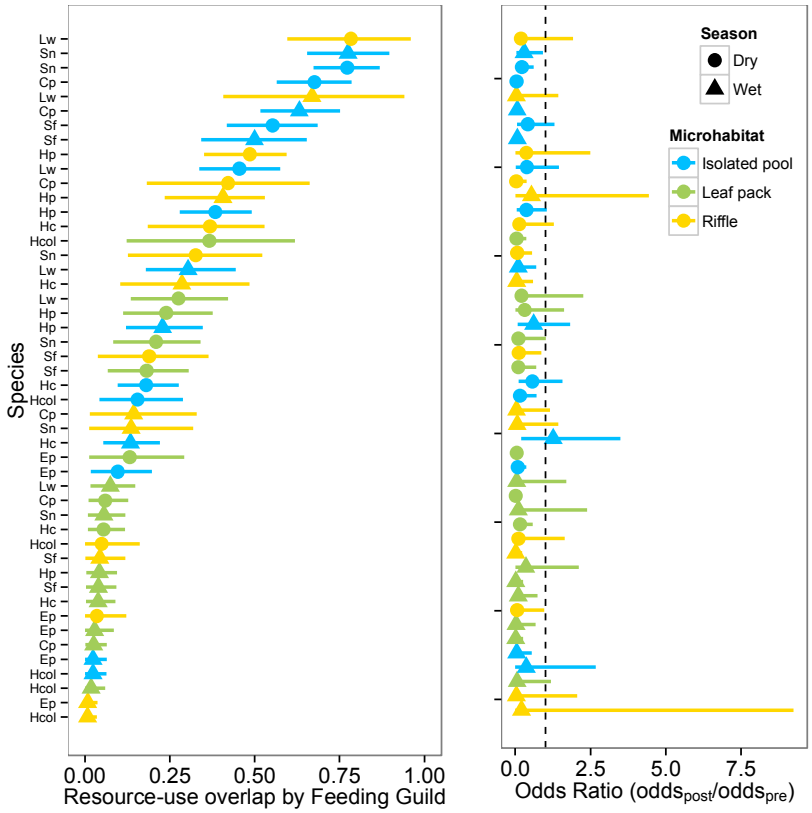

Figure 2.7 Food resource use overlap among species in each season and microhabitat (left) did not predict the odds of decline (right; Pearson's correlation coefficient = 0.20, $t = 1.42$, $df = 46$, $p = 0.15$). Resource use overlap close to zero indicate less resource overlap with other species in the same feeding guild, while values close to one represent more resource overlap with other species in the same feeding guild. Species codes: Hc = *H. colymba*; Hp = *H. palmeri*; Sf = *S. flotator*; Sn = *S. nubicola*; Cp = *C. panamensis*; Lw = *L. warszewitschii*; Hcol = *H. colymbiphyllum*; Ep = *E. prosoblepon*.

Chapter III: CHANGES IN HOST DEMOGRAPHY AFTER A CHYTRIDIOMYCOSIS OUTBREAK OFFER INSIGHT INTO LACK OF AMPHIBIAN ABUNDANCE RECOVERY

Coauthors: REBECCA MCCAFFERY, ANA V. LONGO, KELLY R. ZAMUDIO, & KAREN R. LIPS

Abstract

After an emerging infectious disease (EID) arrives into a naïve host population and causes rapid, widespread host mortality, then the host population must maintain its abundance to avoid extirpation as the pathogen establishes. In the case of the EID chytridiomycosis, caused by the pathogenic fungus *Bactrachochytrium dendrobatidis* (*Bd*), it has caused amphibian mass mortality, species extirpations, and population declines worldwide. For most amphibian populations, we lack demographic data to determine if populations are declining, increasing, or stabilizing. I analyzed five-years (2010−2014) of post-outbreak capture-mark-recapture data for a population of male glass frogs, *Espadarana prosoblepon*, whose population dynamics were studied from 2000−2004 directly before the 2004 chytridiomycosis outbreak in El Copé, Panama. I developed a novel multi-state Jolly-Seber model that accounts for imperfect host and pathogen detection to estimate: monthly pathogen prevalence, population size and growth, monthly apparent host survivorship, and recruitment. Between 2010 and 2014, I captured 202 unique males a total of 426 times. Contrary to our expectations that a hyper-virulent novel pathogen would continue to cause negative effects on host survivorship 10 years post-outbreak, monthly apparent survivorship post-outbreak (~92 − 99%) was nearly identical to survivorship estimates before *Bd* arrival (~ 92 −

94%). Pathogen prevalence ranged between 30 − 90%, while mean infection intensity was consistently low, 56.79 ± 27.43 ZGE. During the dry season, as host infection intensity increased, host survivorship decreased, supporting the hypothesis that higher infection intensity contributes to host mortality. Monthly average *E. prosoblepon* male population size was 111 individuals (95% Credible interval: 97 − 124), which is approximately half of this population's abundance before *Bd* arrival. Mean population growth between sampling occasions varied from 0.92 −1.48. I also found that the per capita entry probability, which quantifies the proportion of new animals entering the population via immigration or reproduction, was less than half of the pre-decline estimate. I conclude that this population has not recovered to pre-decline abundances because of a lack of entries into the population and not mortality of adults. I hypothesize that high survivorship of hosts coupled with low-level chronic infections is best explained by host tolerance to *Bd* infection and resistance to infection build up. My results suggest that wild amphibian populations can adapt via tolerance and resistance to *Bd* presence, but populations may not recover to pre-decline abundances if there are insufficient recruits.

Introduction

The rapid emergence of a virulent fungal pathogen into naïve ecosystems worldwide has decimated amphibian populations (e.g., Lips et al. 2006, Crawford et al. 2010, Fisher et al. 2012). Some of these same host populations, however, continue to persist in the presence of the pathogen after the outbreak. Ideally, to understand how these host populations are affected by pathogen presence, we would compare host survival, recruitment rates, and population sizes before and after pathogen

invasion; but these data rarely exist because either the pathogen has been present for decades (e.g., Murray et al. 2009, Rodriguez et al. 2014) or it is not clear when the pathogen will enter a naïve population. So, the most common approach has been to compare host survival, recruitment, and population sizes between two populations, where one population has the pathogen present and the other population does not (e.g., Muths et al. 2011, Tobler et al. 2012). In this circumstance, though, confounding site effects and host population histories can bias conclusions and makes it unclear how host populations are persisting in the presence of the pathogen.

There are at least two mechanisms that can help explain how host populations are avoiding extirpation when the pathogen establishes. First, the host population can offset pathogen-induced abundance declines with increased recruitment, via reproduction or immigration (e.g., Lampo et al. 2011, Muths et al. 2011). In this case, recruitment rates are high and host survival rates are low, but population size is maintained. Alternatively, the host can cope with pathogen infection by tolerating and/or resisting infection (e.g., Roy and Kirchner 2000, Woodworth et al. 2005, Schneider and Aryes 2008). Host resistance− where the host actively eliminates or limits increases in infection intensity through either adaptive or innate immune defenses– is measured as the inverse of infection intensity, because more resistant hosts should have lower infection intensities. Host tolerance, on the other hand, is the ability to persist with an infection by compensating for any tissue damage caused by the pathogen; it is measured as how quickly the odds of host survivorship change with respect to infection intensity changes. Tolerance is assumed when increases in infection intensity do not produce higher rates of mortality. But host tolerance and

resistance are influenced by seasonality because weather contributes to shifts in host and pathogen biology (Altizer et al. 2006).

In the case of the emerging pathogenic fungus *Batrachochytrium dendrobatidis* (*Bd*), seasonality determines how quickly the pathogen reproduces on an infected host (e.g., Longo et al. 2010). Seasonally lower host survivorship can lead to population declines by at least one of two mechanisms that are not mutually exclusive. First, seasonal weather changes, such as temperature or rainfall, can increase or decrease pathogen growth rates on infected individuals. In the instance of *Bd* in the wet tropics, though, infectious *Bd* zoospores may be mainly affected by temperature variations between seasons because, during the drier season, rainfall may not be low enough to cause pathogen desiccation. This would be measured as both higher host infection intensities and mortality during the cooler season than the hotter season. Alternatively, though, seasonal changes in host social behavior, such as aggregations or activities, can affect pathogen growth on infected hosts (e.g., Altizer et al. 2006, Longo et al. 2010). Less active individuals may be clumping in refugia that assist in pathogen growth (Longo et al. 2010), whereas active individuals may be able to cope minimize or eliminate pathogen infections more readily by thermoregulatory behavior.

The most basic data requirement to make inferences on host survivorship, recruitment, and population size is to identify disease state without error for each individual because state assignment errors can bias model estimates (Kendall 2008, Kéry and Schaub 2012). In the case of *Bd*, infected hosts tend to be misidentified more often as uninfected host when their infection intensities are low (i.e., false

negatives; Lachish et al. 2012, Miller et al. 2012). Low infection intensities are especially common post-outbreak, making this type of error especially problematic (Briggs et al. 2010). But, when pathogen detection probability is available, we can integrate imperfect pathogen detection into the modeling approach by adjusting the observation matrix.

I conducted a capture-mark-recapture study of a population of male *Espadarana prosoblepon* for five years (2010 – 2014) in El Copé, Panama 10 years after the 2004 *Bd* outbreak (Lips et al. 2006). I estimated host survival, recruitment rates, population size, and population growth rate in the presence of *Bd* and determined how host infection intensity affects survivorship seasonally. The ability to understanding how host populations are maintaining abundance in the presence of disease will help reintroduction programs and recovery plans to help boost population recovery.

Methods

Study Species.— Espadarana prosoblepon is a small, nocturnal, arboreal glass frog distributed from Honduras to Ecuador. It inhabits elevations between 20 to 1900 m in humid lowland, premontane, and lower montane zones of wet forests and rainforests (Savage 2002). Within the last several decades, *E. prosoblepon* has declined throughout its range because of deforestation and chytridiomycosis (Lips et al. 2003, Kubicki et al. 2010).

Male *E. prosoblepon* establish territories on overhanging stream vegetation (Savage 2002) where they call to attract females. Amplectic pairs deposit egg clutches onto leaves overhanging the stream. Males are present year-round and often

inhabit the same territories year-round (Robertson et al. 2008; McCaffery and Lips, 2013). Males can live at least five years (McCaffery and Lips, 2013).

Espadarana prosoblepon is one of the most well studied species in El Copé, Panama. In 2004, the arrival of *Bd* at this site caused population declines and extirpations of many species, including *E. prosoblepon* (Lips et al. 2006, Crawford et al. 2010). By the peak of the outbreak, approximately 48% of *E. prosoblepon* individuals were infected and carried average infections of 139 zoospores (Longo et al. *in prep*), and four dead individuals had been found (Tunstall et al. *in prep*). Following the outbreak, *E. prosoblepon* density declined by ~ 70% at this site (Angeli et al. 2014).

Field surveys.— I surveyed four 200-m permanent stream transects in Parque Nacional G. D. Omar Torríjos H., El Copé, Coclé Province, Panama (8°39’57’’N, 80°35’33’’W; 600−900 m) established as part of a long-term amphibian monitoring project (Lips et al. 2003; Figure 3.1). The four stream transects, Casacada, Guabal, Loop, and Silenciosa, are part of the same drainage network, and all streams are < 5 m wide and bordered by dense vegetation. These transects were established in 1998 and were monitored annually from 2000 to 2005. Streams were not monitored in the years following the *Bd* outbreak in 2004, but we resumed surveys in 2010 following similar field methodology to the pre-*Bd* surveys.

Between 2010 and 2014, I surveyed each transect either one or two months during both or one of the wet and dry seasons: July 2010, July 2011, June 2012, July 2012, February 2013, March 2013, June 2013, July 2013, and March 2014. These

months represent our primary sampling periods. Within each month, I surveyed each transect 2–7 times on consecutive nights (mean ± SE: 3.94 ± 0.24; Table A3.1).

Field teams surveyed transects by slowly walking in the middle of streams and capturing amphibians by hand with a fresh pair of latex gloves. Captured individuals were sexed, weighed (g), measured (snout-to-vent length; mm), and swabbed. To test for *Bd* infection, I swabbed the ventral skin surface with a sterile cotton tip swab. Swabs were stored in a capped 2.5 mL tube with 30 µL of 70% ethanol.

I double swabbed a subset of all captured individuals, which included other species, during the sampling occasions: June 2012, July 2012, February 2013, March 2013, and March 2014, twice in sequence and labeled samples as "swab1" and "swab2". These replicate swabs were used to calculate imperfect pathogen detection (Supplement 3.2).

Newly captured individuals were given a unique toe clip combination ranging between one to four toe clips with no more than one toe clip per limb (McCaffery and Lips 2013). I recorded toe clip codes for all recaptured individuals and all individuals were immediately released at the point of capture. I only recorded recaptures on the last sampling occasion following McCaffery and Lips (2013). Ionly analyzed male captures because females were rarely (i.e., < 5% of captures). Females come down from the canopy to the stream to breed and may move across the site more frequently than males (Savage, 2002).

Molecular Analysis.— I tested all skin swabs collected for the presence of *Bd* using PrepMan Ultra® to extract DNA. I tested swabs for *Bd* in singlicate using Taqman

qPCR (Boyle et al. 2004, Hyatt et al. 2007) running 50 cycles. I ran each plate with the Panamanian *Bd* isolate (JEL 423) standards of 0.1, 1, 10, 100, and 1000 *Bd* zoospore genomic equivalents (ZGE) to determine *Bd* presence and infection intensity. I included negative and positive controls in each qPCR plate to estimate rates of false-positives. I categorized individuals as *Bd* positive if amplification occurred before cycle 50 (Briggs et al. 2010). If I captured and swabbed an individual more than once within a month, I calculated the individual's mean infection intensity among swabs for the analysis. Approximately 81% of those individuals had zero ZGE. If I exclude those individuals, the average difference between zoospore loads between the first and last swab collected for a single individual within a month 11.70 ± 8.04 ZGE. I refer to ZGE as infection intensity hereafter.

Statistical Analysis.— I analyzed a five-year (2010-2014) post-outbreak capture-mark-recapture dataset for male *E. prosoblepon* collected during wet and dry seasons using a multi-state Jolly-Seber model within a hierarchical Bayesian framework (Kéry and Schaub 2012). For each disease state (i.e., infected and uninfected), the model quantifies: monthly host survivorship, per-capita entry probability, transition probabilities between disease states, population size, and population growth rates, while accounting for imperfect host and pathogen detection (Figure 3.2).

The multi-state formulation of the Jolly-Seber model includes both state and observation processes to account for imperfect host detection (Kéry and Schaub 2012). The state process describes the true disease state of an individual where the *i*th state is described as: 1 = not entered, 2 = uninfected, 3 = infected, and 4 = dead, and

assumes that an individual moves between the *H* disease states over a finite number of sampling occasions $t = 1, 2, \ldots, n$ (Figure 3.2). For any given individual, the successive disease state is described by a discrete first-order Hidden Markov Model (HMM), where the probability of an individual transitioning from disease state *j* to *i* at time $t-1$ to t only depends on the true state at time $t-1$.

Population size

Using the same modeling approach as McCaffery and Lips 2013, I used a data augmentation method to calculate the true population size of male *E. prosoblepon* along the four sampled transects, N_t, at time *t* as $N_t = \sum_{i=1}^{M} z_{i,t}$, where $z_{i,t}$ is the latent state variable (i.e., the unobserved true state) of the *i*th host at time *t* (Kéry and Schaub 2012), where $z_{i,t} = 1$ if the *i*th host is alive and present in the population, and zero otherwise. I augmented the observed data set *Y* with a large number of all-zero capture-histories, resulting in a larger data set of fixed dimension *M*, where *M* was much greater than *N*, the true population size, to account for individuals never observed but likely present at the site. I estimate population size for June 2011 to July 2013 because there were few captures June 2010 and no new individuals were marked March 2014, precluding us from estimating population size.

Recruitment

I denote the number of new recruits at *t* as $B_t = \sum_{i=1}^{M}(1 - z_{i,t-1})\, z_{i,t}$, and I express the recruitment process as a per-capita entry probability, *f*, computed as $f_t = \frac{B_t}{N_t}$ (Kéry and Schaub 2012). This expresses the fraction of new individuals at *t* per individual

alive at *t*. The recruitment process consists of both immigration and reproduction, which are not distinguishable in our modeling approach.

Survival and disease dynamics

To estimate monthly survival, colonization, and transition rates using a multi-state Jolly-Seber model, I used the transition matrix, Ψ, where the rows represent the past state at *t−1* and the columns represent the state at the current time step, *t*:

$$\Psi_{z_{i,t-1},z_{i,t},j,t} = \begin{bmatrix} 1-\gamma_{2,t}^{M_{j,t}}-\gamma_{3,t}^{M_{j,t}} & \gamma_{2,t}^{M_{j,t}} & \gamma_{3,t}^{M_{j,t}} & 0 \\ 0 & \Phi_{2,j,t}^{M_{j,t}}(1-c^{M_{j,t}}) & \Phi_{2,j}^{M_{j,t}}c^{M_{j,t}} & 1-\Phi_{2,j,t}^{M_{j,t}} \\ 0 & \Phi_{3,j,t}^{M_{j,t}}r^{M_{j,t}} & \Phi_{3,j,t}^{M_{j,t}}(1-r^{M_{j,t}}) & 1-\Phi_{3,j,t}^{M_{j,t}} \\ 0 & 0 & 0 & 1 \end{bmatrix}.$$

For ease of presentation, I dropped the third and fourth index of the matrix used in model formulation and summarized parameter names and definitions (Table 3.1). States in the transition matrix, Ψ, are read from top to bottom and left to right in the order: not entered yet, uninfected, infected, dead. The "not entered yet" category consists of individuals that are not part of the population but may enter, where the parameter $\gamma_{i,t}$ is the state-specific removal entry probability, the probability that an individual in state *i* enters the population at time *t*. The parameter Φ_i is the state-specific apparent monthly survival probability for uninfected (*i* = 2) and infected (*i* = 3) hosts from *t−1* to *t* because I cannot distinguish between emigration and death. Given that the number of months varied between sampling occasions, I adjusted estimates for the cumulative survival across all month between *t−1* to *t* using the notation $M_{j,t}$.

The parameters *c* and *r* are the infection and recovery probabilities, respectively. Conditional on the *j*th host's survival from *t−1* to *t*, a host can become infected, if they were uninfected at *t−1*, or recover from infection, if there were infected at time *t−1*, with probabilities *c* and *r*. I also assume that at most only one state transition occurs between sampling occasions.

For infected individuals, I include the association between survival probability ($\phi_{3,j}$) from time *t*−1 to *t* and the *j*th host's infection intensity at time *t−1* ($ZGE_{j,t-1}$) during the wet and dry seasons ($Season_{t-1}$) as:

$$logit(\phi_{3,j,t}) = \alpha_1 + \beta_1 ZGE_{j,t-1} Season_{t-1},$$

where α_1 is the y-intercept and β_1 is the slope, representing the strength and directionality of the relationship.

Imperfect host and pathogen detection

To estimate monthly host recapture probabilities, I mapped the observation process of the four true states, represented by the rows, onto the three observed states, the columns (i.e., "seen uninfected", "seen infected", and "not seen"), using the observation matrix, π:

$$\pi = \begin{bmatrix} 0 & 0 & 1 \\ p_{2,j,t} & 0 & 1 - p_{2,j,t} \\ p_{3,j,t} e_{j,t} & p_{3,j,t}(1 - e_{j,t}) & 1 - p_{3,j,t} \\ 0 & 0 & 1 \end{bmatrix}.$$

I modified the traditional observation matrix used in multi-state Jolly-Seber models to account for the probability of misclassifying the disease state of the *j*th host at time *t*, $e_{j,t}$, by multiplying the traditional observation matrix by a misclassification matrix (Supplement 3.2; Titman and Sharples 2010).

I define the probability of misclassifying an individual ($e_{j,t}$) as *1− the probability of detecting the pathogen on the jth host given that it is infected at time t*. In my specification, host misclassification occurring at *t* is conditional host detection from *t−1* to *t*. I estimated the probability of misclassifying the disease status of an individual by fitting a separate hierarchical Bayesian model using the double swab samples I collected to calculate pathogen detection probability ($m_{j,t}$) as a function of host infection intensity ($ZGE_{j,t}$) following Miller et al. (2012; Supplement 3.3). Pathogen detection probability (i.e., probability of correctly identifying an infected host when infected) is the complement of misclassification probability (i.e., probability of incorrectly identifying an infected host when infected) where:

$$e_{j,t} = 1 - logit(m_{j,t})$$

$$logit(m_{j,t}) = \alpha_2 + \beta_2 ZGE_{j,t}$$

I also included variation in the state-specific detection probability, $p_{i,j,t}$, as a function of the number of surveys conducted in a given sampling occasion (Table A3.1), where:

$$logit(p_{i,j,t}) = \alpha 2_i + \beta 2 Surveys_{j,t}$$

State-space model formulation

Because there are more than two possible true and observed states, parameter likelihood is based on the categorical distribution, where the state-space model is:

$$z_{i,j,t} | z_{i,j,t-1} = categorical(\Psi_{z_{i,j,t-1},1:4,j,t}),$$

where $z_{i,j,t}$is the latent variable state of the *j*th host at time *t*. And the observation equation linking the true and observed states is:

$$y_{i,j,t}|z_{i,j,t} = categorical(\pi_{z_{i,j,t},1:3,j,t}).$$

Model limitations.— By using a Hidden Markov Model, I assume individuals do not develop acquired immunity and that the only information influencing state changes are the current states and not an individual's entire infection history (Cashins et al. 2013, Ellison et al. 2014, but see McMahon et al. 2014). I also did not include stream transect as a covariate, given that it is a well-mixed population (Robertson et al. 2008, McCaffery and Lips 2013).

Our use of the Jolly-Seber model does not account for the possibility that infection could influence the emigration rate rather than the survival rate (Schmidt 2010), but most individuals move very little over their lifetime and tend to move upstream (Robertson et al. 2008), so I attributed the loss of individuals to death rather than emigration.

Parameter comparisons.— To test our predictions and assess potential differences between parameter estimates of infected and uninfected hosts (i.e., survival and recapture probabilities), I compared the posterior distributions of the parameters. I investigated whether the parameter values were equal by computing the proportion of iterations in the posterior distribution in which one parameter is greater than the other. Extreme proportions (i.e., ≥ 0.95) suggest little overlap in posterior distributions, and I interpreted it as a 95% probability that the first parameter is significantly higher than the second. I considered regression coefficients significant if the 95% credible interval did not overlap with zero on the logit scale.

To estimate population growth rate, I used the equation: $\lambda_t = \frac{N_{t+1}}{N_t}$, where $\lambda_t >$ 1 suggests population growth, $\lambda_t < 1$ indicates population declines, and $\lambda_t = 1$ suggests population stability (Kéry and Schaub 2012). I estimated the population growth rate for the population from 2011 to 2013.

Model fit.— I fit the model using Bayesian methods and estimated the posterior distributions for all parameters using Markov chain Monte Carlo (MCMC) methods implemented in JAGS 4.0.0 in the R environment (R Core Team 2015) using the "jagsUI" package (Kellner, 2015). For all parameters, I used vague priors with a normal distribution (normal(0, 0.368); Lunn et al. 2000). I ran three chains for each parameter, and ran each chain for 20,000 iterations, with a burn-in period of 2,000 iterations, and thinned by 50. I evaluated convergence of chains by visual inspecting trace plots, and using the diagnostics of Gelman, where Rhat < 1.1 (Brooks & Gelman 1998). I also assessed model fits using posterior predictive checks (Gelman et al. 2004), where a value close to 0.5 indicates adequate model fit.

Results

Field summary.— I captured 202 individuals 426 times between 2010 and 2014 (Table 3.2). I captured 143 individuals once, 61 individuals twice, 20 individuals three times, 13 individuals four times, 9 individuals five times, 8 individuals eight times, and 1 individual seven times. I captured several individuals in 2011 and 2014, indicating that individuals live at least four years post-*Bd*.

Approximately 75% of our captures were uninfected (320/426), and all infected individuals had low infection intensities (average infection intensity = 2.93 ± 1.44 ZGE; Figure 3.3). I documented 23 infection events, where an uninfected individual became infected, and 26 recovery events, where an infected host lost an infection.

Our multi-state Jolly-Seber model adjusting for misclassification of disease state fit the data well (Figure A3.1; Bayesian *p*-value = 0.61).

Population growth and abundance.— Most population growth rate estimates overlapped one or were slightly above one, indicating stable population size (Figure 3.3 & 3.4). Monthly estimates of the number of infected individuals each month ranged between 27 and 94 individuals and that of uninfected individuals was between 2 – 60 individuals. Monthly mean prevalence ranged between 30 – 99% (Figure 3.4). Host infection intensity during the dry seasons ranged was 0.23 to 51.89 ZGE, and during the wet season, average monthly infection intensity ranged between 0.13 to 1988.23 (Table 3.2).

Demographic rates.— During the dry season, infection intensity decreased the probability of survival of infected hosts but not during the wet season (95% Credible interval: $\beta_1 wet$ = -0.81 − -0.03, $\beta_1 dry$ = -0.10 – 0.20; Figure 3.6). Average monthly survival probability of infected hosts was 93.76% (95% Credible Interval = 89.46 – 96.02%), and 92.10% for uninfected hosts (95% Credible Interval = 88.38 – 94.77%), and did not differ significantly (Pr(infected > uninfected) = 0.70).

Monthly infection probability was higher (84.53–99.14%) than monthly recovery probability (14.39–76.63%; Pr(infection > recovery) = 1).

Between 2011 to 2014, the average monthly per-capita entry probability, defined as the proportion of new individuals added to the population per individual already present, was 0.06 – 0.34 (Figure 3.6), and the average per-capita entry probability across all sampling occasions was 0.21 (95% Credible interval: 0.16 – 0.26), which is less than half of the average pre-decline estimate (mean: 0.56; 95% Credible interval: 0.54 – 0.58; McCaffery and Lips 2013).

Imperfect pathogen and host detection.— For uninfected hosts, capture probabilities were similar between wet and dry seasons (Pr(wet > dry) = 0.90), but capture probabilities differed between seasons for infected hosts (Pr(wet > dry) = 1; Table 3.3). Capture probability did not differ between infected and uninfected hosts during the wet season (Pr(infected > uninfected) = 0.34) but did differ during the dry season (Pr(infected > uninfected) = 1). For each additional survey conducted each month, the odds of capturing an individual increased by 1.53 (95% Credible interval: 1.22 – 1.98).

Discussion

Male *E. prosoblepon* survivorship post-outbreak was similar to survivorship pre-outbreak (McCaffery and Lips 2013), despite high infection prevalence. Because infected hosts with low-level infections and uninfected hosts had similar survival rates and most individuals had low-level infections, this suggests that animals are not dying from infection.

Espadarana prosoblepon may be tolerating mild infections or limiting pathogen build-up because either extrinsic conditions during the outbreak amplified *Bd*'s impact or this species has adapted to *Bd* via tolerance or resistance. During the chytridiomycosis outbreak in 2004, high species diversity may have caused pathogen amplification (~74 species; Crawford et al. 2010), high host density may have caused high host-to-host *Bd* transmission, and pathogen naivety may have made the amphibian immune system inadequate to fight the pathogen. But, today, in the field and in the lab, when *E. prosoblepon* is infected, they maintain low-level infections (Tunstall et al. *in prep*), suggesting adaptation. If *E. prosoblepon* has managed to adapt to *Bd* infection, it is surprising that their population size is only half of its historic size (McCaffrey and Lips 2013). It is possible, however, that the population is slowly increasing over time and the length of our study only captured a small snapshot. Alternatively, if the population continues increasing and high host density caused large population declines, then I expect that the abundance will plateau rather than producing a large *Bd* outbreak.

The lack of mortality of infected *E. prosoplepon* may be explained by host resistant or tolerance because of a strong innate and/or adaptive immune system that can combat *Bd* growth. Before *Bd*'s arrival in El Copé in 2004, *E. prosoplepon* produced some of the strongest *Bd* inhibitory anti-microbial peptides (AMPs) among all other species tested (Woodhams et al. 2006). Other innate or acquired immune defense against *Bd* that can aid in tissue repair or immunological defense are mutualistic anti-fungal bacteria (e.g., Bell 2012) and MHC expression (Savage and Zamudio 2011, Ellison et al. 2014). Neither of which have been characterized for *E.*

prosoplepon. The AMPs that *E. prosoplepon* produces may not have been enough to prevent the large declines during the outbreak because of other extrinsic factors that amplified *Bd*'s impact (e.g., high species diversity and high host density).

I hypothesize that the primary reason preventing the population from rebounding to its pre-decline size is lower recruitment rates and not high mortality of infected hosts. Recruitment rates may be lower for one of two reasons. First, before *Bd* arrival, lowland *E. prosoplepon* may have colonized our upland population (Robertson et al. 2008), and if the lowland population declined, then it may lead to lower immigration rates. This, however, is unsupported by any of our data, and lower population sizes do not necessarily translate to lower immigration rates. Alternatively, high pathogen-induced mortality of juveniles might decrease recruitment rates to the adult population (e.g., Langhammer et al. 2013, Rachowicz et al. 2006). Because I was unable to mark and track other life stages (e.g., larvae, metamorphs, juveniles), I cannot separate immigration and reproduction from the recruitment process.

During the dry season, higher host mortality was explained by higher host infection intensities, but not during the wet season, which I hypothesize is a result of differences in host activity between seasons. For example, in Puerto Rico during the dry season, *Eleutherodactylus coqui* are less active and clump in humid refugia, where the *Bd* infection intensities of infected hosts rapidly increase (Longo et al. 2010). In El Copé *E. prosoblepon* reproduce less, call less, and are more difficult to detect during the dry season (*Lips pers. obs.*), which was reflected in the lower detection probability. The difference in host mortality between seasons may be the result of differences in habitat use. During the dry season, amphibians are still present

at the site, since they are territorial, but I am not finding them. The next steps to explaining this pattern would be to collect data on seasonal activity, behavioral clumping, and identifying habitat use differences between seasons.

Modeling advances

I developed a novel Jolly-Seber model that allows us to adjust for imperfect pathogen detection. I modified the traditional observation matrix used in Jolly-Seber models by accounting for the misclassification probability of disease state (Supplement 3.2) and provide code (Supplement 3.3) for future studies. Imperfect pathogen detection is a large problem for many host-pathogen systems (e.g., Thompson 2007, Lachish et al. 2012, Miller et al. 2012), and, if I had not included imperfect pathogen detection, my results would have underestimated pathogen prevalence, overestimated mean infection intensity, and introduced bias in both infection and recovery probability estimates (e.g., Lachish et al. 2012, Miller et al. 2012).

Conclusions

Ten years after a chytridiomycosis outbreak, evidence suggests that male *E. prosoblepon* populations are stable, at half their historic abundance, and have not recovered to pre-*Bd* population sizes because of lower recruitment rates rather than high pathogen-induced mortality. These frogs may be tolerating low-level infections and may be resistant to pathogen build up. To understand the evolutionary ecology of host defense, the costs to pathogen defense, and defense-cost trade-offs, the next step

would be understand how this species is tolerating mild infections and resisting pathogen build-up. Conservation biologists trying to preserve amphibian species face the big challenge of reducing *Bd*'s impacts to prevent rapid extinction but not compromising the host adaption to the pathogen.

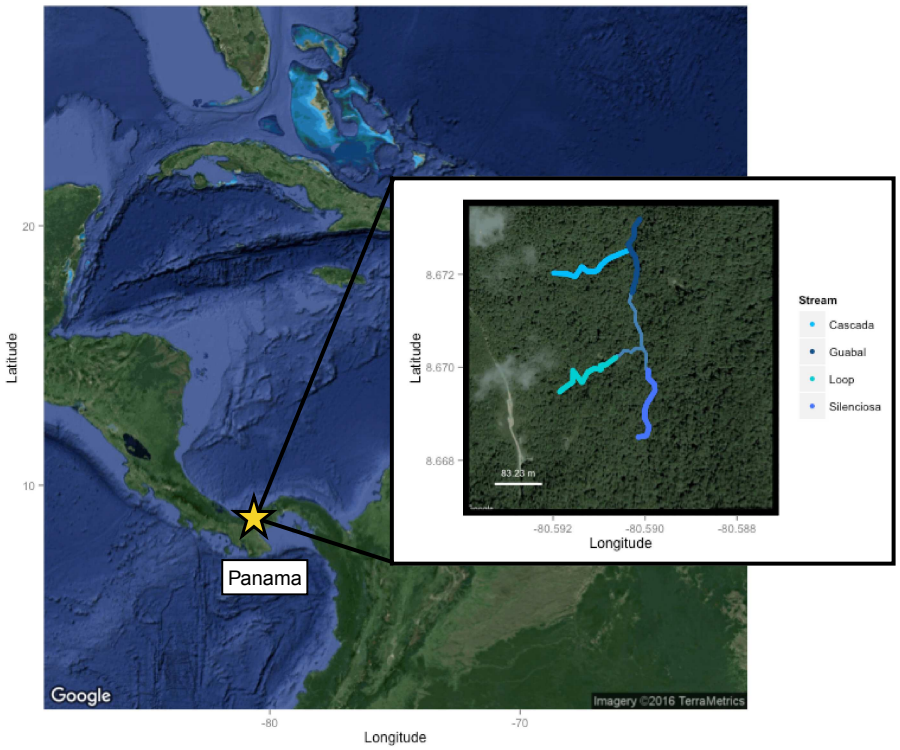

Figure 3.1 Map of study area located in Parque Nacional G. D. Omar Torríjos H., El Copé, Coclé Province, Panama. The four surveyed streams are color-coded in the embedded map.

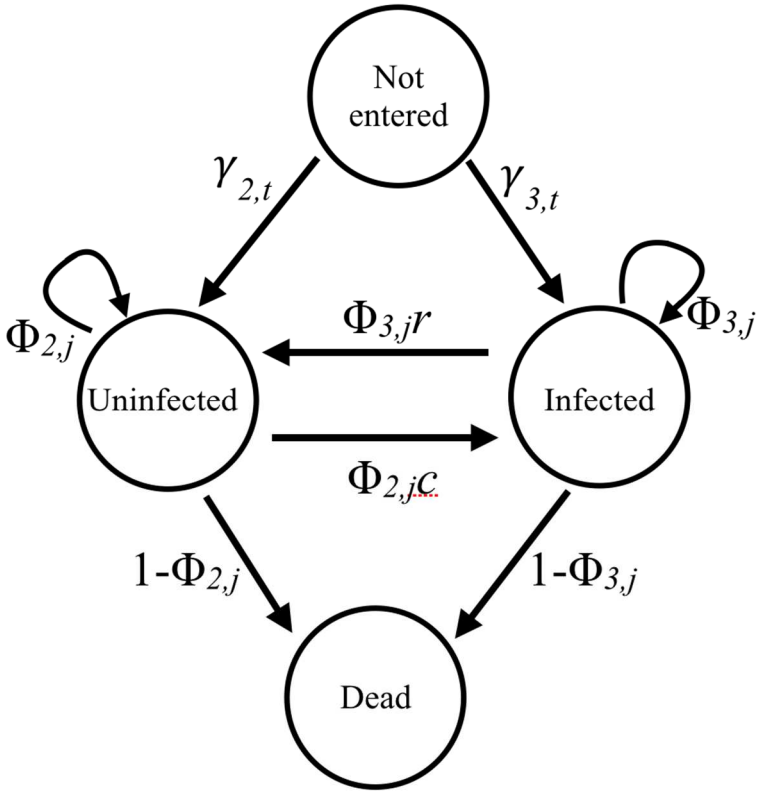

Figure 3.2 Diagram of the *E. prosoblepon* host-pathogen model. The parameters Φ (state-specific monthly survivorship), γ (entry probabilities), and *c/r* (transition probabilities) are all estimated using monthly capture-mark-recapture for the *j*th individual the *t*th season.

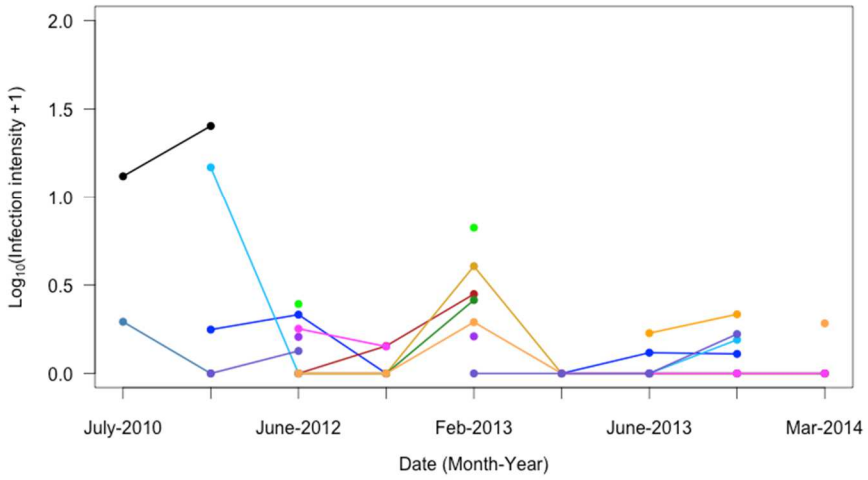

Figure 3.3 Raw infection intensity time series for 13 *E. prosoblepon* male individuals. Each color represents an individual, where lines connect infection histories. Although most infections reach close to zero, there is a ~ 90% chance of missing infections at low infection intensities, making it likely that individuals maintain low-level infections rather than gaining and losing infections.

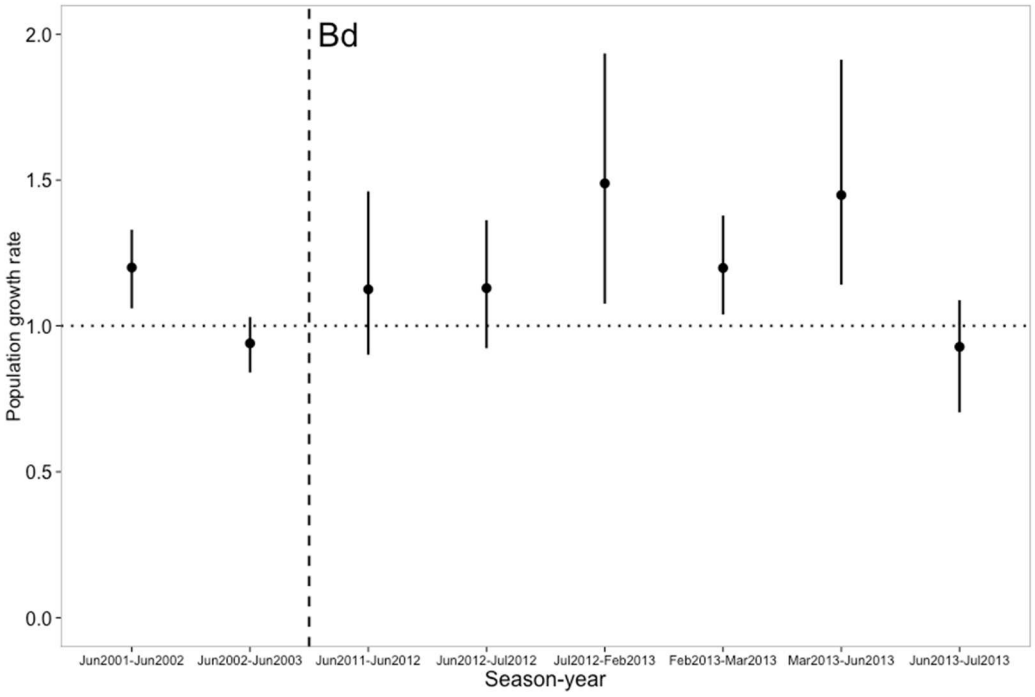

Figure 3.4 Population growth rate before and after the 2004 *Bd* outbreak, identified by the vertical dashed line. Overlap with one, indicated by the horizontal dashed line, suggests consistent population size between sampling occasions, values lower than one indicate declining populations, and values greater than one suggest increasing population size. Pre-*Bd* estimates come from McCaffery and Lips (2013).

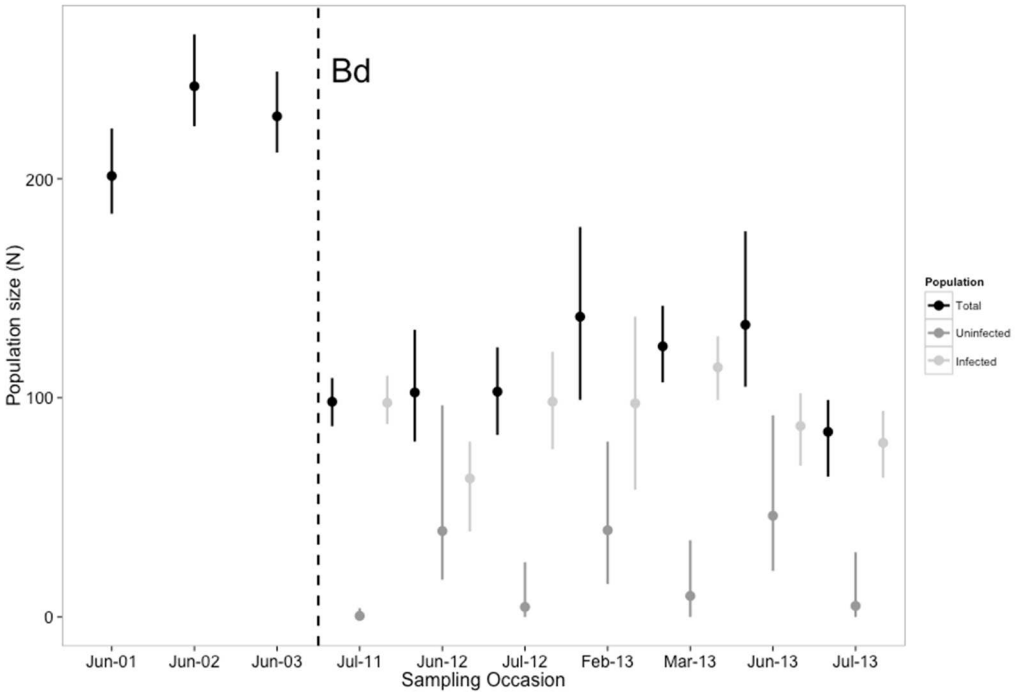

Figure 3.5 Male *E. prosoblepon* population size before (2001-2003; McCaffery and Lips 2013) and after (2011 to 2013) *Bd* arrival in 2004. *Bd* arrival is marked by the vertical dashed line, and total, uninfected, and infected disease states are indicated by colors. Pre-*Bd* estimates come from McCaffery and Lips (2013).

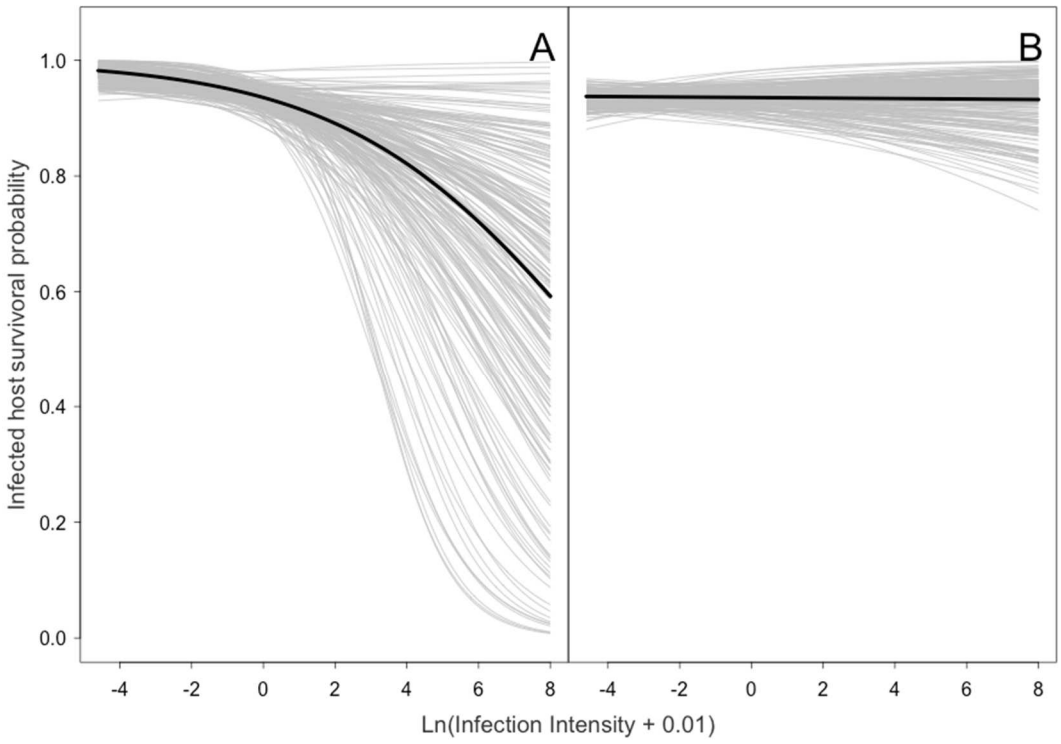

Figure 3.6 Monthly apparent survival probability of infected hosts as it relates to host infection intensity during the (A) dry season and (B) wet season.

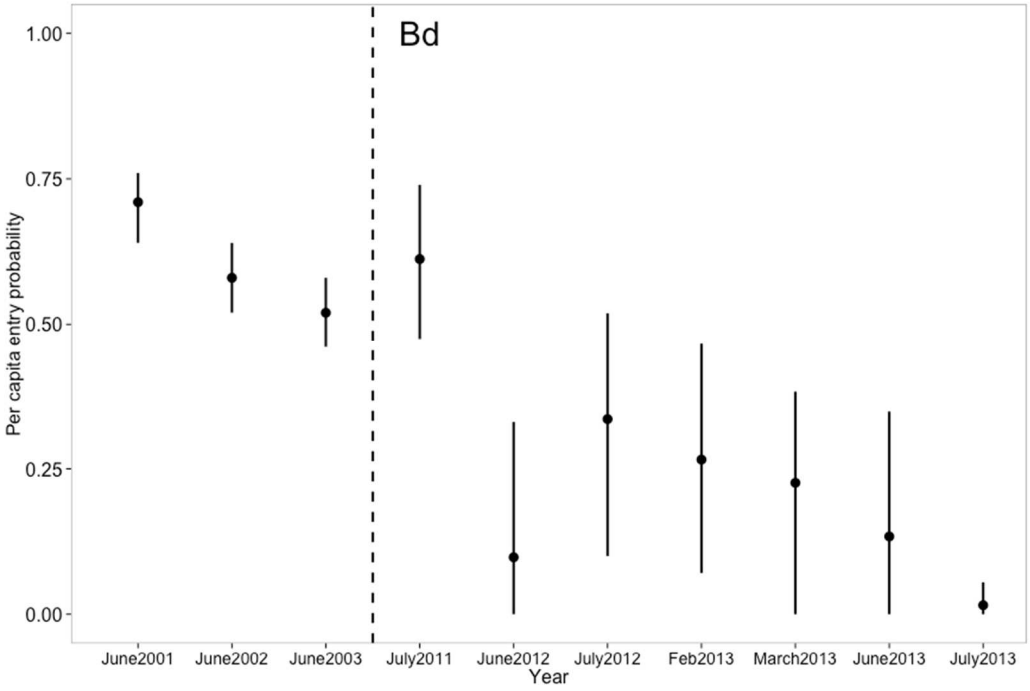

Figure 3.7 The fraction of new individuals entering the population, per capita entry probability, before and after the *Bd* outbreak in 2004, represented by the vertical dashed line. The fraction of individuals entering the population, via immigration and reproduction, across all post-outbreak years is approximately half the rate it was before the *Bd* outbreak. Pre-*Bd* estimates come from McCaffery and Lips (2013).

Table 3.1 Parameter definitions and symbols.

Parameter	Symbol	Definition
Apparent survival	$\Phi_{i,t}$	Probability that an individual in state *i* survives from time *t-1* to time *t*
Capture	$p_{i,t}$	Probability that an individual in state *i* at time *t* is detected
Infection	c	Probability that an uninfected individual time *t-1* will become infected time *t*
Recovery	r	Probability that an infected individual time *t-1* will become uninfected time *t*
Misclassification	$e_{j,t}$	Probability that the *j*th "uninfected" individual at time *t* is incorrectly classified as uninfected
Per-capita entry probability	f_t	The fraction of new individuals at *t* per individual alive at *t*

Table 3.2 Capture effort and infection intensity summary of individuals captured and marked. Few individuals were partially observed, and a majority of individuals were captured not infected. Mean infection[1] and mean infection[2] provide estimates of average host infection intensity without and with including hosts of zero infections, respectively.

	2010	2011	2012		2013			2014		
	Jul	Jul	Jun	Jul	Feb	Mar	Jun	Jul	Mar	Totals
Uninfected	10	33	52	23	23	38	60	46	35	320
Infected	6	11	26	4	16	2	13	14	3	95
Unknown	1	0	2	0	0	4	1	2	1	11
Total No. of individuals	17	44	80	27	39	44	74	62	39	426
Min infection	0.94	0.13	0.20	0.42	0.21	0.23	0.22	0.29	0.22	0.13
Max infection	1988.23	24.37	612.18	8.05	51.89	0.23	40.06	4.41	1.59	1988.23
Mean infection[1]	595.92	5.30	56.12	4.24	5.17	0.42	1.54	0.92	4.52	53.61
Mean infection[2]	17.70	0.28	7.88	0.08	0.40	0.01	0.27	0.06	0.01	2.96

Table 3.3. Capture probability estimates of infected and uninfected hosts during the dry and wet seasons.

Disease status	Season	Mean	95% Credible interval	
Uninfected	Dry	0.24	0.01	0.80
	Wet	0.03	0.01	0.15
Infected	Dry	0.38	0.28	0.48
	Wet	0.62	0.52	0.73

Chapter IV: Modeling post-outbreak disease dynamics in a Neotropical amphibian community.

Coauthors: Elise Zipkin, J. Andrew Royle, Ana V. Longo, Evan H. Campbell Grant, Kelly R. Zamudio, & Karen R. Lips

Abstract

As fungal pathogen outbreaks become more frequent worldwide across taxa, the number of host communities that must cope with pathogen persistence also increases. This rapid shift from outbreak to post-outbreak disease states of host communities has shifted the focus of phenomena from: "what leads to host extinction during a fungal outbreak?" to "how are hosts persisting once the pathogen becomes established?." In the case of chytridiomycosis, the disease caused by the amphibian-killing fungus *Batrachochytrim dendrobatidis* (*Bd*), invasions into naïve populations caused amphibian mass mortality, population declines, and species extirpations, but after the epidemic, the remaining hosts persist at a new stable state with no obvious signs of abundance declines. This pattern can be explained by at least one of three processes: (1) increased host mortality is compensated by increased arrival rates, (2) hosts cope with infections via tolerance and/or resistance and thereby increase their survivorship, or (3) *Bd* transmission risk– the probability a susceptible host becomes infected– varies locally, creating hot- and cold-spots of pathogen transmission and host refugia. To determine which of these processes is contributing to amphibian persistence 10 years after a chytridiomycosis outbreak, I quantified amphibian survival, arrival rates, abundance, change in abundance, and infection processes. I conducted 195 surveys and made 1,700 amphibian captures over a two-year field study along streams and

traits during the wet and dry seasons. Because of sparse data and difficulty in recapturing hosts, I developed a novel multi-state disease-structured Dail-Madsen model to quantify disease dynamics in a multi-species amphibian community of unmarked individuals. I found high *Bd* prevalence, low infection intensities, and high survivorship of uninfected and infected hosts. Contrary to expectations, *Bd* transmission risk did not relate to host density, pathogen prevalence, or infection intensity. I conclude that *Bd* transmission risk is constant across the study site and that infected hosts do not suffer from high rates of pathogen-induced mortality, indicating that hosts cannot avoid *Bd* infection but they need to cope with infections to persist, challenging any future reintroductions of susceptible species.

Introduction

During a multi-host fungal pathogen outbreak, rapid species extinctions and population declines lead to depauperate host communities, where a subset of species remain at lower densities as the pathogen establishes endemically (e.g., Lips et al. 2006). As the numbers of multi-host fungal pathogen outbreaks become more frequent worldwide− such as white-nose syndrome outbreaks, snake fungal disease epidemics, and chytridiomycosis (Fisher et al. 2012)− so have the number of host communities persisting with the pathogen post-outbreak. This particular phenomenon raises the question of how hosts persist alongside a highly virulent fungal pathogen (e.g., Fisher et al. 2012), which would aid in conservation efforts to preserve the hosts remaining in these communities and provide baseline information for communities where species reintroductions are planned.

After a severe disease outbreak, hosts may persist with the pathogen through at least one of three possible processes. First, the number of arriving hosts, via immigration or reproduction can counterbalance high pathogen-induced mortality of infected host. Under this scenario, I expect to see that the number of individuals arriving compensates for the number of individuals lost due to infection, such that there are no changes in host abundance (e.g., Lampo et al. 2011, Maslo et al. 2015). This type of compensation is similar to either source-sink dynamics or the 'rescue effect', where site colonization prevents host extinction. Alternatively, if the host is either resistant or tolerant to the pathogen (Roy and Kirchner 2000), then the health of the infected host is no longer significantly affected by infection (e.g., Gonzalez et al. 2013, Vander Wal et al. 2013). This would be reflected as similar survivorship between infected and uninfected hosts. And lastly, if pathogen transmission risk− the probability that a susceptible becomes infected− varies locally, then hot- and cold-spots of pathogen infections and host refugia can act as primary breeding sites (i.e., pathogen growth on infected hosts or host reproduction) to promote both pathogen and host persistence in spatially separate locations.

In the case of the amphibian-killing fungal pathogen, *Bactrachochytrium dendrobatidis* (*Bd*), before invasion, tropical amphibian communities are characterized by high abundance and diversity (Crawford et al. 2010), and when *Bd* arrives, we repeatedly observe a rapid rise in pathogen prevalence among hosts and high host infection intensity >1,000 ZGE (Longo et al. *in prep*, Tunstall et al. *in prep*). At high *Bd* infection intensities, host mortality increases (e.g., Savage and Zamudio 2011, Heard et al. 2015, Grogan et al. 2016), and within several months,

these amphibian communities are left with a subset of species at lower densities as the pathogen establishes (Smith et al. 2009, Crawford et al. 2010, Angeli et al. 2014). To identify how hosts are coping with infection and offsetting possible pathogen-induced abundance declines, ideally, we would mark hosts and track their survival and infection status over time for several species to obtain estimates of survival, arrival, and abundance, while correcting for imperfect host detection– the probability of detecting an individual given it is present (e.g., capture-mark-recapture analysis). However, most of the remaining communities post-outbreak are characterized by a few remaining species at such low abundances that require extensive investment of time to capture, mark, and recapture enough individuals to generate reliable estimates. This makes it increasingly difficult to obtain survival, arrival, and abundance estimates.

This clash between ecological difficulty in tracking individuals (i.e., low counts and lots of zeros) and statistical challenges (i.e., inability to estimate parameters) was partially reconciled by Royle (2004) when he showed that it was possible to estimate population size from temporally repeated counts of organisms and to account for imperfect detection without having to uniquely identify individuals, commonly referred to as the *N*-mixture model. The key idea was to view site-specific population sizes as independent random variables scattered according to a probability distribution (e.g., Poisson) and that populations at each sampling location are closed with respect to migration, births, and deaths throughout the study. In 2011, Dail and Madsen further generalized the *N*-mixture model to estimate open population abundances, while accounting for imperfect detection. They did this by

assuming that the abundance for any site depends only on the abundance the previous time step and that the difference between abundances across time is the sum of two processes: survival and arrivals. Although these estimates do not technically estimate parameter rates the same way of capture-mark-recapture models, both modeling approaches estimate related quantities. Zipkin et al. (2014) further proposed that this class of model could also accommodate populations structured by age, size, sex, or disease, representing a valuable advance in the estimation of population dynamics for multistate data from unmarked individuals.

To determine which of the three processes listed above are contributing to the persistence of the few remaining sparse amphibians following a chytridiomycosis outbreak in El Copé, Panama, I created a multi-state disease-structured Dail-Madsen model for unmarked individuals that corrects for imperfect host and pathogen detection probability to estimate: disease state-specific survivorship, arrival rates, detection probability, recovery and infection probabilities, community abundance, and the change in abundance across years. I conducted 195 surveys and made 1,700 amphibian captures over a two-year field study along streams and trails during the wet and dry seasons. I hypothesized that amphibian persistence was driven by local variation in transmission risk, rather than higher arrival rates or host resistance/tolerance. I predicted that areas with higher host density would have higher rates of *Bd* infection because as host density increases, the number of host contacts increases and may drive the rise in *Bd* infections. Spatial variation in host density would create host refugia and *Bd* infection hot- and cold-spots, allowing for host and pathogen persistence. Our study provides a new way of understanding population and

disease dynamics of rare species in species-rich communities, which are typically underrepresented and difficult to study, that help conservation agencies target recovery efforts intended to buffer or stop species declines.

Methods

Study site.— I sampled four-200 m stream and three-400 m trail transects in Parque Nacional G. D. Omar Torríjos Herrera, Coclé Province, El Copé, Panama (8° 40' N, 80° 37' 17'' W, Lips et al. 2003). The park spans elevations from 500 – 1000 m and is located on the continental divide.

This site experiences both a dry (December to April) and wet (May to November) season. I recorded daily minimum/ maximum temperatures and rainfall using a min/max thermometer and rain gauge along the continental divide, and I recorded hourly temperatures every 60 to 80 meters along each transects using ibuttons®.

The total seasonal rainfall during the wet seasons in 2012 and 2013 was 259.98 cm and 245.92 cm, respectively, while the 2013 and 2014 dry seasons experienced 120.21 cm and 121.46 cm (Table A4.1; Figure A4.1). The average daily minimum/maximum temperatures during the 2012 and 2013 wet seasons were 19.75°C /26.27°C and 19.70°C /28.56°C, respectively, while the 2013 and 2014 dry seasons were 19.57°C /23.98°C and 18.57°C /25.14°C (Figure A4.1). Temperatures along stream and trail transects were similar within a season, and mean maximum daily temperature was higher during the wet season than the dry season (Figure A4.2 and A4.3).

Field surveys.— I surveyed all amphibians along seven pre-established 200 or 400 m transects (Lips et al. 2006), and I divided the transects in 20 m adjacent sections called "sites" for a total of 40 riparian and 59 terrestrial sites. I assumed that no births, deaths, immigration, or emigration occurred within each site within seasons but that these factors could change between seasons (MacKenzie and Royle 2005).

Field teams of two to three people conducted visual encounter surveys by slowly walking each transect and using visual and audio cues to locate all amphibians within 2 m of the stream bank or trail. I used a fresh pair of latex powder-free gloves when handling each individual. To estimate *Bd* infection status, upon capture, I swabbed all individuals following the swabbing technique described by Hyatt et al. (2007) using a sterile cotton tipped swab, and I stored the swabs in capped tubes with 30 μL of 70% ethanol. All individuals were released at the original point of capture.

I surveyed each transect six to eight times (1900 hrs to 0100 hrs) over two wet and two dry seasons, which constitute our primary sampling periods. Within each primary sampling period, I aggregated surveys into two secondary sampling periods of 3−4 consecutive nights each. To determine if the site-closure assumption was violated between the secondary periods within each primary period, I calculated site-specific differences in the number of captured infected and uninfected hosts between the first and second set of secondary surveys. I found no differences in the number of captures for either infected or uninfected hosts (Figure A4.4 & Figure A4.5), indicating that the closure assumption was reasonable based on the patterns in our observed capture data.

Molecular Analysis.— I tested all skin swabs collected for the presence of *Bd* using PrepMan Ultra® to extract DNA. I tested swabs for *Bd* in singlicate using Taqman qPCR (Boyle et al. 2004, Hyatt et al. 2007) running 50 cycles. I ran each plate with the Panamanian *Bd* isolate (JEL 423) standards of 0.1, 1, 10, 100, and 1000 *Bd* zoospore genomic equivalents (ZGE) to determine *Bd* presence and infection intensity. I included negative and positive controls in each qPCR plate to ensure that false-positives were negligible. I categorized individuals as *Bd*-positive if amplification occurred before cycle 50 (Briggs et al. 2010). I considered low-level zoospore detections on the skin surface (ZGE 0.001−1) as *Bd*+. I refer to ZGE as infection intensity hereafter.

Multi-state disease-structured Dail-Madsen model.— I developed a multi-state disease-structured model to estimate survivorship, arrival rates, abundance, changes in abundance, transmission risk and recovery, and individual detection probability of uninfected and infected hosts (Table 4.1).

Over 75% of amphibians captures were from four species of two families: *Espadarana prosoblepon* and *Sachatamia albomaculata* of Family Centrolenidae, and *Pristimantis cruentus* and *Pristimantis cerasinus* of Family Craugastoridae. I collected less than 15 samples for over 65% of species (24 of 37 species; Table 4.1). I provide a summary of species-specific estimates of pathogen prevalence and mean zoospore load across the entire two-year study (Table 4.1). Because most of these species share habitats and likely transmit *Bd* infections, I pooled all species data into the model. This modeling approach assumes that all species have a similar response

to *Bd* infection and transmission risks. By doing so, I lose inference on species-specific responses and contributions to disease dynamics, such as pathogen amplification (e.g., DiRenzo et al. 2014) or dilution (e.g., Searle et al. 2011), but this approach better evaluates how the persisting amphibian community copes with infection.

I extended the open *N*-mixture model (Dail and Madsen 2011) to incorporate disease state-structured dynamics following Zipkin et al. (2014). Our interest lies in modeling $N_{i,j,t}$, the true abundance of each host by disease state i (1 = uninfected, 2 = not infected) at site j during each season t. I assume that changes in abundance occur monthly through births, deaths, immigration, and emigration.

I model initial abundance for uninfected ($i = 1$) and infected ($i = 2$) states during the first season ($t = 1$) using a positive discrete distribution:

$$N_{i,j,1} \sim Pois(\lambda_i),$$

such that the expected abundance λ_i was the same across all j sites but differed by disease state. Although parameter estimates in the model likely vary between stream and trails, the low number of individuals detected during sampling did not allow for habitat-specific covariates in the model to be identifiable. I provide raw estimates of differences between habitats and seasons (Table 4.2).

I modeled subsequent seasons ($t \geq 2$) by considering the number of individuals that are gained (G_i) at each site j, the number of individuals that survived (S_i) in each disease state i, and the number of individuals that transition between disease states (T_i). I thus assume that the local abundance at site j follows a Markovian process where local abundance at season t and site i is only dependent upon the abundance at

all sites during the previous season. The number of uninfected and infected individuals that are gained at each site in each season, $t \geq 2$, was specified as:

$$G_{i,j,t} \sim Pois(\gamma_{i,t})$$

where γ_i is the expected number of uninfected ($i = 1$) and infected ($i = 2$) individuals that arrive between seasons $t-1$ and t. Note that our model cannot distinguish between immigration and reproduction, or between emigration and death.

To estimate the number of individuals that survive and transition disease states monthly, I developed a transition matrix, Ψ, where the rows represent the current state (uninfected, infected, and dead) and the columns represent the state at the following time step:

$$\Psi = \begin{bmatrix} \Phi_1^{M_{j,t}}(1 - c_j^{M_{j,t}}) & \Phi_1^{M_{j,t}} c_j^{M_{j,t}} & 1 - \Phi_1^{M_{j,t}} \\ \Phi_2^{M_{j,t}} r_j^{M_{j,t}} & \Phi_2^{M_{j,t}}(1 - r_j^{M_{j,t}}) & 1 - \Phi_2^{M_{j,t}} \\ 0 & 0 & 1 \end{bmatrix}.$$

The parameter Φ_i is the monthly survival probability for uninfected ($i = 1$) and infected ($i = 2$) individuals with expected state-specific survival from season $t-1$ to t the cumulative survival for all month during that time period ($M_{j,t}$). The number of months between seasons varied, with 7, 3−4, and 7−8 months between the end of sampling in season $t = 1, 2, 3$ and the start of sampling in season $t+1$. I accounted for the difference in time between seasons, here and in all subsequent state transitions, by assuming that all transitions were constant and equal across each time period by including the variable $M_{j,t}$ as the number of months between seasons $t-1$ and t at site j. The parameters c_j and r_j are the transmission risk and recovery probabilities, respectively, at each site j. With this specification, individuals experience the survival probability associated with their disease state from season $t-1$ to t, and conditional on

their survival, individuals can become infected (if they were uninfected at $t-1$) or recover (if they were infected at time t) with probabilities c and r. Thus, the number of individuals that survive (S_i) within each disease state i:

$$S_{i,j,t} \sim Bin\left(N_{i,j,t-1}\Psi_{i,i}\right)$$

and the number of individuals that transition between disease state i to ii ($T_{i(ii),j,t}$) follow:

$$T_{i(ii),j,t} \sim Bin\left(N_{i,j,t-1}\Psi_{i,ii}\right)$$

where the notation $i(ii)$ represents a transition from state i to ii (e.g., state 1 to 2 or state 2 to 1, where 1 = uninfected and 2 = infected). Finally, I assumed that the number of individuals gained within each disease state i, site j, and season t (G_i) is described by a Poisson process, where:

$$G_{i,j,t} \sim Poisson\left(\gamma_{i,t}\right).$$

with $\gamma_{i,t}$are the state-specific arrival rates each season t.

To test our hypotheses related to transmission risk, I modeled infection probability in relation to: host density ($N_{j,t}$), infection intensity ($I_{j,t}$), pathogen prevalence ($Prev_{j,t}$), and site-specific variation (β_j). Each covariate ($cov_{j,t}$) was run in a separate model, such that:

$$logit(c_j) = \alpha 1 + \beta 1 cov_{j,t}.$$

I derived host density and pathogen prevalence from the model as: $N_{j,t} = N_{1,j,t} + N_{2,j,t}$ and $Prev_{j,t} = \frac{N_{2,j,t}}{N_{j,t}}$, respectively. I specified site-specific variation in infection probability as a random effect: $\beta_j \sim normal(0, \sigma^2)$. I calculated infection intensity ($I_{j,t}$) as the sum of the infection intensities of all infected hosts captured at site j

during replicate survey *k* in season *t*, and then, averaging the total number of zoospores across replicate surveys 1:*k*. Here, I assume that the sum of all host infection intensities correlates to the total amount of shed free-living *Bd* because host infection intensity correlates strongly to *Bd* shedding rates (Reeder et al. 2012, DiRenzo et al. 2014).

The state-specific total abundances for individuals in disease state *i* at a given site *j* each season *t* is then determined by:

$$N_{i,j,t} = G_{i,j,t} + S_{i,j,t} - T_{i(ii),j,t} + T_{ii(i),j,t}$$

where the average abundance at a site *j* is the sum of arrival, survival, transition to the disease state, and the loss of individuals transitioning to the other disease state. I assume that the transition between disease states occurs monthly with a fixed probability.

Imperfect host and pathogen detection.—I consider the observation process consisting of two parts− imperfect detection of the host and of the pathogen. First, I model the state-specific detection probability at each site *j* during replicate survey *k* and season *t* as:

$$y_{i,j,k,t} \sim Bin(N_{i,j,t} p_{i,j,t}),$$

where $y_{i,j,k,t}$ is the apparent number of individuals in each state after correcting for misclassified hosts, and $p_{i,j,t}$ is the state-specific detection probability. I included the number of observers ($Obs_{j,t}$) as a covariate of the state-specific detection probability using the logit transformation and specifying:

$$logit(p_{i,j,t}) = \alpha 2_i + \beta 2 Obs_{j,t}$$

Next, I accounted for pathogen detection probability, specifically incorrectly classifying infected hosts as uninfected caused by qPCR error. I modeled the observed number of infected individuals ($m_{2,j,k,t}$)as:

$$m_{2,j,k,t} \sim Bin(y_{2,j,k,t}\tau_{j,k,t})$$

where $y_{2,j,k,t}$ is the apparent number of infected individuals at site *j* survey replicate *k* and season *t*, and $\tau_{H,t}$is the probability of correctly assigning disease state as a function of infection intensity:

$$logit(\tau_{j,k,t}) = \alpha 3 + \beta 3ZGE_{j,k,t}$$

I estimated $\tau_{j,k,t}$ by averaging the ln(infection intensity + 0.01) of all individuals at site *j* replicate *k* and season *t*, and using informative priors, where $\alpha 3 \sim dunif(0.25, 1.32)$ and $\beta 3 \sim dunif(0.14, 0.51)$, following Miller et al. (2012).

The observed number of uninfected individuals is then the sum of the number of misclassified individuals and the true observed uninfected individuals:

$$m_{1,j,k,t} = (y_{2,j,k,t} - m_{2,j,k,t}) + y_{1,j,k,t}.$$

I did not include hosts with partially observed state detections (i.e., found alive, but disease state unknown; Conn and Cooch 2009, Zipkin et al. 2015) because I could not identify the two latent partially observed variables in the model.

Parameter comparisons.—To determine significant differences between parameter estimates of infected and uninfected hosts, I compared the posterior distributions for the parameters of interest (Ruiz-Gutierrez et al. 2010). I investigated whether the parameter values were equal by computing the proportion of iterations in the posterior distribution in which one parameter is greater than the other. Extreme proportions

(i.e., ≥ 0.95) suggest little overlap in posterior distributions, and I interpreted it as a 95% probability that the first parameter is significantly higher than the second. I also considered regression coefficients meaningful if the 95% credible interval did not overlap with zero on the logit scale.

To estimate the change in community abundance, I used the equation: $\lambda_t = \frac{N_{t+1}}{N_t}$, where $\lambda_t > 1$ suggests abundance growth, $\lambda_t < 1$ indicates abundance declines, and $\lambda_t = 1$ suggests abundance stability (Kéry and Schaub 2012). I estimated the change in community and disease state abundance between each season.

Model fit.— I fit my model using Bayesian methods and estimated the posterior distributions for all parameters using Markov chain Monte Carlo (MCMC) methods implemented in JAGS 4.0.0 in the R environment (R Core Team 2015) using the "jagsUI" package (Kellner, 2015). For most parameters, I used vaguely informative normal priors (normal(0, 0.368)). I ran three chains for each parameter, and ran each chain for 50,000 iterations, with a burn-in period of 10,000 iterations, and thinned by 50. I evaluated convergence of chains by visual inspecting trace plots, and using the diagnostics of Gelman, where Rhat < 1.1 (Brooks & Gelman 1998). I also assessed model fits using posterior predictive checks (Gelman et al. 2004), where a value close to 0.5 indicates adequate model fit and extreme values close to either 0 or 1 indicate poor model fit.

Results

Field summary.— I made 1,700 amphibian captures, of which 1,129 were uninfected, 366 were infected, and 205 were unknown (Table 4.2). Each season, the total number of infected hosts captured ranged between 43−160 (17−28% of captures), while the number of uninfected host captures were between 191−410 (71−82% of captures). Between zero and seven hosts were caught during a single survey at each 20 m site (Table 4.3). Iconducted a total of 45 to 53 surveys per season, with six to eight surveys per 20 m site.

I captured 37 species, of which 26 species were found in both streams and trails, while the other 11 were only found in one habitat. I caught 23−24 species in the wet seasons and 25−28 species in the dry seasons, of which 32 species were caught in both wet and dry seasons and 5 were only found in one season (Table 4.3; Figure A4.6).

Infection intensities were uniformly low across species. Average species-level infection intensities were less than 100 ZGE for 89% of species (Table 4.1), and 98% of individuals had infection intensities less than 100 ZGE (Table 4.2). At the site level, average host infection intensity ranged between 82 to 202 ZGE, and pathogen prevalence ranged between 62 to 69%, when uncorrected for imperfect pathogen detection (Table 4.3).

Multi-state disease-structured Dail-Madsen model.— My model fit the data well (Figure A4.7 & A4.8). Apparent monthly survival probability of infected hosts was greater than the apparent monthly survival probability of uninfected hosts (Table 4.4;

Pr(infected > uninfected) = 0.97), likely because most infected individuals captured had infections < 100 ZGE that do not substantially impact host survivorship (e.g., Savage and Zamudio 2011, Heard et al. 2015, Grogan et al. 2016).

The amphibian site arrival rates (number of frogs season^{-1}) did not differ between the infected and uninfected classes during either of the dry to wet season transition (Table 4.4; Pr(infected > uninfected) = 0.48), but site arrival rates were higher for the infected class than the uninfected class from the dry to wet transition (Pr(infected > uninfected) = 0.96).

Amphibian abundance was higher during the wet season than in the dry season (Figure 4.1). From the wet to dry season transition, amphibian abundance fell by approximately 100 individuals, suggesting abundance declines between seasons ($\lambda < 1$), whereas community abundance gained those individuals back from the dry to wet season (Figure 4.1 & 4.2). Annually, however, amphibian abundance was similar between wet 2012 and wet 2013 ($\lambda = 1.03$; 95% Credible interval: 0.82−1.24) and between dry 2013 and dry 2014 ($\lambda = 1.05$; 95% Credible interval: 0.87−1.22). After correcting for imperfect pathogen detection, pathogen prevalence was consistently between 50 − 90% among sites (Figure 4.3).

Host density, pathogen prevalence, and infection intensity did not predict *Bd* infection probability (Supplement 4.1), although these factors varied among sites (Figure A4.9). I found little variation in average monthly *Bd* transmission risk among sites, where it was consistently between 16 − 17% when site was included as a random effect in the model (Figure 4.4; Table A4.1). Average monthly transmission

risk and recovery probabilities did not differ (Table 4.1; Pr(infection > recovery) = 0.51).

I found that individual detection probability of uninfected hosts differed between seasons (Pr(wet > dry) = 0.96; Table 4.1), but not for infected hosts (Pr(wet > dry) = 0.63; Table 4.4). I also found that individual detection probability did not differ between infected and uninfected hosts during either the wet or dry seasons (Pr(wet infected > wet uninfected) = 0.72; Pr(dry infected > dry uninfected) = 0.94). For each every additional person searching on a survey, the odds of detecting an amphibian increased by 1.47 (95% Credible interval: 1.17 − 1.85).

Discussion

Within 10 years after a chytridiomycosis outbreak in El Copé, Panama, less than half of the original amphibian species are persisting at low abundances and suffering little to no negative direct impacts on survivorship (Crawford et al. 2010). Among adults, *Bd* prevalence was high, but average infection intensity tended to be low. Amphibian abundance did not change annually, and given that host monthly survivorship was high and arrival rates reflected seasonal fluctuations, regardless of host infection status, it seems unlikely that *Bd* is causing significant declines in abundance or that infected host mortality is compensated by higher arrival rates, implying that the persistence of amphibians alongside the fungal pathogen *Bd* may be due to the hosts ability to cope with pathogen infection.

The low pathogen-induced mortality rates are typical of low-level infections, and these are the norm for most species and individuals across habitats and seasons. I propose that these hosts are able to limit the build of disease through resistance or

they are able to compensate for disease-induced damage through tolerance (Roy and Kirchner 2000). During the outbreak, host infection intensities were orders of magnitude higher than those reported here, reaching over 100,000 ZGE for some species (Longo et al. *in prep*, Tunstall et al. *in prep*). The rapid rise and spread of *Bd* throughout this amphibian community could have been the results of naivety to the pathogen, high species diversity, and/or high host density. Today, however, ten years after the outbreak, species diversity is less than half of the original 74 species community (Crawford et al. 2010) and abundance is much lower, making it likely that *Bd* infection of susceptible hosts does not occur as rapidly or repeatedly as it use to. Because infection intensity is low, pathogen prevalence is high among hosts, and monthly recovery probability is less than 50%, this indicates that hosts are able to tolerate low-level infections and prevent the amplification of their infections.

The high host survival estimates for each disease class, the high pathogen prevalence, and low-level infection intensities I report are similar to the estimates for the amphibians remaining in the Sierra Nevada of California post-*Bd* outbreaks (Briggs et al. 2010). In the California system, a single species, *Rana muscosa*, dominates the landscape where isolated lakes may create literal zoospore pools where amphibians bathe. In contrast, the El Copé system has > 35 species that occupy primarily leaf litter and vegetation in forest and riparian habitats where temperatures in most habitats are ideal for *Bd* growth year-round (i.e., 17°−24°C; Piotrowski et al. 2004). In both cases, amphibians occupy habitats that may promote abiotic persistence of *Bd* in an environmental reservoir.

Bd transmission risk did not relate to host density or pathogen prevalence, indicating that transmission risk may not entirely operate by direct host-to-host contacts. For most infectious diseases, host-to-host contacts are the primary mechanism that drives transmission risk (McCallum et al. 2001), but in the *Bd* system, environmental *Bd* reservoirs, where the pathogen can persist outside of the host, may be regulating *Bd* transmission risk. Given the consistency in *Bd* transmission risk among sites, the *Bd* environmental reservoir may by uniformly distributed across the study area because the cloud forest is consistently cool and moist year-round, offering optimal *Bd* growth (e.g., Piotrowski et al. 2004). Previous evidence confirms that *Bd* can occur outside the host (e.g., Johnson and Speare 2003, 2005, Mitchell et al. 2008, Chesnut et al. 2015), but I do not know how long or if *Bd* can reproduce outside the host. From our analysis, if *Bd* only persisted outside of the host for short periods of time, then *Bd* transmission risk should have correlated to infection intensity, a quantity directly proportional to *Bd* shedding rates (e.g., Reeder et al. 2012, DiRenzo et al. 2014), but I did not find support for this hypothesis. I also did not find support for the hypothesis that *Bd* transmission risk is correlated with host density or pathogen prevalence, which leads us to conclude that the idea of an environmental *Bd* reservoir may persist for longer periods of time or *Bd* reproduces outside of the host. The next steps to understanding *Bd* environmental reservoirs and transmission risk are to collect environmental samples of *Bd*, test for zoospore viability (Maguire et al. 2016), and monitor samples overtime for evidence of zoospore reproduction.

Seasonal changes in abundance, where wet season abundance was higher than dry season abundance, may be attributed to seasonal breeding or behavior changes in some amphibian species. First, some species may be entering the site between the dry to wet season to reproduce and leave the site between the wet to dry season (Wells, 2007), which would manifest as seasonal fluctuations in amphibian abundance. Unfortunately, since individuals of many Neotropical species are difficult to track, especially over long distances, we lack information on the breeding biology of most species. Alternatively, individuals may be remaining at the site year-round, but their behavior changes seasonally, where they may be seeking refugia (e.g., Longo & Burrowes 2010). By doing so, the detection portion of the model must consider host availability: i.e., the proportion of time the individual is active and available to be detected (e.g., Diefenbach et al. 2007). However, because I found almost all species in both wet and dry seasons, I hypothesize that individuals are remaining at the site and are not available for detection during the dry season. *A priori* I did not consider host availability and did not collect appropriate data, which would have consisted of monitoring individuals and recording the proportion of time they are active, i.e., available to be detected.

Modeling limitations

Our original approach to understanding host persistence following the pathogen outbreak was to collect capture-mark-recapture data of eight focal species to estimate species-specific estimates of survival, arrival, and abundance for each disease class. Because two years of intensive surveys yielded low recapture rates, I

was unable to pursue this analysis. Therefore, the modeling approach taken here represents a valuable advance towards estimating disease dynamics from unmarked individuals when data are sparse and hosts are difficult to detect (e.g., Dail and Madsen 2011, Zipkin et al. 2014). Ideally, I would have used a multi-species multi-state disease-structured open population model, allowing estimates for species-specific survival, arrival, and abundance for each disease class. Again, the sparse data prevented modeling species separately to identify species-specific effects, such as pathogen amplification, dilution, or transmission risk. For communities that have experienced mass mortality where few hosts remain and capture-mark-recapture is impractical and costly, the ability to extract parameter estimates for survival, arrival, and abundance from unmarked individuals provides the opportunity to study these difficult to monitor persisting hosts.

Conclusions

Similar to other post-outbreak communities, such as bats affected by white-nose syndrome (Hoyt et al. 2015), the persisting host community is represented by fewer species at lower abundances. During the outbreak, high prevalence and infection intensity lead to host extinction and declines, but post-outbreak, high prevalence and low infection intensity allow the remaining hosts to persist alongside the pathogen. These consistent patterns worldwide bring up new questions on host persistence, such as: how long will the persisting hosts remain? Are the populations stable or unstable? Will future outbreaks abolish the persisting hosts? And are species community composition or host density the key to explaining the differences between

outbreak and post-outbreak disease dynamics? Here, I have taken the first steps to understanding the patterns and processes contributing to host persistence after a severe multi-host fungal pathogen outbreak. These results, data, and modeling approach are of interest to conservation biologists interested in obtaining unbiased estimates of amphibian abundance, to epidemiologists dealing with sparse datasets and difficult to detect species, and to amphibian reintroduction programs that need to evaluate the health of amphibian populations prior to species reintroductions.

Table 4.1 List of parameters in the model along with definitions and units. Note that apparent survival does not distinguish between death and emigration, and arrival rates do not separate births and immigration.

Parameter	Name	Units	Definition
S_i	Apparent survival	Monthly probability (0-1)	Apparent monthly survival probability in state *i* from time *t*-1 to *t*
$\gamma_{i,t}$	Arrival rate	Number of frogs arriving season^{-1}	Seasonal arrival rate from season *t-1* to *t*
$p_{i,j,t}$	Detection	Individual probability (0-1)	Individual detection probability during survey *j* at site *i* in season *t*
c_j	Transmission risk	Monthly probability (0-1)	Monthly probability that an individual gains infection from time *t-1* to *t* given it was not infected at *t-1*
r_j	Recovery	Monthly probability (0-1)	Monthly probability that an individual loses infection from time *t-1* to *t* given it was infected at *t-1*
$N_{i,j,t}$	Abundance	Number of frogs	Abundance of amphibians in state *i* at site *j* at time *t*
λ_t	Change in abundance	Seasonal rate of increase	Change in community abundance from season *t-1* to *t*

Table 4.2 Summary of amphibian captures with the number of samples collected, mean zoospore load, number of *Bd* positive and negative swabs, and pathogen prevalence for each species. The majority of samples were collected from four species of two families highlighted in bold.

Genus	Species	Family	No. of samples	Mean zoospore load	No. *Bd* positive	No. *Bd* negative	Pathogen prevalence
Agalychnis	*callidryas*	Hylidae	1	0.00	0	1	0.00
Bolitaglossa	*schizodactyla*	Plethodontidae	16	106.78	4	10	0.25
Centrolene	*sp.*	Centrolenidae	1	0.59	1	0	1.00
Chaunus	*marinus*	Bufonidae	6	0.00	0	5	0.00
Cochorenella	*eukenemos*	Centrolenidae	6	0.12	1	5	0.17
Craugastor	*bransfordi*	Craugastoridae	1	0.00	0	1	0.00
Craugastor	*crassidigitus*	Craugastoridae	25	5.41	3	21	0.12
Craugastor	*fitzingeri*	Craugastoridae	11	3.70	4	6	0.36
Craugastor	*mask*	Craugastoridae	1	0.00	0	1	0.00
Craugastor	*sp.*	Craugastoridae	3	0.48	1	0	0.33
Diasporus	*"orange"*	Eleutherodactylidae	55	66.28	11	33	0.20
Diasporus	*"peep"*	Eleutherodactylidae	19	14.56	3	13	0.16
Diasporus	*sp.*	Eleutherodactylidae	17	0.25	1	9	0.06
Diasporus	*"tock"*	Eleutherodactylidae	10	1.63	3	6	0.30
Espadarana	*prosoblepon*	Centrolenidae	**729**	6.64	133	537	0.18
Hyalinobatrachium	*colymbiphyllum*	Centrolenidae	31	15.14	3	24	0.10
Hyalinobatrachium	*sp.*	Centrolenidae	1	0.00	0	1	0.00

Hyalinobatrachium	*vireovittatum*	Centrolenidae	5	--	0	0	--
Hyloscurtis	*colymba*	Hylidae	4	555.75	3	0	0.75
Hyloscurtis	*palmeri*	Hylidae	13	76.87	6	6	0.46
Lithobates	*warszewitschii*	Ranidae	1	6.35	1	0	1.00
Oedipina	*sp.*	Plethodontidae	2	0.00	0	2	0.00
Pristimantis	*caryophyllaceus*	Craugastoridae	6	4.20	2	4	0.33
Pristimantis	*cerasinus*	Craugastoridae	**227**	49.56	63	145	0.28
Pristimantis	*cruentus*	Craugastoridae	**188**	176.13	51	123	0.27
Pristimantis	*educatoris*	Craugastoridae	1	0.00	0	1	0.00
Pristimantis	*museosus*	Craugastoridae	10	776.94	5	5	0.50
Pristimantis	*pardalis*	Craugastoridae	43	1.70	13	28	0.30
Pristimantis	*ridens*	Craugastoridae	9	0.49	2	5	0.22
Pristimantis	*sp.*	Craugastoridae	65	102.92	7	11	0.11
Pristimantis	*talamancae*	Craugastoridae	1	0.00	0	1	0.00
Rhaebo	*haematiticus*	Bufonidae	13	0.45	3	6	0.23
Sachatamia	*albomaculata*	Centrolenidae	**155**	89.74	39	98	0.25
Sachatamia	*ilex*	Centrolenidae	15	0.17	2	13	0.13
Silverstoneia	*sp.*	Dendrobatidae	2	0.22	1	1	0.50
Smilisca	*phaeota*	Hylidae	1	0.00	0	1	0.00
Smilisca	*silia*	Hylidae	6	0.00	0	6	0.00
	Total		1700	57.31	366	1129	0.32

Table 4.3 Summary of field samples. For each habitat and season-year, I include host density, pathogen prevalence, host infection intensity, and microclimate minimum, maximum, mean, and standard error.

	No. of host per 20 m site				Pathogen prevalence		Host infection intensity				Microclimate			
Habitat	Min	Max	Mean	SE	Mean	SE	Min	Max	Mean	SE	Min	Max	Mean	SE
Trail	0.00	6.00	1.23	0.06	0.65	0.02	0.00	8738.79	69.46	38.49	18.51	24.06	21.08	0.23
Stream	0.00	7.00	2.33	0.11	0.68	0.01	0.00	19107.08	188.48	121.19	18.64	24.15	21.14	0.27

	No. of host per 20 m site				Pathogen prevalence		Host infection intensity				Microclimate			
Season	Min	Max	Mean	SE	Mean	SE	Min	Max	Mean	SE	Min	Max	Mean	SE
Wet 2012	0.00	7.00	2.33	0.15	0.69	0.02	0.00	1733.40	82.09	26.70	19.04	23.84	21.36	0.25
Dry 2013	0.00	3.00	1.16	0.09	0.62	0.04	0.00	1839.62	26.30	19.83	18.64	22.54	20.50	0.24
Wet 2013	0.00	7.00	1.79	0.14	0.66	0.03	0.00	8738.79	158.92	92.43	19.07	24.15	21.62	0.25
Dry 2014	0.00	6.00	1.42	0.11	0.69	0.03	0.00	19107.08	202.88	193.09	19.30	22.68	21.00	0.35

Table 4.4 Summary of model output. Monthly survival, detection, recovery, and transmission risk of infected and uninfected hosts. Site arrival rates are reported as the number of frogs per season. For parameter units and definitions, see Table 1.

	Mean	Standard deviation	95% Credible interval	
Uninfected host				
Apparent survival	0.90	0.02	0.86	0.95
Arrival rate wet to dry	0.07	0.07	0.01	0.21
Arrival rate dry to wet	0.83	0.21	0.43	1.24
Detection Dry	0.07	0.02	0.03	0.12
Detection Wet	0.12	0.02	0.08	0.17
Infected host				
Apparent survival	0.95	0.01	0.92	0.97
Arrival rate wet to dry	0.08	0.09	0.01	0.28
Arrival rate dry to wet	1.53	0.35	0.87	2.22
Detection Dry	0.13	0.02	0.08	0.19
Detection Wet	0.14	0.02	0.1	0.19
Infection dynamics				
Recovery	0.16	0.12	0.01	0.43
Transmission risk	0.16	0.13	0.01	0.47
Between site variation	0.44	0.45	0.00	1.39

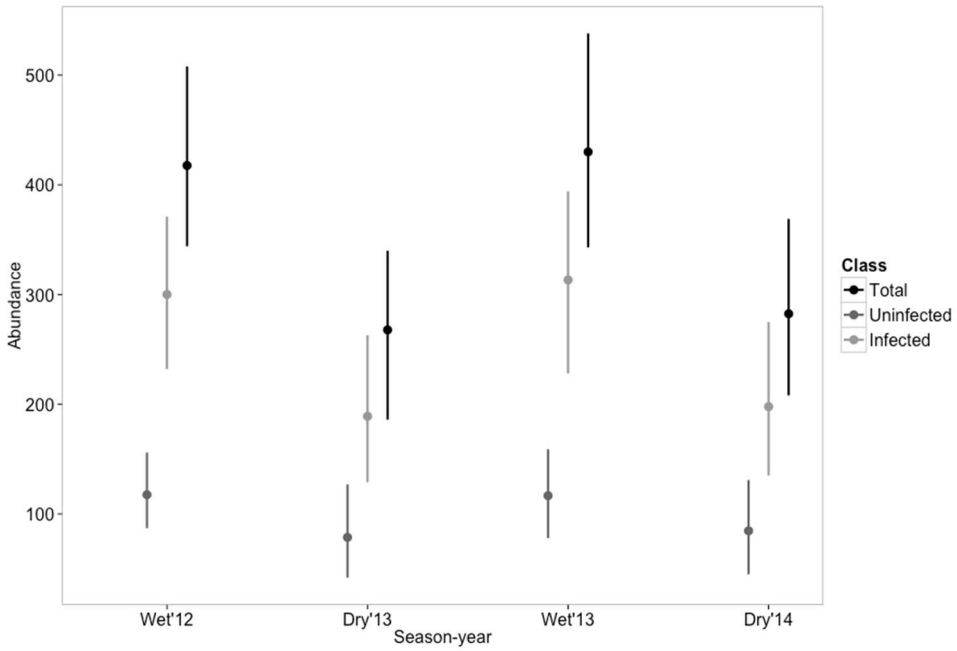

Figure 4.1 Amphibian abundance by disease class across the two-year study during each season. Abundance was lower during the dry season than the wet season, but pathogen prevalence was consistently between 50−90%, regardless of season.

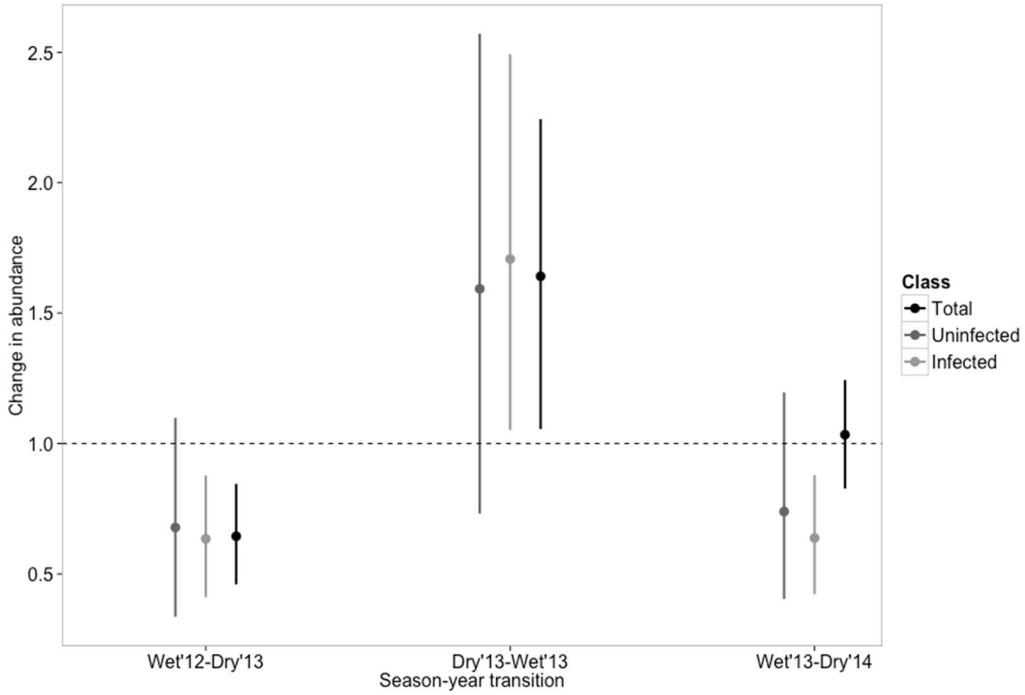

Figure 4.2 Change in abundance over the two-year study by disease class. Abundance decreased from wet to dry season transitions but showed signs of increasing from the dry to wet season transitions.

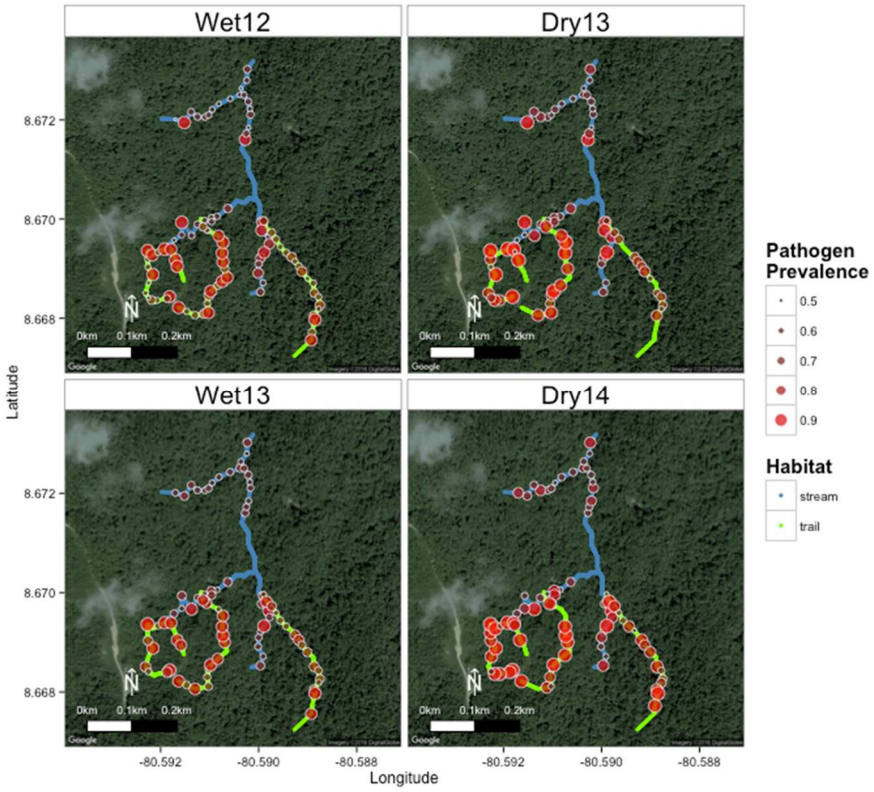

Figure 4.3 Model output of predicted pathogen prevalence each season at each site. Each point represents a 20-m site. Size and color of points indicate the average pathogen prevalence. Habitat type is color coded by blue (stream) and green (trails).

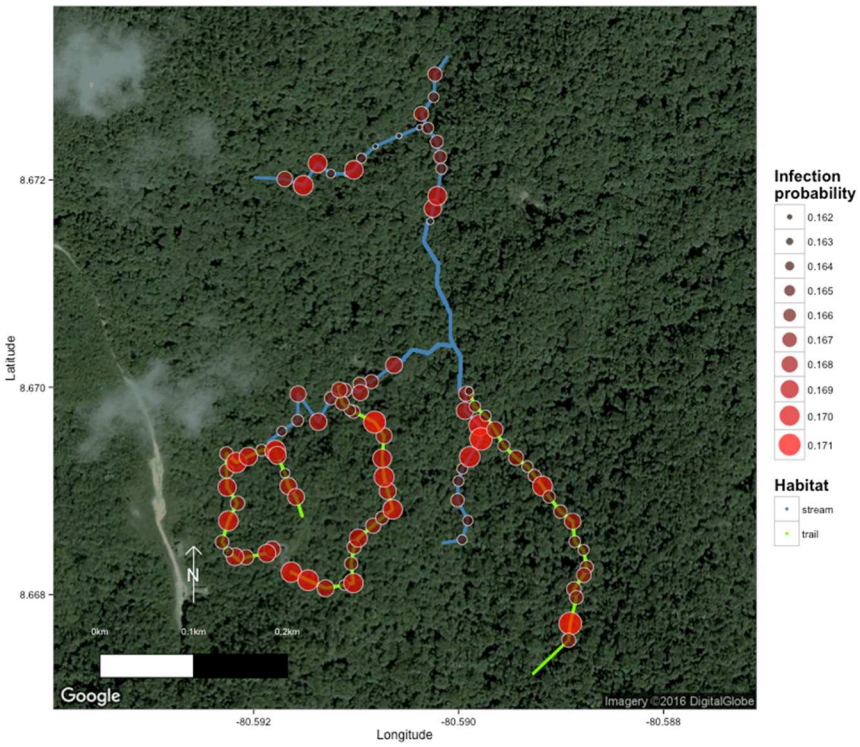

Figure 4.4 Model output of average *Bd* transmission risk among 20-m sites. Each point represents a 20-m site. Size and color of points represents the average infection probability. Habitat type is color coded by blue (stream) and green (trails).

Chapter V: SYNTHESIS

In this dissertation, I answered several unresolved questions (Chapter I) and provided new analytical tools to estimate host survival, recruitment, and abundance populations using both marked and unmarked individuals, using a Neotropical amphibian community as an example. Herein, I provide a synthesis of the chapters, expanding how they fit together and in a larger scientific context.

I. Adults and tadpole community declines

Previous studies have documented the decline of the amphibian adult community in El Copé, Panama (e.g., Lips et al. 2006, Crawford et al. 2010). Here, I document the loss of the larval stages of those species (Chapter I), showing that tadpole declines were much more rapid, severe, and long lasting than the adult declines. The decline of tadpoles was more severe because of both direct and indirect effects. Indirectly, tadpole abundance declined because of the loss of adults to disease, which would reduce larval abundance. Directly, tadpoles can also be affected by *Bd* infection, and although mortality was not observed, infection does affect feeding and likely causes sublethal effects, such as reduced body fitness. It is likely that tadpoles persist at the site at extremely low abundances because adults still persist, but this does not take away from the large discrepancy in declines between adults and tadpoles. These results also corroborate the explanation for the lack of *Espadarana prosoblepon* abundance recovery, which I hypothesize, is caused by the lack of recruits and not pathogen-induced mortality (Chapter II).

Within 10 years of the *Bd* outbreak in El Copé, Panama, it is also clear that neither adults (Chapter II & IV) nor tadpoles (Chapter I) have recovered to pre-*Bd* abundance estimates. It is unclear if a full recovery is even possible. In Chapter IV, I found that individuals in El Copé are infected at low infection intensities and that infected hosts have high survivorship, therefore it seems as though the lack of recovery is occurring somewhere in-between the egg to the adult stage. To better understand where the population size bottleneck is occurring, the next steps would be to track number of egg clutches, quantify egg clutch size, and monitor hatching and metamorphosis success. With this information, initiating reintroduction programs could help aid in population recovery.

II. How are amphibians persisting where Bd is present?

From this dissertation, we now know that amphibians in at least one site in the Neotropics can persist in the presence of *Bd* at stable abundances over time and that they do not show signs of a slow drift to extinction, which before was unclear (Chapters III & IV). Our analyses and data suggest that adult amphibians are no longer suffering high mortality rates from *Bd* infections (Chapters III & IV). Therefore, the next steps to determine how adults are surviving would be to disentangle between host adaptation via tolerance/resistance to pathogen infection and decreases in pathogen virulence.

Currently, there are efforts to quantify host adaptive immune responses (i.e., quantifying MHC expression) using amphibian samples in museums and the field before, during, and after *Bd* outbreak. This research will elucidate evolutionary

mechanisms of amphibians to *Bd* infection. Specifically, examining if MHC diversity correlates with species survival. This type of information would help predict the potential for evolutionary resistance or tolerance in other wild populations.

Alternatively, it is possible that *Bd* virulence has decreased since the outbreak, but there is mixed evidence from laboratory cultures showing both pathogen virulence attenuation and amplification over time (Langhammer et al. 2013, Voyles et al. 2014). Interestingly, Brem et al. (2013) showed that *Bd* virulence can increase when it is transmitted among frogs in the laboratory. Fortunately, during the *Bd* outbreak in El Copé, several samples of the pathogen were collected from dying amphibians and cryopreserved. Therefore, if I collect a sample of *Bd* today in El Copé, Panama from a dying individual, I could compare the virulence between the two isolates, providing insights to if *Bd* virulence has changed over time in this population.

III. Advances to statistical models

The multi-state disease-structured model presented in Chapter IV enables the estimation of survivorship, recruitment, and population size for unmarked infected and uninfected individuals, while accounting for imperfect host and pathogen detection. The data required for this modeling approach is typical of any long-term monitoring program where individual are not marked, such as data routinely collected by individual researchers of the United States Geological Survey (USGS). This analysis provides them with the opportunity to extract critical information, such as survivorship, recruitment, and population size over time, without the extra effort or

costs of intensive capture-mark-recapture studies. These new methods also allow non-profit organizations and government agencies to gather data on more species for less money with statistically robust conclusions that have the potential to increase their success rates on species conservation and biodiversity.

IV. What are other species-specific patterns of Bd infection and survival post-outbreak?

My goal here is to place the patterns I documented for *E. prosoblepon* infection and survivorship (Chapter III) in a larger context, posing the question: "what are other species-specific patterns of *Bd* infection and survival post-outbreak?" I recognize that there is not enough data or published studies to create a complete diagram on all post-outbreak species responses, but I synthesize what I know so far. I only include amphibian-*Bd* capture-mark-recapture studies that report infected and uninfected host survivorship, and infection and recovery probabilities; and, I distinguished three general host-pathogen post-outbreak patterns: where infected hosts carry seasonal, acute, or chronic *Bd* infections. Throughout, this section, I relate how the combination of species infection patterns and their survivorship may translate to species *Bd* tolerance or resistance.

First, *Bd* infections were characterized by seasonal fluctuations in *Bd* infection probability and host survivorship that may be driven by fluctuations in temperature, precipitation, host density, or breeding behavior differences between seasons. The Australian frog *Litoria rheocola* falls into this category, where it experiences seasonal *Bd* infections, with higher infection probabilities during the cooler winter months

when pathogen growth is favored (Sapford et al. 2015, Grogan et al. 2016). As infection probability peaks, host survivorship drops to its lowest. Interestingly, though, this species also has high *Bd* recovery rates, where the host clears or loses their infections rapidly, suggesting that there may be host resistance or that high temperatures help the host clear their infection. Therefore, it seems as though the combination of seasonal infection fluctuations, high *Bd* recovery, and low host density may be preventing severe pathogen outbreaks for this species in Australia.

Next, the host-pathogen post-outbreak pattern I identified was characterized by acute *Bd* infections and high host mortality, likely a result of sustained *Bd* virulence despite more than 30 years of host-pathogen co-occurrence (Murray et al. 2009). Here, infected cascade treefrogs, *Litoria pearsoniana*, in Australia rapidly gain and lose *Bd* infections year-round, and infected hosts experience a 38% decrease in survivorship if they maintain infection. Because individuals do not sustain infections through time, there is little evidence that these hosts are tolerant, but because individuals do repeatedly lose their infections, this suggests at least some host resistance or use of hotter microhabitats to clear infections. The host-pathogen interactions at this site resembles outbreak dynamics, where *Bd* causes high rates of host mortality, more than typical post-outbreak dynamics, given that there is still high pathogen-induced mortality rates despite more than 30 years of host-pathogen co-occurrence.

And finally, the third *Bd*-amphibian pattern I characterized was chronic low-level *Bd* host infections, likely a result of host tolerance and resistance, decreased pathogen virulence, or the prevention of pathogen-build up in hot, dry environments.

These amphibians may have strong innate and/or acquired immune defenses that include: anti-fungal bacteria (e.g., Bell et al. 2013, Belden et al. 2015), anti-microbial peptides (e.g., Woodhams et al. 2006), and MHC gene expression (e.g., Savage and Zamudio 2011, Ellison et al. 2014, Savage and Zamudio 2016). Both *Rana muscosa* (Briggs et al. 2010) and *Espadarana prospoblepon* fall into this category. For both of these species, *Bd* prevalence among hosts is consistently high and adults do not suffer pathogen-induced mortality, likely because infection intensities are low or pathogen virulence has decreased since the outbreak. From a conservation perspective, ideally, after an outbreak, most *Bd*-amphibian interactions would fall into this category, where the host and pathogen can co-occur without substantial negative impacts on host population persistence.

V. Conservation implications

Nearly one-third (32%) of the world's amphibian species are known to be threatened or extinct, 43% are not threatened, and 25% have insufficient data to determine their threat status (2008 IUCN Red List of Threatened Species). As many as 159 amphibian species may already be extinct, where at least 38 species are known to be extinct, one is extinct in the wild, and the other 120 species have not been found in recent years and are possibly extinct. At least 42% of all species have declining populations, suggesting that the number of threatened species is expected to rise. In contrast, less than one percent of species show population increases. The largest numbers of threatened species occur in the Neotropics, especially in Colombia (214), Mexico (211), and Ecuador (171).

Governments and conservation organizations use estimates of population abundance provided by scientists to inform their decisions. In a world where *Bd* is widespread, though, amphibian population estimates are even more difficult to obtain for many Neotropical species or communities, creating the problem where the limited resources we have are not necessarily going to the species or communities that need them the most. Therefore, having robust estimates of population size helps identify the most at-risk species, prioritize conservation actions, and design management strategies for the recovery of wild amphibian populations. Our current species conservation approach does not necessarily align with providing resources to areas that need it the most (e.g., McClananhan and Rankin 2016). I provide new analytical tools to help deal with evaluating the impacts of *Bd* on amphibian adults and tadpoles at other locations that are plagued by low counts and difficult to recapture amphibians (Chapter IV). And for the first time, I provide a data on the responses of two life stages for the El Copé amphibian community following *Bd* invasion, and I describe how adults are persisting alongside a hyper-virulent pathogen.

Appendices

Figure A2.1 Bayesian posterior predictive check, where I compare our data set and simulated data sets to expected values. The average difference between our data set and the simulated data set to expected values should be close to 0.5, indicating that the model fits well. Extreme differences between our data set and the simulated data set to the expected values (i.e., 0.05 or 0.95) indicate poor model fit.

Figure A2.2 Summary results from the simulation model used to determine the number of sites to sample and the number of times to survey a site. As root mean squared error increases (y-axis), parameter precision estimates decrease. I vary species rarity (occupancy probability = 0.1 to 0.9) and detectability (detection probability = 0.1 to 0.9), and determine the number of surveys (thick lines) to conduct per site, when a different number of sites are sampled (x-axis, range: 5 – 50).

Figure A3.1 Depiction of the Bayesian posterior predictive check (i.e., Bayesian p-value) for the multi-state Jolly-Seber model, where values near 0.5 represent the model fits the data well and extreme values (i.e., 0.05 or 0.95) is poor model fit. T^{obs} is the Freeman-Tukey test statistic from the observed data, while T^{rep} is Freeman-Tukey test statistic from the replicated dataset.

Figure A4.1 Difference in the number of observed individuals infected between the second and first aggregated sampling occasions within a season. Panels A, B, C, and D represent the four seasons I sampled individuals.

Figure A4.1 Weather patterns at the site from a weather station located along the continental divide. Black bars represent total rainfall (cm) on the left y-axis, while the red (maximum daily temperature) and blue (minimum daily temperature) lines correspond to the daily extreme temperature on the right y-axis.

Figure A4.2 Summary of daily minimum (blue) and maximum (red) habitat temperatures along each stream transect each season surveyed.

Figure A4.3 Summary of daily minimum (blue) and maximum (red) habitat temperatures along each trail transect each season surveyed.

Figure A4.4 Difference in the number of observed individuals uninfected between the second and first aggregated sampling occasions within a season. Panels A, B, C, and D represent the four seasons I sampled individuals.

Figure A4.5 Difference in the number of observed individuals infected between the second and first aggregated sampling occasions within a season. Panels A, B, C, and D represent the four seasons I sampled individuals.

Figure A4.6 Community composition differences between (A) seasons and (B) habitats. There were very few differences in seasonal community composition, suggested by the large overlap in ellipses, while streams and trails shared few common species. NMDS stress was 0.17. Ellipses represent 95% confidence intervals around the centroid. Points represent community assemblage per transect in each season each year.

Figure A4.7 Bayesian posterior predictive check for the (A) infected and (B) uninfected models, where values near 0.5 suggest good model fit. Extreme values (i.e., ≤ 0.05 or ≥ 0.95) suggest poor model fit to data.

Figure A4.8 Bayesian posterior predictive check for the infected model during (A) wet 2012, (B) dry 2013, (C) wet 2013, and (D) dry 2014.

Figure A4.9 Host density, pathogen prevalence, and infection intensity variation between wet (o) and dry (+) seasons for each 20 m site. Host density and pathogen prevalence estimates are from the model output, while pathogen density- the sum of host infection intensity at each 20 m site- was calculated from the raw data.

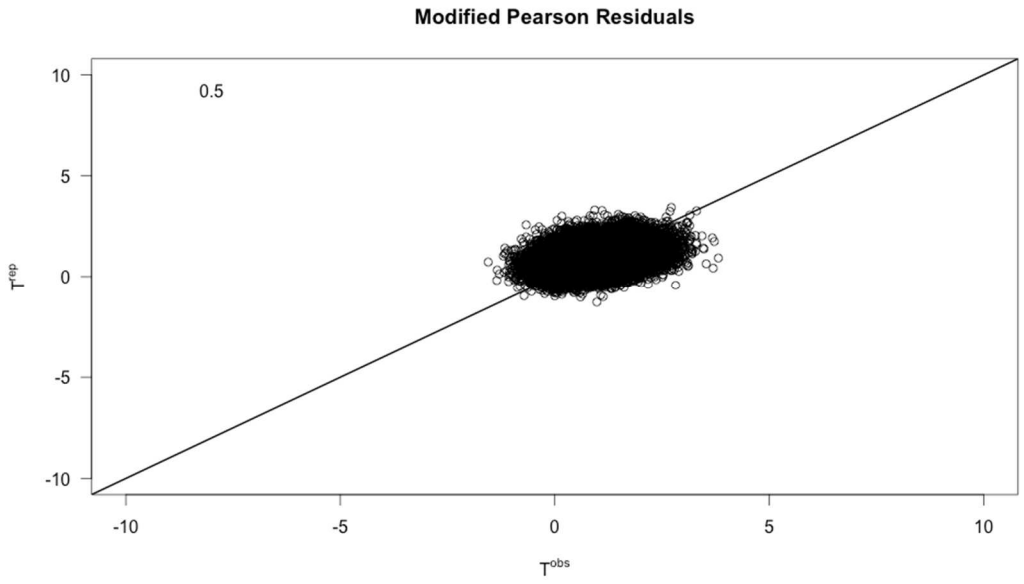

Figure A2.1

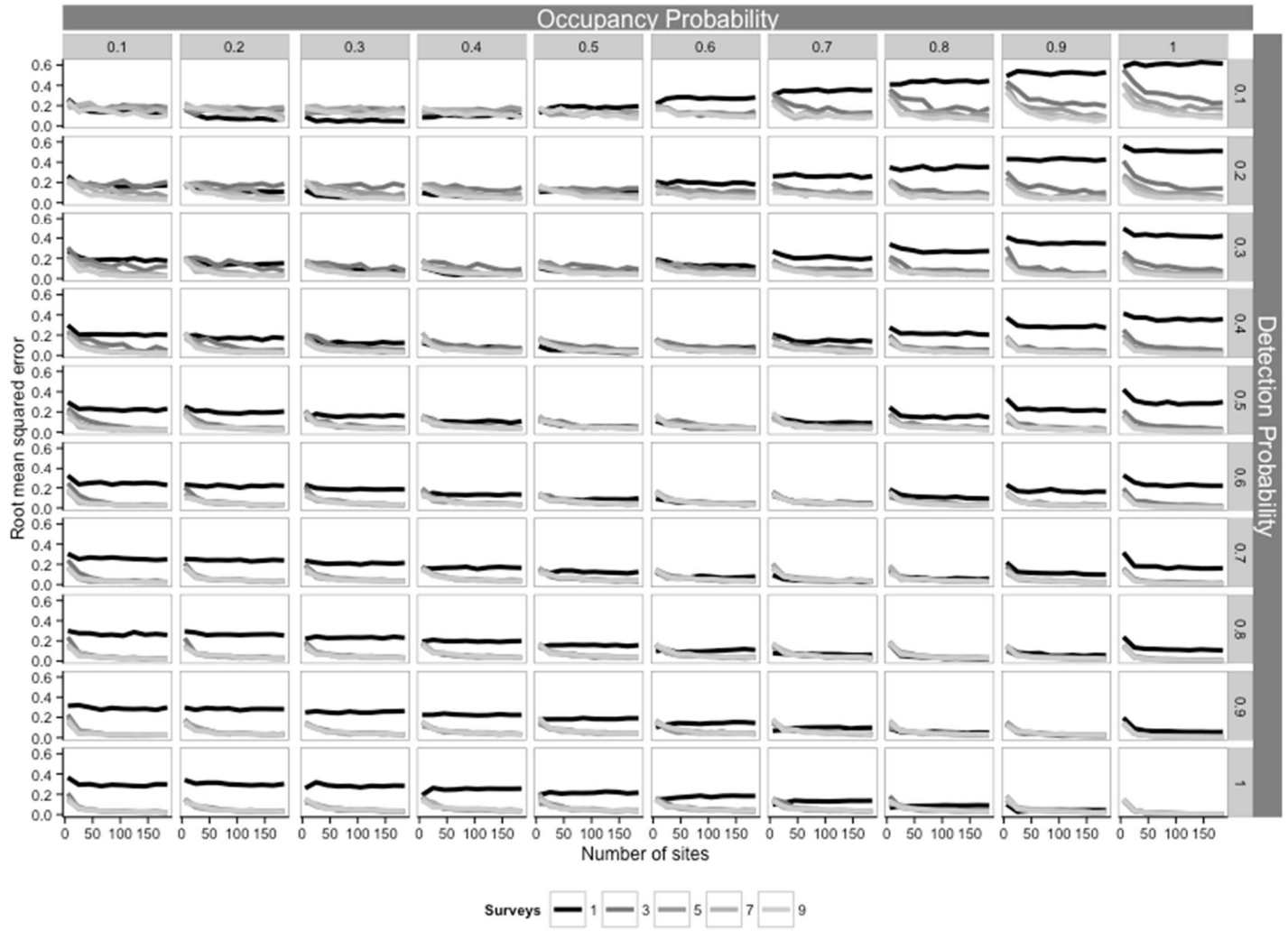
Occupancy Probability
0.1
0.2
0.3
0.4
0.5
0.6
0.7
0.8
0.9
1
Detection Probability
Root mean squared error
0.0
0.2
0.4
0.6
0 50 100 150
Number of sites
Surveys
1
3
5
7
9

Figure A2.2

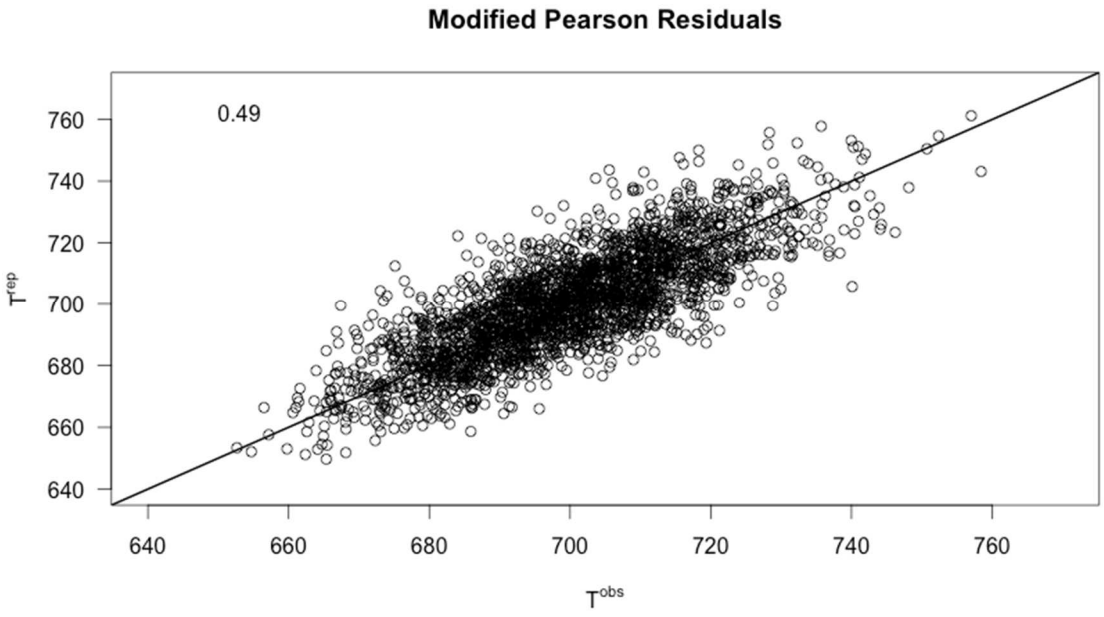
Modified Pearson Residuals
0.49
760
740
720
700
680
660
640
640
660
680
700
720
740
760
T^rep
T^obs

Figure A3.1

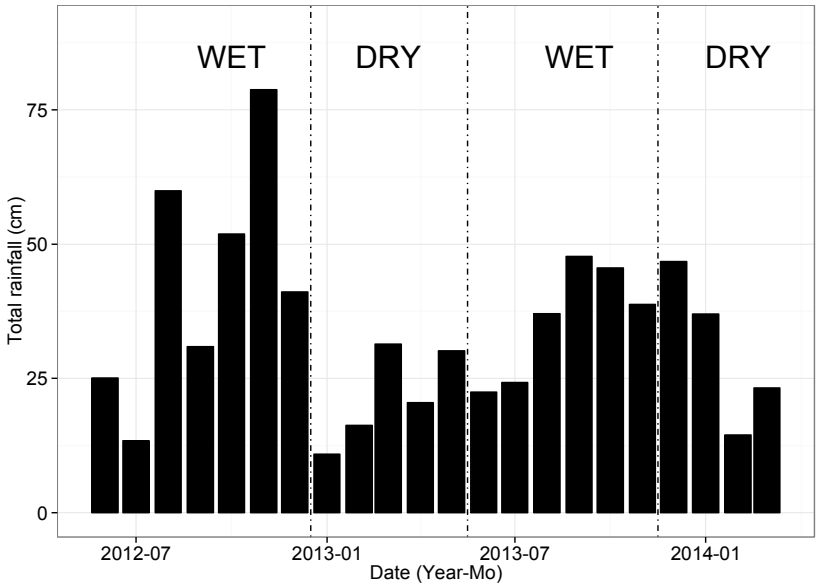
WET
DRY
WET
DRY
75
50
25
0
Total rainfall (cm)
2012-07
2013-01
2013-07
2014-01
Date (Year-Mo)

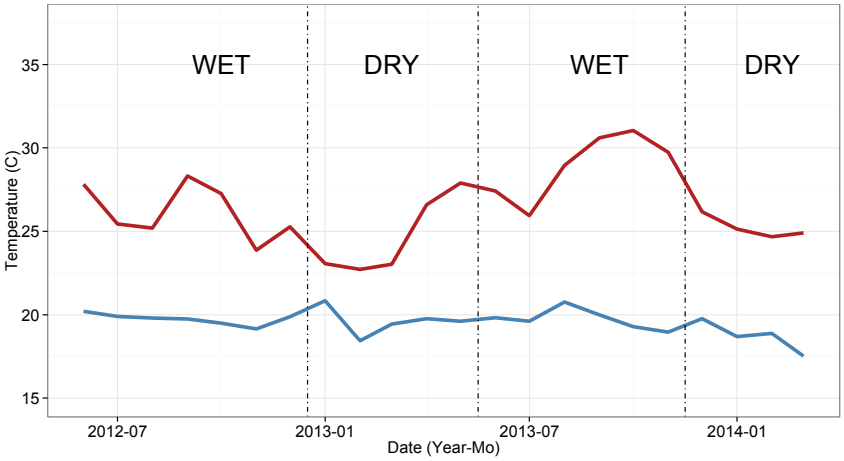
WET
DRY
WET
DRY
35
30
25
20
15
Temperature (C)
2012-07
2013-01
2013-07
2014-01
Date (Year-Mo)

Figure A4.1

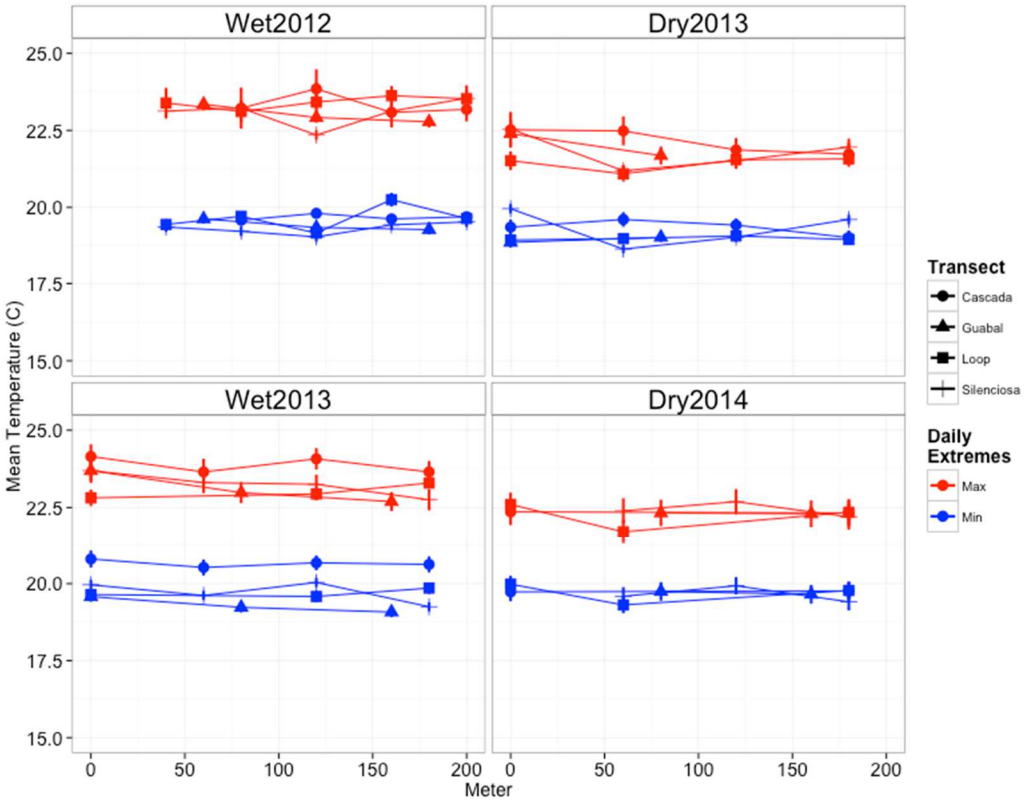
Wet2012
Dry2013
Wet2013
Dry2014
Mean Temperature (C)
25.0
22.5
20.0
17.5
15.0
0
50
100
150
200
Meter
Transect
Cascada
Guabal
Loop
Silenciosa
Daily Extremes
Max
Min

Figure A4.2

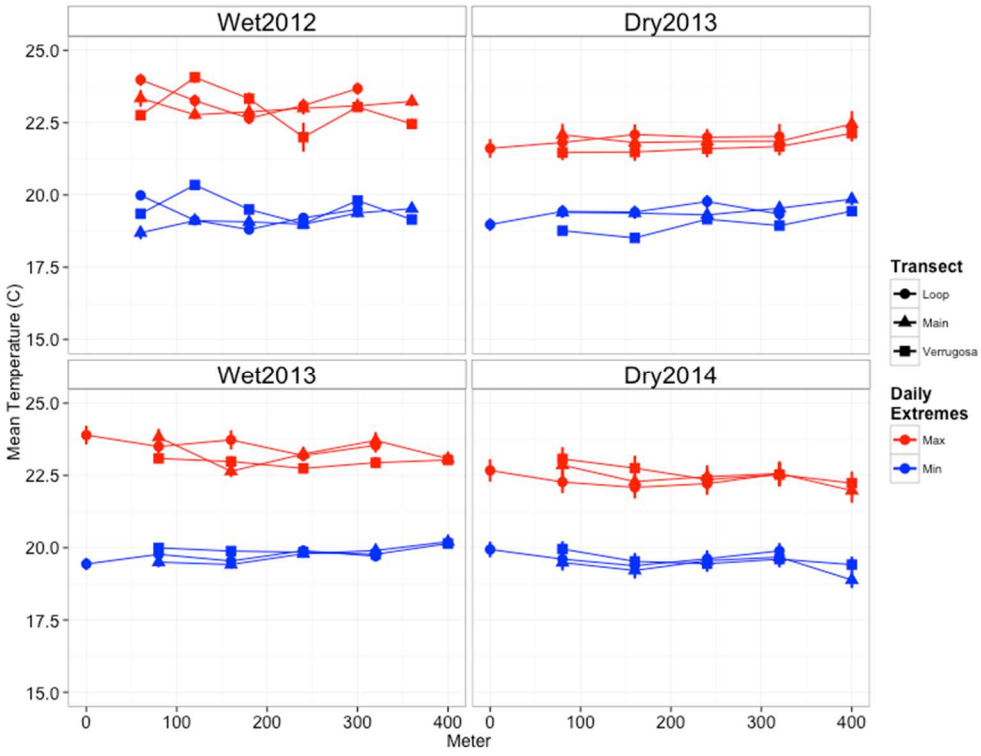
Wet2012
Dry2013
Wet2013
Dry2014
Mean Temperature (C)
25.0
22.5
20.0
17.5
15.0
0
100
200
300
400
Meter
Transect
Loop
Main
Verrugosa
Daily Extremes
Max
Min

Figure A4.3

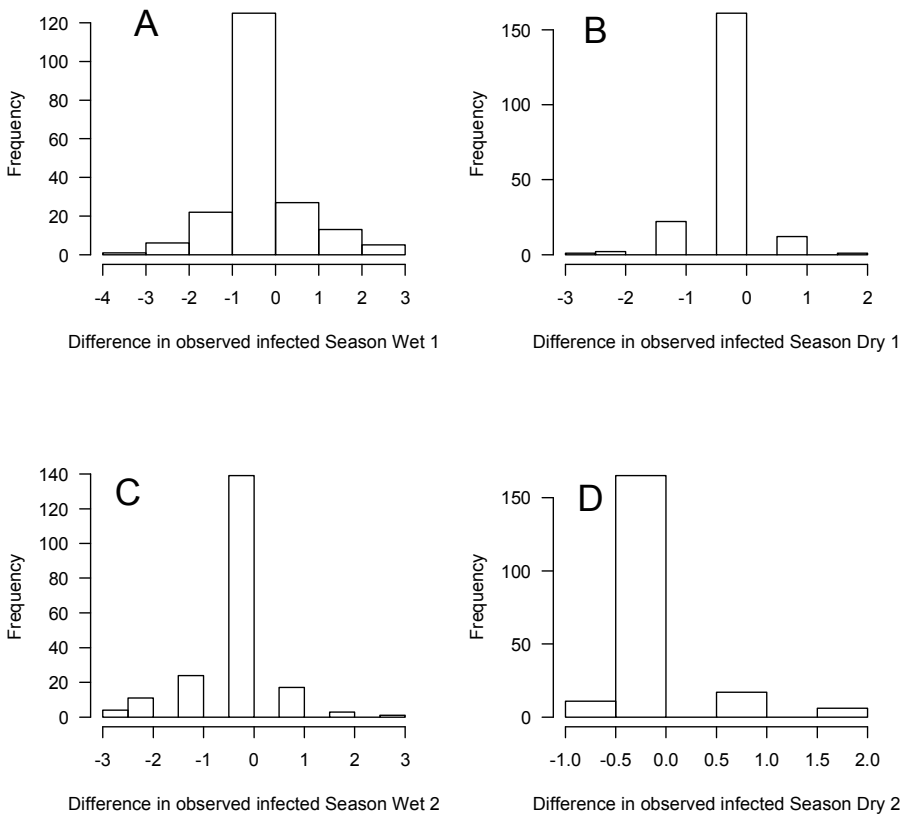
A
Frequency
120
100
80
60
40
20
0
-4 -3 -2 -1 0 1 2 3
Difference in observed infected Season Wet 1
B
Frequency
150
100
50
0
-3 -2 -1 0 1 2
Difference in observed infected Season Dry 1
C
Frequency
140
120
100
80
60
40
20
0
-3 -2 -1 0 1 2 3
Difference in observed infected Season Wet 2
D
Frequency
150
100
50
0
-1.0 -0.5 0.0 0.5 1.0 1.5 2.0
Difference in observed infected Season Dry 2

Figure A4.4

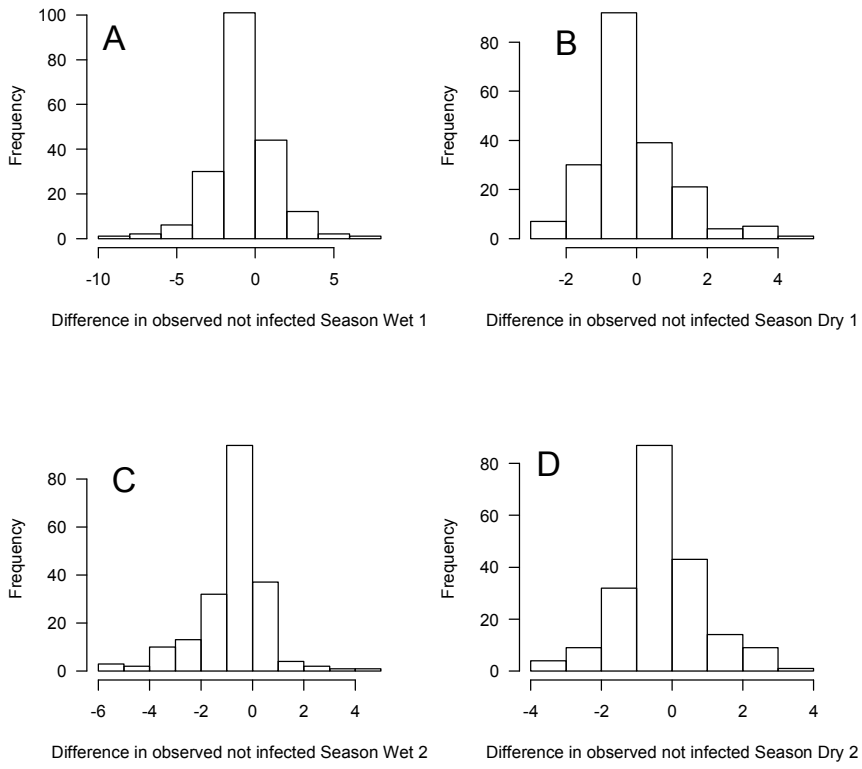
A
B
C
D
Frequency
Difference in observed not infected Season Wet 1
Difference in observed not infected Season Dry 1
Difference in observed not infected Season Wet 2
Difference in observed not infected Season Dry 2

Figure A4.5

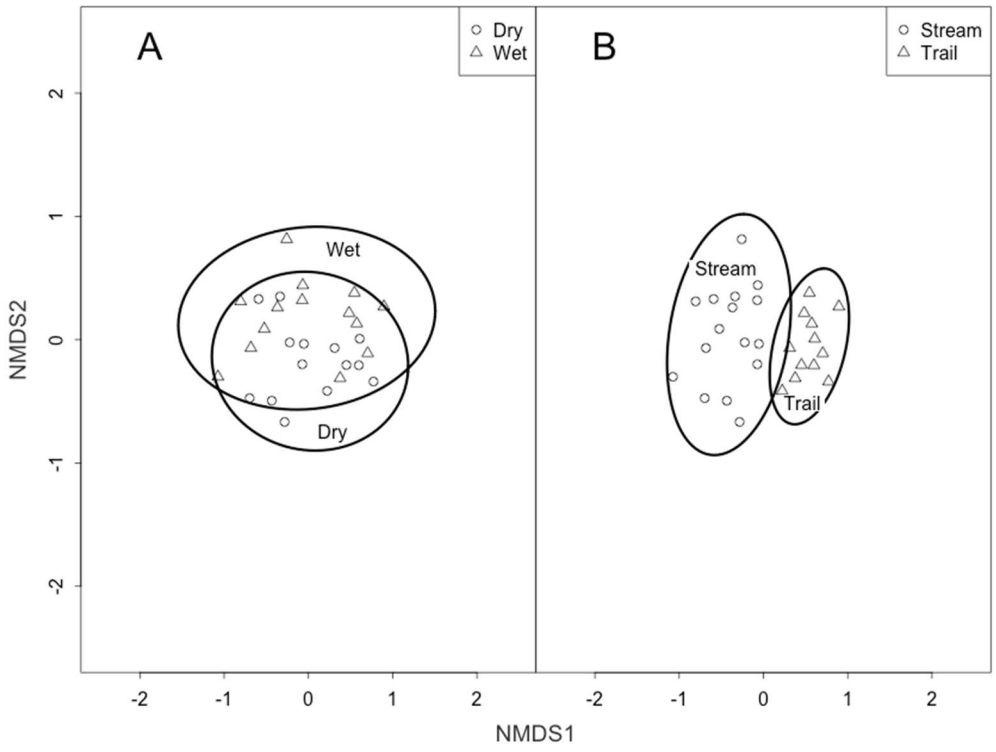
A
Dry
Wet
Wet
Dry
B
Stream
Trail
Stream
Trail
NMDS2
NMDS1
-2
-1
0
1
2

Figure A4.6

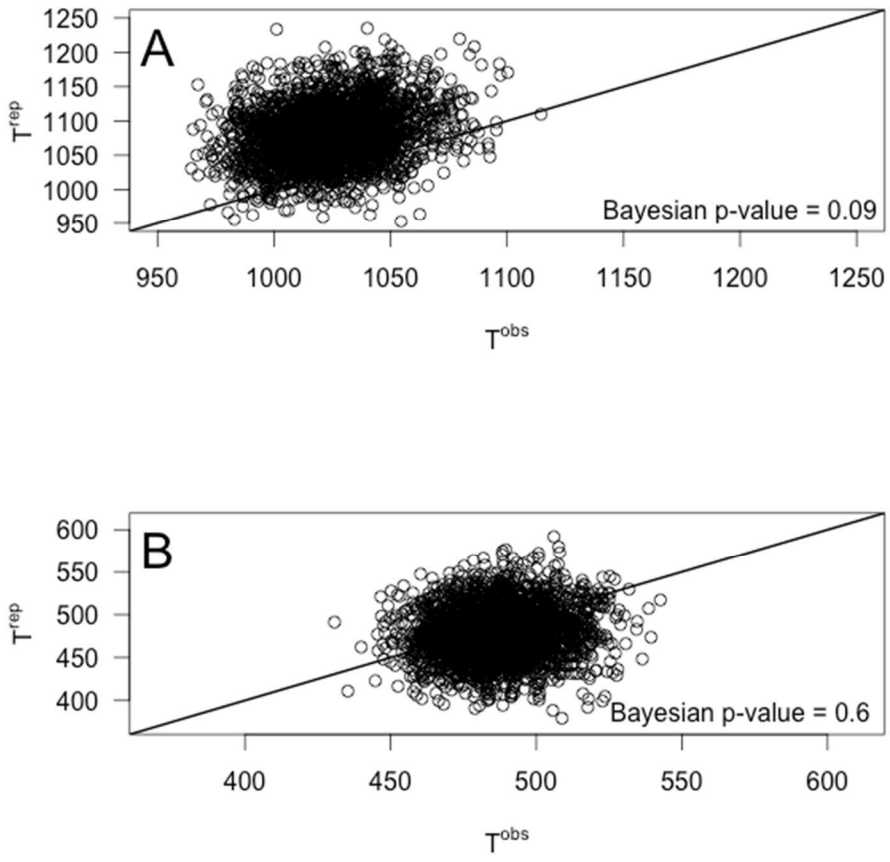
A
Bayesian p-value = 0.09
T^{rep}
T^{obs}
1250
1200
1150
1100
1050
1000
950
950
1000
1050
1100
1150
1200
1250
B
Bayesian p-value = 0.6
T^{rep}
T^{obs}
600
550
500
450
400
400
450
500
550
600

Figure A4.7

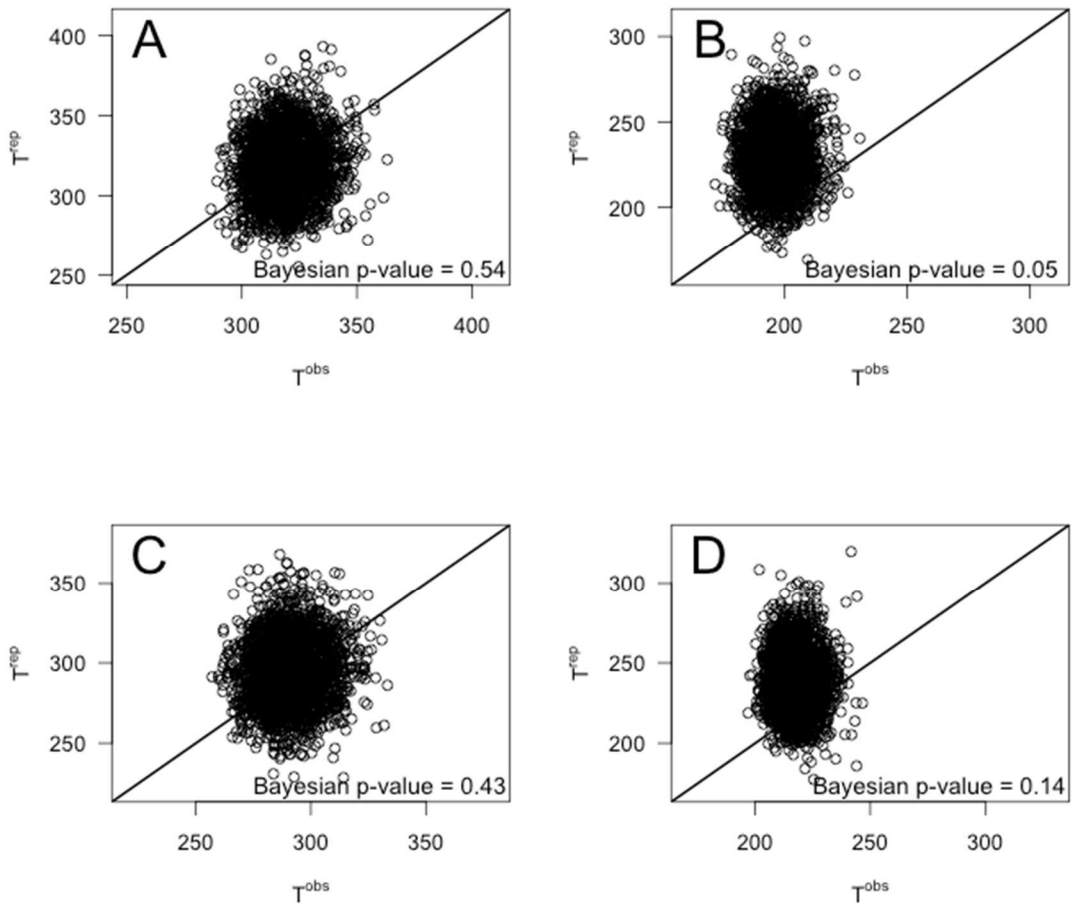
A
Bayesian p-value = 0.54
B
Bayesian p-value = 0.05
C
Bayesian p-value = 0.43
D
Bayesian p-value = 0.14
T^rep
T^obs

Figure A4.8

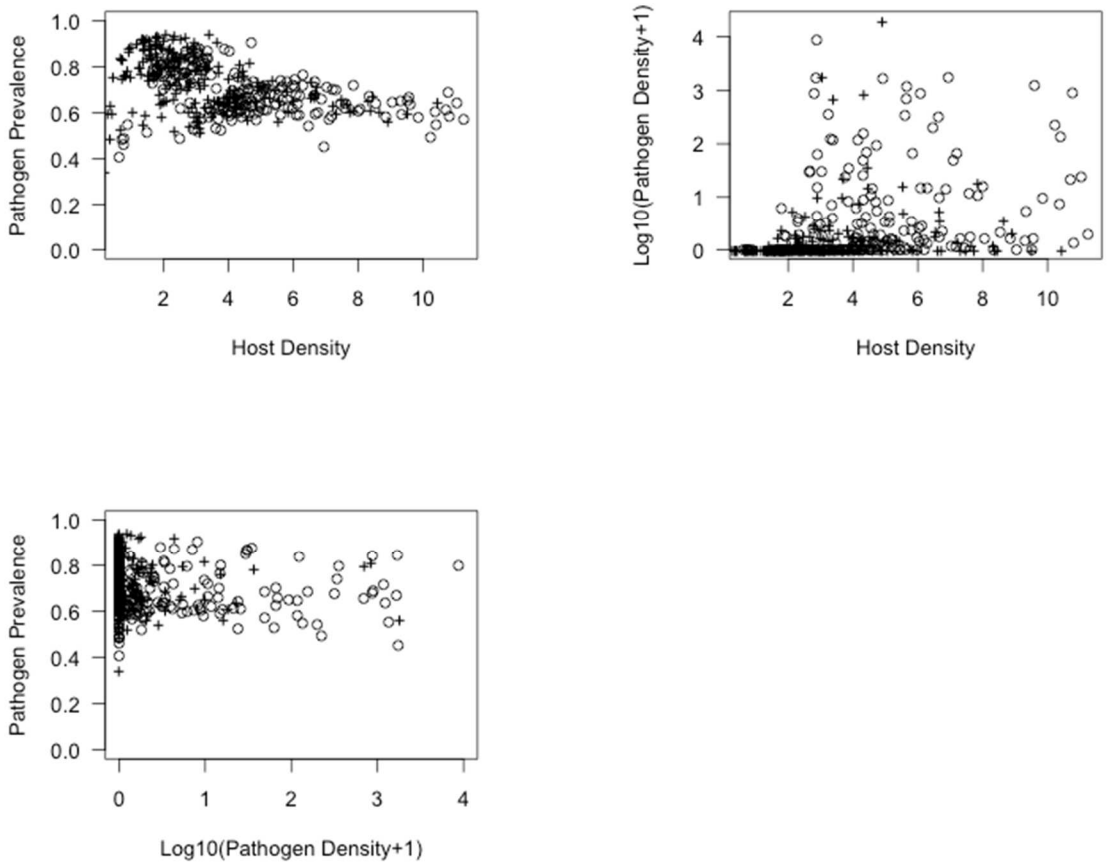
Pathogen Prevalence
Host Density
Log10(Pathogen Density+1)
Host Density
Pathogen Prevalence
Log10(Pathogen Density+1)

Figure A4.9

APPENDIX TABLES

Table A2.1 Summary of months and years that streams were sampled. The adjacent stream is a stream section located between Guabal and Silenciosa. Monthly sampling of microhabitats occurred for the first two years, and annually thereafter, excluding 2012 and 2013.

Month year	Guabal	Silenciosa	Cascada	Loop	Adjacent stream
June 2003 - August 2004	X	X	X	X	
September 2004 *Bd* arrives	X	X	X	X	
October 2004 - August 2005	X	X	X	X	
July 2006					X
July 2007					X
August 2008					X
August 2009	X				
March/April 2010	X				
February 2011	X				
March 2014	X	X		X	

Table A2.2. Summary of the percent occurrence of species in each microhabitat for sampling seasons 2003-2004 and 2004-2005. n equals the total number of samples collected. The number in parentheses represents the raw number of samples the species occurred in. September 2004 was not included in the table. NA indicated no samples taken. --- indicates no individuals found.

		June 2003 - August 2004			October 2004 - August 2005		
Genus species	Microhabitat	Wet (n = 248)	Dry (n = 172)	Total (n = 420)	Wet (n = 224)	Dry (n = 156)	Total (n = 380)
Atelopus varius	Leaf Pack	---	---	---	---	---	---
	Isolated Pool	---	---	---	---	---	---
	Riffle	---	---	---	---	---	---
	Pool	---	100(2)	100(2)	NA	NA	NA
Silverstoneia flotator	Leaf Pack	27.52(1)	---	14.73(1)	---	---	---
	Isolated Pool	66.7(46)	70.86(37)	68.63(83)	100(10)	96.53(22)	97.56(32)
	Riffle	0.18(2)	4.00(6)	1.95(8)	---	3.47(1)	2.44(1)
	Pool	5.6(12)	25.14(4)	14.68(16)	NA	NA	NA
Colostethus panamensis	Leaf Pack	16.55(1)	74.06(6)	61.75(7)	---	---	---
	Isolated Pool	63.26(21)	15.95(19)	26.07(40)	100(2)	100(1)	100(3)
	Riffle	---	---	---	---	---	---
	Pool	20.19(9)	9.99(4)	12.17(13)	NA	NA	NA
Silverstoneia nubicola	Leaf Pack	---	---	---	---	---	---
	Isolated Pool	70.9(12)	56.81(11)	63.95(23)	100(5)	100(4)	100(9)

	Riffle	---	17.48(4)	8.62(4)	---	---	---
	Pool	29.1(12)	25.71(5)	27.43(17)	NA	NA	NA
Allobates talamancae	Leaf Pack	---	---	---	---	---	---
	Isolated Pool	---	---	---	---	100(1)	100(1)
	Riffle	---	---	---	---	---	---
	Pool	---	---	---	NA	NA	NA
Colostethus spp.	Leaf Pack	---	---	---	---	---	---
	Isolated Pool	100(1)	---	100(1)	---	---	---
	Riffle	---	---	---	---	---	---
	Pool	---	---	---	NA	NA	NA
Hyloscirtus colymba	Leaf Pack	72.95(2)	92.33(9)	89.74(11)	---	86.48(2)	39.56(2)
	Isolated Pool	8.19(12)	2.99(18)	3.68(30)	99.79(15)	9.14(14)	58.32(29)
	Riffle	2.49(12)	1.06(9)	1.25(21)	0.21(1)	4.38(3)	2.12(4)
	Pool	16.37(12)	3.62(6)	5.33(18)	NA	NA	NA
Hyloscirtus palmeri	Leaf Pack	48.56(2)	---	37.45(2)	---	88.95(1)	79.54(1)
	Isolated Pool	40.84(7)	9.7(5)	33.71(12)	92.8(5)	1.99(2)	11.6(7)
	Riffle	0.89(6)	27.53(9)	6.99(15)	7.2(1)	9.06(3)	8.87(4)
	Pool	9.7(13)	62.77(5)	21.85(18)	NA	NA	NA
Lithobates warszewitschii	Leaf Pack	---	---	---	---	---	---
	Isolated Pool	26(3)	---	0.49(3)	---	100(2)	100(2)

	Riffle	---	0.04(1)	0.04(1)	---	---	---
	Pool	74(6)	99.96(2)	99.48(8)	NA	NA	NA
Espadarana prosoblepon	Leaf Pack	---	99.68(8)	99.53(8)	---	---	---
	Isolated Pool	100(1)	0.32(2)	0.47(3)	---	---	---
	Riffle	---	---	---	---	---	---
	Pool	---	---	---	NA	NA	NA
Sachatamia							
albomaculata	Leaf Pack	---	99.82(1)	99.82(1)	---	---	---
	Isolated Pool	---	0.18(1)	0.18(1)	---	---	---
	Riffle	---	---	---	---	---	---
	Pool	---	---	---	NA	NA	NA
Sachatamia ilex	Leaf Pack	---	---	---	---	---	---
	Isolated Pool	100(1)	---	100(1)	---	---	---
	Riffle	---	---	---	---	---	---
	Pool	---	---	---	NA	NA	NA
Hyalinobatrachium							
colymbiphyllum	Leaf Pack	100(1)	99.66(3)	99.7(4)	---	---	---
	Isolated Pool	---	0.34(1)	0.3(1)	100(1)	---	100(1)
	Riffle	---	---	---	---	---	---
	Pool	---	---	---	NA	NA	NA

Teratohyla spinosa	Leaf Pack	---	---	---	---	---	---
	Isolated Pool	100(1)	---	100(1)	---	---	---
	Riffle	---	---	---	---	---	---
	Pool	---	---	---	NA	NA	NA
Centrolene spp	Leaf Pack	98.89(1)	99.53(2)	99.19(3)	---	---	---
	Isolated Pool	1.11(2)	0.47(1)	0.81(3)	---	---	---
	Riffle	---	---	---	---	---	---
	Pool	---	---	---	NA	NA	NA

Table A2.3 Summary of tadpole detection probabilities in microhabitats from occupancy model.

Microhabitat	Mean	Median	SD	Lower	Upper
IsoPool + LeafPack	0.41	0.41	0.02	0.36	0.47
Riffle	0.13	0.13	0.03	0.08	0.20

Table A2.4 Summary of AICc, differences in AICc (dAICc) scores, and model weights for macro-evolutionary model of species vulnerability to *Bd*, quantified using last Julian Day a species was last observed at the site. The Brownian model was the model of best fit, indicating a phylogenetic signal to the order of species losses.

Model name	AICc	dAICc	Model weights
Brownian	149.48	0	0.71
OU	152.77	3.28	0.13
Lambda	153.25	3.76	0.10
White noise	155.31	5.83	0.03

Table A2.5 Summary of logistic regression results next to summary of occupancy model results. In general, the logistic regression results were less than the occupancy model results.

				Logistic			Occupancy		
Species	Year	Microhabitat	Season	Mean	Lower	Upper	Mean	Lower	Upper
Hyalinobatrachium colymbiphyllum	Pre	Isolated pool	Dry	0.05	0.01	0.11	0.1	0.02	0.20
Lithobates warszewitschii	Pre	Isolated pool	Dry	0.05	0.01	0.11	0.11	0.02	0.22
Espadarana prosoblepon	Pre	Isolated pool	Dry	0.08	0.02	0.15	0.15	0.04	0.29
Hyloscirtus palmeri	Pre	Isolated pool	Dry	0.13	0.05	0.21	0.25	0.11	0.41
Silverstoneia nubicola	Pre	Isolated pool	Dry	0.25	0.14	0.37	0.46	0.26	0.65
Hyloscirtus colymba	Pre	Isolated pool	Dry	0.36	0.24	0.49	0.65	0.48	0.82
Colostethus panamensis	Pre	Isolated pool	Dry	0.41	0.28	0.54	0.66	0.48	0.83
Silverstoneia flotator	Pre	Isolated pool	Dry	0.65	0.53	0.78	0.9	0.81	0.97
Lithobates warszewitschii	Pre	Leaf pack	Dry	0.01	0	0.03	0.02	0	0.06
Silverstoneia nubicola	Pre	Leaf pack	Dry	0.02	0	0.04	0.03	0	0.09
Hyloscirtus palmeri	Pre	Leaf pack	Dry	0.04	0	0.09	0.09	0.01	0.2
Silverstoneia flotator	Pre	Leaf pack	Dry	0.04	0	0.1	0.09	0.01	0.21
Hyalinobatrachium colymbiphyllum	Pre	Leaf pack	Dry	0.06	0.01	0.13	0.13	0.01	0.29
Colostethus panamensis	Pre	Leaf pack	Dry	0.17	0.06	0.3	0.33	0.11	0.57
Espadarana prosoblepon	Pre	Leaf pack	Dry	0.17	0.06	0.3	0.37	0.12	0.62
Hyloscirtus colymba	Pre	Leaf pack	Dry	0.24	0.11	0.38	0.46	0.21	0.73
Hyalinobatrachium colymbiphyllum	Pre	Riffle	Dry	0.01	0	0.03	0.04	0	0.12
Espadarana prosoblepon	Pre	Riffle	Dry	0.01	0	0.03	0.05	0	0.16
Lithobates warszewitschii	Pre	Riffle	Dry	0.02	0	0.04	0.07	0	0.21
Colostethus panamensis	Pre	Riffle	Dry	0.02	0	0.05	0.09	0	0.27

Silverstoneia nubicola	Pre	Riffle	Dry	0.06	0.01	0.13	0.28	0.04	0.58
Silverstoneia flotator	Pre	Riffle	Dry	0.13	0.04	0.22	0.56	0.23	0.91
Hyloscirtus palmeri	Pre	Riffle	Dry	0.18	0.08	0.29	0.67	0.37	0.96
Hyloscirtus colymba	Pre	Riffle	Dry	0.22	0.11	0.34	0.9	0.72	1
Hyalinobatrachium colymbiphyllum	Pre	Isolated pool	Wet	0.01	0	0.03	0.02	0	0.06
Espadarana prosoblepon	Pre	Isolated pool	Wet	0.01	0	0.03	0.02	0	0.06
Lithobates warszewitschii	Pre	Isolated pool	Wet	0.03	0	0.07	0.06	0.01	0.14
Hyloscirtus palmeri	Pre	Isolated pool	Wet	0.1	0.04	0.17	0.21	0.07	0.36
Silverstoneia nubicola	Pre	Isolated pool	Wet	0.17	0.08	0.27	0.36	0.16	0.57
Hyloscirtus colymba	Pre	Isolated pool	Wet	0.2	0.11	0.31	0.4	0.2	0.62
Colostethus panamensis	Pre	Isolated pool	Wet	0.32	0.2	0.44	0.64	0.43	0.86
Silverstoneia flotator	Pre	Isolated pool	Wet	0.63	0.5	0.76	0.91	0.81	0.99
Lithobates warszewitschii	Pre	Leaf pack	Wet	0	0	0.01	0.01	0	0.03
Silverstoneia nubicola	Pre	Leaf pack	Wet	0	0	0.02	0.01	0	0.04
Espadarana prosoblepon	Pre	Leaf pack	Wet	0.01	0	0.03	0.02	0	0.06
Hyalinobatrachium colymbiphyllum	Pre	Leaf pack	Wet	0.01	0	0.04	0.03	0	0.08
Silverstoneia flotator	Pre	Leaf pack	Wet	0.02	0	0.06	0.04	0	0.11
Colostethus panamensis	Pre	Leaf pack	Wet	0.03	0	0.07	0.07	0	0.17
Hyloscirtus palmeri	Pre	Leaf pack	Wet	0.03	0	0.07	0.07	0	0.17
Hyloscirtus colymba	Pre	Leaf pack	Wet	0.04	0	0.09	0.08	0.01	0.18
Hyalinobatrachium colymbiphyllum	Pre	Riffle	Wet	0	0	0.01	0.01	0	0.04
Espadarana prosoblepon	Pre	Riffle	Wet	0	0	0.01	0.01	0	0.04
Lithobates warszewitschii	Pre	Riffle	Wet	0	0	0.02	0.02	0	0.09
Colostethus panamensis	Pre	Riffle	Wet	0.01	0	0.02	0.04	0	0.13
Silverstoneia nubicola	Pre	Riffle	Wet	0.01	0	0.03	0.05	0	0.17
Silverstoneia flotator	Pre	Riffle	Wet	0.04	0	0.09	0.24	0.01	0.58

Hyloscirtus palmeri	Pre	Riffle	Wet	0.11	0.04	0.2	0.55	0.21	0.95
Hyloscirtus colymba	Pre	Riffle	Wet	0.17	0.07	0.27	0.79	0.49	1
Hyalinobatrachium colymbiphyllum	Post	Isolated pool	Dry	0.01	0	0.03	0.02	0	0.06
Lithobates warszewitschii	Post	Isolated pool	Dry	0.02	0	0.06	0.05	0	0.13
Espadarana prosoblepon	Post	Isolated pool	Dry	0.01	0	0.03	0.02	0	0.06
Hyloscirtus palmeri	Post	Isolated pool	Dry	0.05	0.01	0.11	0.12	0.02	0.24
Silverstoneia nubicola	Post	Isolated pool	Dry	0.08	0.02	0.15	0.17	0.04	0.32
Hyloscirtus colymba	Post	Isolated pool	Dry	0.25	0.14	0.38	0.08	0.01	0.19
Colostethus panamensis	Post	Isolated pool	Dry	0.04	0	0.1	0.53	0.29	0.78
Silverstoneia flotator	Post	Isolated pool	Dry	0.42	0.27	0.57	0.78	0.58	0.96
Lithobates warszewitschii	Post	Leaf pack	Dry	0	0	0.01	0.01	0	0.03
Silverstoneia nubicola	Post	Leaf pack	Dry	0	0	0.01	0.01	0	0.02
Hyloscirtus palmeri	Post	Leaf pack	Dry	0.02	0	0.05	0.01	0	0.05
Silverstoneia flotator	Post	Leaf pack	Dry	0.01	0	0.03	0.04	0	0.1
Hyalinobatrachium colymbiphyllum	Post	Leaf pack	Dry	0.01	0	0.02	0.01	0	0.04
Colostethus panamensis	Post	Leaf pack	Dry	0.01	0	0.02	0.01	0	0.04
Espadarana prosoblepon	Post	Leaf pack	Dry	0.02	0	0.05	0.04	0	0.11
Hyloscirtus colymba	Post	Leaf pack	Dry	0.07	0.01	0.14	0.13	0.02	0.29
Hyalinobatrachium colymbiphyllum	Post	Riffle	Dry	0	0	0.01	0.01	0	0.04
Espadarana prosoblepon	Post	Riffle	Dry	0	0	0.01	0.01	0	0.04
Lithobates warszewitschii	Post	Riffle	Dry	0	0	0.02	0.02	0	0.1
Colostethus panamensis	Post	Riffle	Dry	0	0	0.01	0.01	0	0.03
Silverstoneia nubicola	Post	Riffle	Dry	0.01	0	0.02	0.05	0	0.17
Silverstoneia flotator	Post	Riffle	Dry	0.02	0	0.06	0.19	0	0.55
Hyloscirtus palmeri	Post	Riffle	Dry	0.06	0.01	0.12	0.46	0.08	0.91
Hyloscirtus colymba	Post	Riffle	Dry	0.06	0.01	0.13	0.61	0.2	1

Hyalinobatrachium colymbiphyllum	Post	Isolated pool	Wet	0.01	0	0.02	0	0	0.01
Espadarana prosoblepon	Post	Isolated pool	Wet	0	0	0.01	0.01	0	0.04
Lithobates warszewitschii	Post	Isolated pool	Wet	0	0	0.02	0.01	0	0.03
Hyloscirtus palmeri	Post	Isolated pool	Wet	0.07	0.02	0.13	0.14	0.03	0.27
Silverstoneia nubicola	Post	Isolated pool	Wet	0.07	0.02	0.13	0.15	0.03	0.29
Hyloscirtus colymba	Post	Isolated pool	Wet	0.22	0.12	0.33	0.45	0.24	0.68
Colostethus panamensis	Post	Isolated pool	Wet	0.06	0.01	0.11	0.12	0.02	0.24
Silverstoneia flotator	Post	Isolated pool	Wet	0.19	0.1	0.29	0.44	0.19	0.69
Lithobates warszewitschii	Post	Leaf pack	Wet	0	0	0	0	0	0.01
Silverstoneia nubicola	Post	Leaf pack	Wet	0	0	0.01	0	0	0.01
Espadarana prosoblepon	Post	Leaf pack	Wet	0	0	0	0	0	0.01
Hyalinobatrachium colymbiphyllum	Post	Leaf pack	Wet	0	0	0.01	0	0	0.02
Silverstoneia flotator	Post	Leaf pack	Wet	0	0	0.01	0	0	0.01
Colostethus panamensis	Post	Leaf pack	Wet	0	0	0.01	0	0	0.02
Hyloscirtus palmeri	Post	Leaf pack	Wet	0.01	0	0.04	0.03	0	0.08
Hyloscirtus colymba	Post	Leaf pack	Wet	0.01	0	0.02	0.01	0	0.04
Hyalinobatrachium colymbiphyllum	Post	Riffle	Wet	0	0	0	0	0	0.01
Espadarana prosoblepon	Post	Riffle	Wet	0	0	0	0.01	0	0.03
Lithobates warszewitschii	Post	Riffle	Wet	0	0	0	0	0	0.02
Colostethus panamensis	Post	Riffle	Wet	0	0	0.01	0.01	0	0.03
Silverstoneia nubicola	Post	Riffle	Wet	0	0	0.01	0.01	0	0.05
Silverstoneia flotator	Post	Riffle	Wet	0	0	0.01	0.01	0	0.05
Hyloscirtus palmeri	Post	Riffle	Wet	0.05	0.01	0.11	0.42	0.07	0.91
Hyloscirtus colymba	Post	Riffle	Wet	0.02	0	0.06	0.26	0	0.79

Table A2.6 Summary of simulation results for species that vary in occupancy and detection probability. The first and second numbers represent the recommended number of sites and number of repeated surveys per site to conduct if 0.1 is the desired root mean squared error of estimates. Bold values represent number of sites, while the value directly below the bold number represents the number of surveys per site.

		Occupancy Probability								
		0.1	0.2	0.3	0.4	0.5	0.6	0.7	0.8	0.9
Detection Probability	0.1	**145**	**45**	**5**	**5**	**85**	**85**	**45**	**65**	**65**
		9	1	1	1	3	3	5	9	9
	0.2	**45**	**45**	**25**	**5**	**65**	**5**	**25**	**25**	**25**
		9	9	1	1	9	7	7	5	9
	0.3	**25**	**25**	**25**	**25**	**25**	**25**	**25**	**25**	**25**
		9	7	7	1	1	7	9	5	5
	0.4	**25**	**25**	**25**	**25**	**5**	**25**	**25**	**25**	**25**
		7	7	7	1	1	1	3	3	3
	0.5	**25**	**25**	**25**	**25**	**25**	**25**	**25**	**25**	**25**
		5	7	5	1	1	1	5	3	3
	0.6	**25**	**25**	**25**	**25**	**25**	**5**	**25**	**25**	**25**
		5	5	3	3	1	1	1	3	3
	0.7	**25**	**25**	**25**	**25**	**25**	**25**	**5**	**25**	**25**
		5	3	3	3	3	1	1	1	3
	0.8	**25**	**25**	**25**	**25**	**25**	**5**	**5**	**25**	**25**
		3	3	3	3	3	1	1	1	1
	0.9	**25**	**25**	**25**	**25**	**25**	**25**	**5**	**5**	**25**
		3	3	3	3	3	3	1	1	1

Table A3.1 Number of surveys per month in each stream.

Stream	Year	Month	Surveys
Cascada	2010	Jul	2
Cascada	2011	Jul	4
Cascada	2012	Jun	6
Cascada	2012	Jul	2
Cascada	2013	Feb	5
Cascada	2013	Mar	2
Cascada	2013	Jun	4
Cascada	2013	Jul	3
Cascada	2014	Mar	7
Guabal	2010	Jul	3
Guabal	2011	Jul	4
Guabal	2012	Jun	6
Guabal	2012	Jul	2
Guabal	2013	Feb	3
Guabal	2013	Mar	4
Guabal	2013	Jun	3
Guabal	2013	Jul	4
Guabal	2014	Mar	7
Loop	2010	Jul	4
Loop	2011	Jul	4
Loop	2012	Jun	6
Loop	2012	Jul	2
Loop	2013	Feb	6
Loop	2013	Jun	4
Loop	2013	Jul	3
Loop	2014	Feb	3
Loop	2014	Mar	5
Silenciosa	2010	Jul	3
Silenciosa	2011	Jul	4
Silenciosa	2012	Jun	5
Silenciosa	2012	Jul	2
Silenciosa	2013	Feb	3
Silenciosa	2013	Mar	4
Silenciosa	2013	Jun	3
Silenciosa	2013	Jul	4
Silenciosa	2014	Mar	7

Table A4.1 Random effect summary for between site variations in *Bd* transmission risk.

Transect	Meter	Mean	Standard deviation	95% Credible interval	
Cascada	0	-0.04	0.63	-1.54	1.28
Cascada	100	-0.04	0.60	-1.33	1.20
Cascada	120	-0.03	0.60	-1.36	1.27
Cascada	140	0.01	0.62	-1.20	1.46
Cascada	160	0.02	0.67	-1.31	1.48
Cascada	180	0.00	0.63	-1.58	1.24
Cascada	20	-0.04	0.61	-1.38	1.15
Cascada	40	-0.04	0.56	-1.33	1.11
Cascada	60	-0.02	0.59	-1.32	1.17
Cascada	80	0.01	0.64	-1.32	1.44
Guabal	0	-0.03	0.60	-1.27	1.25
Guabal	100	-0.01	0.62	-1.41	1.34
Guabal	120	-0.02	0.62	-1.18	1.30
Guabal	140	0.00	0.58	-1.20	1.37
Guabal	160	-0.02	0.59	-1.29	1.28
Guabal	180	0.00	0.61	-1.52	1.19
Guabal	20	0.01	0.62	-1.37	1.32
Guabal	40	0.01	0.63	-1.53	1.28
Guabal	60	-0.02	0.64	-1.45	1.34
Guabal	80	-0.01	0.61	-1.47	1.21
LoopStream	0	0.01	0.65	-1.44	1.34
LoopStream	100	-0.01	0.63	-1.48	1.23
LoopStream	120	0.01	0.63	-1.27	1.41
LoopStream	140	0.00	0.62	-1.36	1.36
LoopStream	160	-0.01	0.64	-1.18	1.56
LoopStream	180	-0.02	0.59	-1.45	1.21
LoopStream	20	-0.01	0.63	-1.49	1.32
LoopStream	40	-0.01	0.62	-1.34	1.44
LoopStream	60	0.00	0.59	-1.30	1.38
LoopStream	80	-0.01	0.61	-1.39	1.35
LoopTrail	0	0.00	0.64	-1.40	1.41
LoopTrail	100	-0.01	0.61	-1.35	1.36
LoopTrail	120	0.02	0.65	-1.36	1.46
LoopTrail	140	0.00	0.64	-1.28	1.42
LoopTrail	160	0.01	0.61	-1.18	1.45
LoopTrail	180	-0.01	0.62	-1.28	1.43
LoopTrail	20	0.01	0.64	-1.48	1.21

LoopTrail	200	-0.01	0.64	-1.48	1.24
LoopTrail	220	0.02	0.64	-1.21	1.47
LoopTrail	240	0.01	0.63	-1.34	1.42
LoopTrail	260	-0.02	0.67	-1.36	1.54
LoopTrail	280	0.02	0.62	-1.22	1.44
LoopTrail	300	0.01	0.64	-1.30	1.46
LoopTrail	320	-0.02	0.64	-1.32	1.52
LoopTrail	340	0.01	0.64	-1.36	1.40
LoopTrail	360	0.01	0.68	-1.36	1.52
LoopTrail	40	0.00	0.66	-1.31	1.46
LoopTrail	60	0.01	0.66	-1.46	1.30
LoopTrail	80	-0.02	0.60	-1.26	1.37
MainTrail	0	0.02	0.63	-1.41	1.42
MainTrail	100	-0.01	0.69	-1.47	1.37
MainTrail	120	-0.01	0.68	-1.59	1.30
MainTrail	140	0.01	0.66	-1.30	1.40
MainTrail	160	0.00	0.62	-1.16	1.52
MainTrail	180	-0.01	0.66	-1.47	1.35
MainTrail	20	0.02	0.63	-1.25	1.64
MainTrail	200	0.02	0.63	-1.25	1.52
MainTrail	220	0.01	0.65	-1.37	1.55
MainTrail	240	0.02	0.65	-1.26	1.46
MainTrail	260	0.01	0.59	-1.18	1.37
MainTrail	280	0.00	0.68	-1.32	1.53
MainTrail	300	0.03	0.64	-1.49	1.30
MainTrail	320	-0.01	0.62	-1.53	1.18
MainTrail	340	-0.02	0.60	-1.41	1.13
MainTrail	360	-0.01	0.62	-1.35	1.29
MainTrail	380	0.00	0.65	-1.34	1.33
MainTrail	40	0.01	0.63	-1.28	1.49
MainTrail	60	-0.02	0.63	-1.46	1.20
MainTrail	80	0.02	0.60	-1.20	1.41
Silenciosa	0	0.00	0.63	-1.29	1.35
Silenciosa	100	-0.02	0.61	-1.41	1.28
Silenciosa	120	-0.02	0.61	-1.31	1.22
Silenciosa	140	-0.01	0.62	-1.50	1.26
Silenciosa	160	-0.02	0.63	-1.55	1.06
Silenciosa	180	-0.02	0.65	-1.51	1.26
Silenciosa	20	0.01	0.66	-1.42	1.32
Silenciosa	40	0.02	0.64	-1.34	1.33
Silenciosa	60	0.03	0.62	-1.23	1.23
Silenciosa	80	0.02	0.64	-1.25	1.47
Verrugosa	0	-0.03	0.64	-1.38	1.50

Verrugosa	100	0.00	0.63	-1.31	1.38
Verrugosa	120	-0.02	0.62	-1.34	1.40
Verrugosa	140	-0.01	0.64	-1.60	1.26
Verrugosa	160	0.02	0.63	-1.31	1.45
Verrugosa	180	-0.01	0.58	-1.24	1.30
Verrugosa	20	-0.02	0.60	-1.26	1.52
Verrugosa	200	-0.01	0.64	-1.40	1.30
Verrugosa	220	0.00	0.63	-1.57	1.27
Verrugosa	240	-0.02	0.64	-1.32	1.49
Verrugosa	260	-0.02	0.63	-1.36	1.42
Verrugosa	280	-0.01	0.64	-1.41	1.27
Verrugosa	300	0.00	0.61	-1.34	1.23
Verrugosa	320	0.00	0.66	-1.40	1.32
Verrugosa	340	-0.01	0.63	-1.38	1.34
Verrugosa	360	0.03	0.63	-1.38	1.38
Verrugosa	380	-0.01	0.69	-1.38	1.61
Verrugosa	40	-0.02	0.62	-1.25	1.39
Verrugosa	60	0.00	0.63	-1.39	1.30
Verrugosa	80	-0.01	0.62	-1.26	1.35

Supplement

SUPPLEMENT 2.1

STATISTICAL ANALYSIS

Optimizing species detection and sampling schemes

```
# Define function to simulate data

data.fn <- function(R = h, T = n,
                    psi = g,
                    p = f){

  # Create empty data frames
  y <- array(NA, dim = c(R, T))

  z <- rbinom(R, 1, psi)

  prob <- z * p

  for(j in 1:T){

    y[,j] <- rbinom(R, 1, prob)

  }

  return(list(R = R, T = T,
              psi = psi, p = p,
              z = z, y = y))
}

# Define model in BUGS language

sink("model.txt")
cat("
model{

# Priors

psi ~ dunif(0,1)
p ~ dunif(0,1)

# Ecological model for the true abundance

for(i in 1:R){

      z[i] ~ dbern(psi)

}

# Obervational model

for(i in 1:R){

 for(j in 1:T){

           p.eff[i,j] <- z[i] * p

           y[i,j] ~ dbern(p.eff[i,j])             # Detection
```

```
            y.new[i,j] ~ dbern(p.eff[i,j])         # Simulated data

      } #js

} #is

}
", fill = TRUE)
sink()

# Monitor Parameters
params <- c("psi", "p")

# MCMC settings
ni <- 10000
nt <- 10
nb <- 100
nc <- 3

# Create vectors with parameters for simulated data
Tpsi <- seq(from = 0.1, to = 1, by = 0.1)

Tp <-  seq(from = 0.1, to = 1, by = 0.1)

sit <- seq(from = 5, to = 200, by = 20)

surv <- seq(from = 1, to = 10, by = 2)


nsheet <- length(Tpsi) * length(Tp) * length(sit) * length(surv)
nrow <- 25
ncol <- 8

# Create empty matrix to store data
store <- array(NA, dim = c(nrow, ncol, nsheet))

colnames(store) <- c("True_psi", "True_p", "Nsurveys", "Nsites",
 "Psi_Mean", "SD", "ylo", "yhi")

Nsheet <- 1


for(g in Tpsi){                  # Psi

 for(f in Tp){                   # p

      for(h in sit){             # site

      for(n in surv){            # Number of surveys  (4)

        for(q in 1:25){          # number of simulated data sets

# Simulate the data
sodata <- data.fn(R = h, T = n,
                  psi = g,
                  p = f)

# Bundle the data
win.data <- list(y = sodata$y, R = nrow(sodata$y), T =
 ncol(sodata$y))

# Create initial values
zst <- apply(win.data$y, 1, max, na.rm = T)
```

```
inits <- function() {list(z = zst)}

# Run the model
output2 <- run.jags(data = win.data,  inits = inits, monitor =
 params, burnin = nb, model = "model.txt", sample = ni, n.chains =
 nc, method = "parallel")

 # Save the output

 store[q, 1, Nsheet] <- sodata$psi

 store[q, 2, Nsheet] <- sodata$p

 store[q, 3, Nsheet] <- sodata$T

 store[q, 4, Nsheet] <- sodata$R

 store[q, c(5,6,7,8), Nsheet] <- c(output2$summaries[1,4],
 output2$summaries[1,5], output2$summaries[1,1],
 output2$summaries[1,3])

                 }
Nsheet <- Nsheet + 1
          }
     }
 }
}
```

SUPPLEMENT 3.1

To correct for misclassification of individual disease state, I multiplied the traditional host observation matrix (*d*) used to correct for host detection probability by a misclassification matrix (*g*) used to adjust for imperfect pathogen detection probability on the host, where:

$$d = \begin{bmatrix} 0 & 0 & 1 \\ p_{2,j,t} & 0 & 1 - p_{2,j,t} \\ 0 & p_{3,j,t} & 1 - p_{3,j,t} \\ 0 & 0 & 1 \end{bmatrix}$$

$$g = \begin{bmatrix} 1 & 0 & 0 \\ e_{j,t+1} & (1 - e_{j,t+1}) & 0 \\ 0 & 0 & 1 \end{bmatrix}$$

SUPPLEMENT 3.2

Methods

I double swabbed a subset of all individuals captured in streams, including other species, twice in sequence and labeled samples as "swab1" and "swab2" (Table S1). By including all species in the analysis, I am assuming that pathogen detection probability does not vary by species identification, and that pathogen detection heterogeneity is only attributed to the number of zoospores a host carries.
These replicate swabs were used to estimate imperfect pathogen detection that was used in the multi-state Jolly-Seber model.

I tried to run this analysis with only the double swabs collected for *E. prosoblepon,* but there were not enough samples to calculate imperfect pathogen detection, where credible intervals were very large. I double swabbed 70 *E. prosoblepon*. Of the 70 double swabs, 21 individuals tested *Bd* positive at least once, with 17 individuals testing positive once and four individuals testing positive twice.

Statistical analysis

First, I modeled *Bd* prevalence (ψ) as the proportion of individuals that are infected. The probability that the *i*th individual is infected is a Bernoulli random variable where:

$$z_i \sim \text{Bernoulli}(\psi).$$

I included season and habitat covariates in the prevalence model, where I expected that the proportion of individuals infected differ between seasons and habitat, such that:

$$\square\square\square\square\square(\square_{\square}) = \square 1 + \square 1\square\square\square_{\square} + \square 2\square\square\square\square\square\square_{\square}.$$

I modeled pathogen detection probability on the *i*th infected host on the *j*th swab sample as:

$$\square_{\square,\square}|\square_{\square} \sim \square\square\square\square(\square_{\square,\square}),$$

so that pathogen detection probability is Bernoulli distributed with probability if the individual is infected, , and zero if it is not. I included the relationship between detection probability and infection intensity of the *i*th host (modeled below) as:

$$\square\square\square\square\square(\square_{\square,\square}) = \square 2 + \square 3\square_{\square}.$$

Next, I considered host infection intensity. If the *i*th individual is infected ($\square_{\square}$= 1), then the log-transformed infection intensity ($\square_{\square}$) is a random sample from a normal distribution with mean $\square_{\square}$, and standard deviation, $\square$:

$$\square_{\square}|\ \square_{\square} \sim \square\square\square\square\square\square\square(\square_{\square}, \square).$$

I allowed the average infection intensity of the *i*th infected host to vary by season and habitat:

$$\square_{\square} = \square 3 + \square 4\square\square\square_{\square} + \square 5\square\square\square\square\square\square_{\square}.$$

I also accounted for measurement error in host infection intensity, where multiple swabs of the same individual can give different estimates of infection intensity. I assumed that infection intensity measurement error of the *j*th sample on the *i*th host is a draw from a normal distribution with error, $\square$:

$$\square_{\square} \sim \square\square\square\square\square\square\square(\square_{\square}, \square).$$

Model fit

I fit our model using Bayesian methods and estimated the posterior distributions for all parameters using Markov chain Monte Carlo (MCMC) methods implemented in JAGS 4.0.0 in the R environment (R Core Team 2015) using the "jagsUI" package (Kellner, 2015). I log transformed the data. For all parameters, Iused non-informative normal priors (i.e., normal(0, 0.368); Lunn et al. 2000). I ran three chains for each parameter and ran each chain for 50,000 iterations, with a burn-in period of 10,000 iterations, and thinned by 50. I evaluated convergence of chains by visual inspecting trace plots, and using the diagnostics of Gelman, where Rhat < 1.1 (Brooks & Gelman 1998). I also assessed model fits using posterior predictive checks (Gelman et al. 2004), where a value close to 0.5 indicates adequate model fit.

Results

I swabbed 434 individuals from 23 species (Table S1). I collected 148 and 286 in streams during the dry season and during the two wet seasons. I double swabbed 99 individuals during the entire study, with 53 during the dry and 46 during the two wet seasons. Of the 99 double swabbed individuals, a total of 34 individuals tested positive at least once, with 26 testing positive once, and 8 were positive twice, where qPCR was > 0 ZGE. Our data fit the detection-adjusted models well (Fig S1).

Pathogen detection probability increased as individual infection intensity increased (Fig. S2). Detection probability reached ~99.99% around 54 ZGE.

Table S1 Summary of species included in the imperfect pathogen detection analysis and the number of samples collected for each. All of these species are primarily riparian.

Genus	Species	No. of samples
Boltiglossa	*schizodactyla*	2
Centrolene	*sp.*	2
Craugastor	*sp.*	2
Diasporus	*"orange"*	2
Espadarana	*prosoblepon*	261
Hyalinobatrachium	*colymbiphyllum*	18
Hyalinobatrachium	*vireovittatum*	1
Hyloscirtus	*colymba*	2
Hyloscirtus	*palmeri*	4
Oedipina	*sp.*	1
Pristimantis	*cerasinus*	4
Pristimantis	*cruentus*	17
Pristimantis	*museosus*	7
Pristimantis	*pardalis*	1
Pristimantis	*ridens*	2
Pristimantis	*sp.*	3
Rhaebo	*haematiticus*	2
Sachatamia	*albomaculata*	55
Sachatamia	*ilex*	7
Silverstoneia	*sp.*	29
Silverstoneia	*flotator*	8
Smilisca	*silia*	2
Smilisca	*sp.*	2
	Total	434

Table S2 Summary of the posterior distributions from the model. All parameters were back transformed to their original scale, except detection probability on the logit scale. Bold values are the ones I used in the multi-state Jolly-Seber model.

	Mean	95% Credible interval	
Infection intensity (ZGE)			
Dry	0.77	0.23	0.97
Wet	0.56	0.1	0.95
Stream	0.8	0.28	0.97
Standard deviation	16.25	4.57	43.2
Prevalence (Infected/Total)			
Dry	0.65	0	1887
Wet	1.39	0	3663
Stream	0.33	0	16.03
Measurement error			
Error	4.55	2.82	9.52
Detection probability (logit)			
Alpha	**-0.37**	**-1.26**	**0.42**
Beta	**0.89**	**0.34**	**1.41**

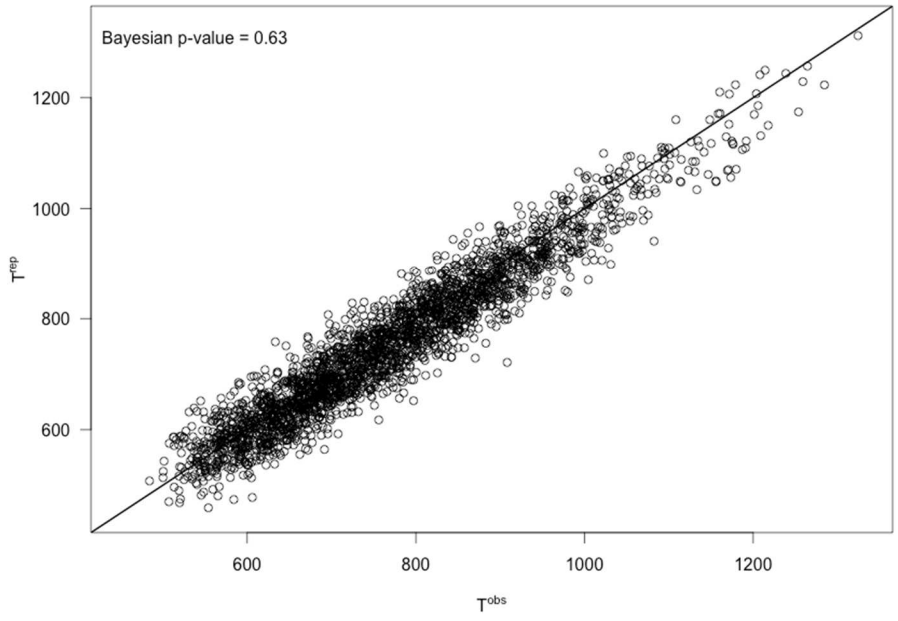

Figure S1 Bayesian posterior predictive check, where I compare our data set and simulated data sets to expected values. The average difference between our data set and the simulated data set to expected values should be close to 0.5, indicating that the model fits well. Extreme differences between our data set and the simulated data set to the expected values (i.e., 0.05 or 0.95) indicate poor model fit.

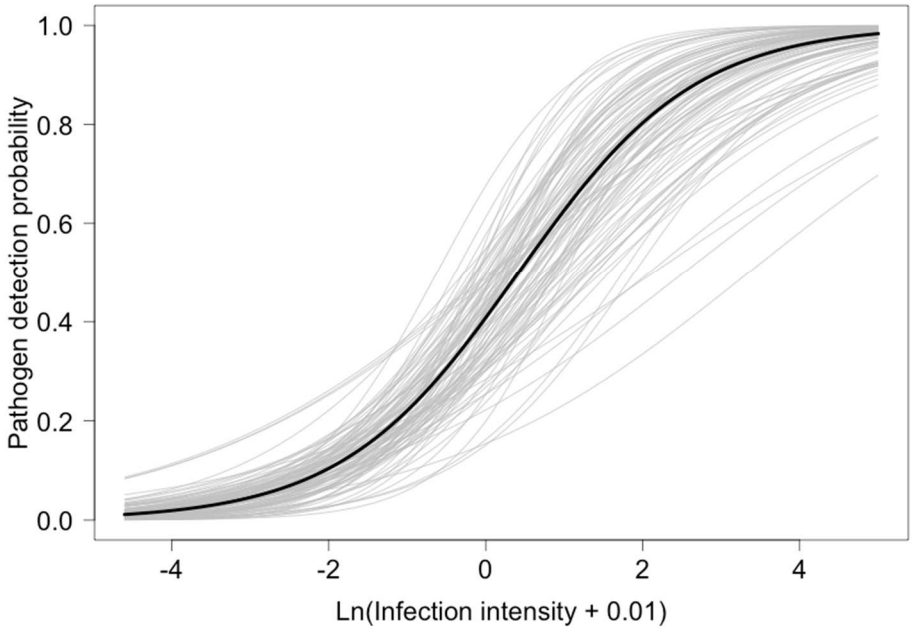

Figure S2 The relationship between pathogen detection probability and individual infection intensity on the natural log scale caused by swabbing error. The dark line is the mean posterior distribution estimates, and light gray lines represent model iterations.

SUPPLEMENT 3.3

Code to analyze a multi-state Jolly-Seber model with imperfect host and pathogen detection in JAGS.

```
#------------- Analysis of the model

sink("CJS.txt")
cat("
model{

# Priors and constraints

for(t in 1:(n.occasions-1)){

    gamma1[t] ~ dunif(0, 1)
    gamma2[t] ~ dunif(0, 1)

}

alpha_A1 ~ dnorm(0, 0.368)
alpha_A2 ~ dnorm(0, 0.368)

alpha_AB ~ dnorm(0, 0.368)
alpha_BA ~ dnorm(0, 0.368)

beta_p ~ dnorm(0, 0.368)

for(m in 1:2){

  alpha_muB[m] ~ dnorm(0, 0.368)
  alpha_muA[m] ~ dnorm(0, 0.368)

  beta_A[m] ~ dnorm(0, 0.368)

}

#------- Logit scale

for(i in 1:nind){

  for(t in 1:(n.occasions - 1)){

    lphiA[i, t] <- alpha_A1
    lphiB[i, t] <- alpha_A2 + beta_A[det2[i, t]] * II[i,t]

    lpsiAB[i, t] <- alpha_AB
    lpsiBA[i, t] <- alpha_BA
    lpA[i, t] <- alpha_muA[det2[i, t]] + beta_p * survs[i,t]
    lpB[i, t] <- alpha_muB[det2[i, t]] + beta_p * survs[i,t]

  }

}

#----- Misclassification probability

#---- Priors based off double swab analysis
```

```
mu ~ dunif(-3.650, -3.075)
sigma ~ dunif(1.753, 2.339)
sigma.error ~ dunif(1.359, 1.765)

tau <- 1/ (sigma * sigma)
tau.error <- 1/ (sigma.error * sigma.error)

alpha_I ~ dunif(-0.468, 0.690)
beta_I ~ dunif(0.604, 1.045)

for(t in 1:n.occasions){

  for(i in 1:nind){

  # True infection
    x[i, t] ~ dnorm(mu, tau)

  # Observed infection
    II[i, t] ~ dnorm(x[i, t], tau.error)

    leI2[i,t] <- alpha_I + beta_I * x[i, t]

  }
}

#--------- Probability scale

for(i in 1:nind){

  for(t in 1:(n.occasions - 1)){

    phiA[i, t] <- exp(lphiA[i, t]) / (1+ exp(lphiA[i, t]))
    phiB[i, t] <- exp(lphiB[i, t]) / (1+ exp(lphiB[i, t]))

    psiAB[i, t] <- exp(lpsiAB[i, t]) / (1+ exp(lpsiAB[i, t]))
    psiBA[i, t] <- exp(lpsiBA[i, t]) / (1+ exp(lpsiBA[i, t]))

    pA[i, t] <- exp(lpA[i, t]) / (1+ exp(lpA[i, t]))
    pB[i, t] <- exp(lpB[i, t]) / (1+ exp(lpB[i, t]))
  }

  for(t in 1:n.occasions){

    eI[i, t] <- 1 - (exp(leI2[i, t]) / (1 + exp(leI2[i, t])))

  }

}

#----------- Define state-transition and observational matrix

for(i in 1:nind){

  for(t in 1:(n.occasions-1)){

# Define probabilities of state S(t+1) given S(t)

    ps[1, i, t, 1] <- 1 - gamma1[t] - gamma2[t]
    ps[1, i, t, 2] <- gamma1[t]
    ps[1, i, t, 3] <- gamma2[t]
    ps[1, i, t, 4] <- 0

    ps[2, i, t, 1] <- 0
```

```
    ps[2, i, t, 2] <- phiA[i, t]^days[i,t] * (1- psiAB[i,
t]^days[i,t])
    ps[2, i, t, 3] <- phiA[i, t]^days[i,t] * psiAB[i, t]^days[i,t]
    ps[2, i, t, 4] <- 1-phiA[i, t]^days[i,t]

    ps[3, i, t, 1] <- 0
    ps[3, i, t, 2] <- phiB[i, t]^days[i,t] * psiBA[i, t]^days[i,t]
    ps[3, i, t, 3] <- phiB[i, t]^days[i,t] * (1 - psiBA[i,
t]^days[i,t])
    ps[3, i, t, 4] <- 1 - phiB[i, t]^days[i,t]

    ps[4, i, t, 1] <- 0
    ps[4, i, t, 2] <- 0
    ps[4, i, t, 3] <- 0
    ps[4, i, t, 4] <- 1

# Define probabilities of O(t) given S(t)

# Seen in A
    po[1, i, t, 1] <- 0
    po[1, i, t, 2] <- 0
    po[1, i, t, 3] <- 1

# Seen in B
    po[2, i, t, 1] <- pA[i, t]^days[i,t]
    po[2, i, t, 2] <- 0
    po[2, i, t, 3] <- (1 - pA[i, t]^days[i,t])

# Dead
    po[3, i, t, 1] <- pB[i, t]^days[i,t] * eI[i, t+1]
    po[3, i, t, 2] <- pB[i, t]^days[i,t] * (1- eI[i, t+1])
    po[3, i, t, 3] <- (1 - pB[i, t]^days[i,t])

    po[4, i, t, 1] <- 0
    po[4, i, t, 2] <- 0
    po[4, i, t, 3] <- 1


  } #ts

} # is

#----------------- Likelihood

for(i in 1:nind){

#---------- Define latent state at first capture

      z[i, 1] <- 1                  # Everyone is in state 1 at first
occasion    # Not entered

      for(t in 2:n.occasions){

            # Observation process: draw O(t) given S(t)

                  y[i, t] ~ dcat(po[z[i, t], i, t-1, ])
      y.new[i, t] ~ dcat(po[z[i, t], i, t-1, ])

            # State process: draw S(t) given S(t-1)

                  z[i, t] ~ dcat(ps[z[i, t-1], i, t-1, ])
      }

} # is
```

```
#--------- Calculate derived population parameters

for (t in 1:(n.occasions-1)){

  qgammaN[t] <- 1-gamma1[t]
  qgammaI[t] <- 1-gamma2[t]

}

cprobN[1] <- gamma1[1]
cprobI[1] <- gamma2[1]


for (t in 2:(n.occasions-1)){

    cprobN[t] <- gamma1[t] * prod(qgammaN[1:(t-1)])
    cprobI[t] <- gamma2[t] * prod(qgammaI[1:(t-1)])

} #ts

psiN <- sum(cprobN[])          # Inclusion probability
psiI <- sum(cprobI[])         # Inclusion probability

for (t in 1:(n.occasions-1)){
    bN[t] <- cprobN[t] / psiN      # Entry probability
    bI[t] <- cprobI[t] / psiI      # Entry probability
} #t

for (i in 1:nind){
   for (t in 2:n.occasions){
    alN[i,t-1] <- equals(z[i,t], 2)
    alI[i,t-1] <- equals(z[i,t], 3)
   } #t
  for (t in 1:(n.occasions-1)){
    dN[i,t] <- equals(z[i,t]-alN[i,t],0)
    dI[i,t] <- equals(z[i,t]-alI[i,t],0)
  } #t
    aliveN[i] <- sum(alN[i,])
    aliveI[i] <- sum(alI[i,])
} #i

for (t in 1:(n.occasions-1)){

NN[t] <- sum(alN[,t])        # Actual population size
NI[t] <- sum(alI[,t])        # Actual population size

BN[t] <- sum(dN[,t])         # Number of entries
BI[t] <- sum(dI[,t])         # Number of entries

Ntot[t] <- NN[t] + NI[t]

} #t

for (i in 1:nind){
    wN[i] <- 1-equals(aliveN[i],0)
    wI[i] <- 1-equals(aliveI[i],0)
} #i
    NsuperN <- sum(wN[])            # Superpopulation size
    NsuperI <- sum(wI[])            # Superpopulation size

      Nsuper <- sum(NsuperN, NsuperI)

#---- Calculate average infection intensity
```

```
for(t in 1:(n.occasions-1)){

    inf[t] <- mean(alI[,t] * x[,t])
      # All the ones that were alive + infected = alI[,t]
      # The corrected infection intensity = x[, t]
}

#----- These are the ones you want it to report

#---------------- Calculate Bayesian posterior predictive check

for(t in 1:(n.occasions-1)){

  for(i in 1:nind){

    for(s in 1:state){

       r[s, i, t] <- ifelse(y[i, t+1] == s, 1, 0)

   r.new[s, i, t] <- ifelse(y.new[i, t+1] == s, 1, 0)

    }
  }
}


for(t in 1:(n.occasions-1)){

  for(s in 1:state){

    # sum across individuals in each state, each time period

    R_state[s, t] <- sum(r[s, , t])

    R_state.new[s, t] <- sum(r.new[s, , t])

  }

}

for(t in 1:(n.occasions-1)){

  for(s in 1:state){

      for(i in 1:nind){

          muy[i, t, s] <-  ps[z[i, t], i, t, z[i, t+1]] * po[z[i, t],
i, t, s]

      }

      PO_expt[s, t] <- sum(0.01, sum(muy[ , t, s]))

  }

}

#--------- Posterior predictive check

for(t in 1:(n.occasions-1)){

  for(s in 1:state){
```

```
    E.act[s, t] <- pow(pow(R_state[s, t], 0.5) - pow(PO_expt[s, t],
0.5), 2)

    E.new[s, t] <- pow(pow(R_state.new[s, t], 0.5) - pow(PO_expt[s,
t], 0.5), 2)


  }

}


zzz.fit <- sum(E.act[,])
zzz.fit.new <- sum(E.new[,])


}
", fill = TRUE)
sink()
```

Model output for (1) null model, (2) host density, (3) pathogen prevalence, and (4) infection intensity effects on *Bd* transmission risk.

(1) Infection ~ 1

JAGS output for model 'model2.txt', generated by jagsUI.
Estimates based on 3 chains of 70000 iterations,
burn-in = 20000 iterations and thin rate = 50,
yielding 3000 total samples from the joint posterior.
MCMC ran in parallel for 30.804 minutes at time 2016-04-09 08:54:31.

	mean	sd	2.5%	50%	97.5%	overlap0	f	Rhat	n.eff
alpha.lamN	0.187	0.184	-0.155	0.183	0.581	TRUE	0.857	1.012	1177
alpha.lamI	1.082	0.135	0.821	1.080	1.353	FALSE	1.000	1.004	472
alpha_N	2.659	0.509	1.818	2.592	3.818	FALSE	1.000	1.007	3000
alpha_I	2.858	0.379	2.220	2.820	3.681	FALSE	1.000	1.007	1771
gammaN[1]	-2.382	1.198	-4.776	-2.194	-0.548	FALSE	0.999	1.024	92
gammaN[2]	-0.763	0.752	-3.175	-0.584	0.101	TRUE	0.948	1.072	64
gammaI[1]	-2.951	1.243	-4.898	-3.025	-0.556	FALSE	0.995	1.005	1100
gammaI[2]	0.272	0.648	-1.048	0.378	0.957	TRUE	0.818	1.059	439
alpha_IN	-1.610	0.973	-3.848	-1.462	-0.145	FALSE	0.989	1.000	3000
mu	-1.422	1.024	-3.736	-1.270	0.100	TRUE	0.957	1.000	3000
alpha.pN[1]	-1.968	0.213	-2.417	-1.965	-1.568	FALSE	1.000	1.014	317
alpha.pN[2]	-2.461	0.315	-3.159	-2.452	-1.869	FALSE	1.000	1.020	278
alpha.pI[1]	-1.778	0.178	-2.130	-1.777	-1.442	FALSE	1.000	1.001	1665
alpha.pI[2]	-1.795	0.211	-2.230	-1.781	-1.412	FALSE	1.000	1.009	2555
beta.pN	0.490	0.147	0.209	0.489	0.780	FALSE	1.000	1.002	886
zzzfitN	296.042	14.293	270.473	295.279	326.615	FALSE	1.000	1.017	619
zzzfitN.new	282.662	23.666	239.295	281.690	332.927	FALSE	1.000	1.004	711
zzzfitI2	632.938	17.711	600.198	632.363	669.215	FALSE	1.000	1.004	799
zzzfitI2.new	660.024	34.337	595.248	658.559	731.584	FALSE	1.000	1.003	517
NT[1]	416.593	41.815	346.000	412.000	512.000	FALSE	1.000	1.008	560
NT[2]	288.685	45.022	212.000	285.000	389.000	FALSE	1.000	1.013	819
NT[3]	433.347	51.391	345.000	430.000	543.000	FALSE	1.000	1.002	2380
NT[4]	305.442	47.366	228.000	300.000	410.000	FALSE	1.000	1.008	2891
NNT[1]	121.705	20.847	91.000	119.000	168.000	FALSE	1.000	1.047	635
NNT[2]	86.478	27.108	49.000	82.000	148.025	FALSE	1.000	1.042	331
NNT[3]	123.340	23.502	87.000	120.500	177.000	FALSE	1.000	1.027	197
NNT[4]	92.588	27.424	55.975	88.000	161.000	FALSE	1.000	1.028	542
NIT[1]	294.888	35.995	233.000	291.500	375.000	FALSE	1.000	1.005	354
NIT[2]	202.207	38.328	144.000	197.000	296.000	FALSE	1.000	1.018	662
NIT[3]	310.007	44.293	236.000	306.000	411.025	FALSE	1.000	1.001	2696
NIT[4]	212.853	40.444	153.000	206.000	307.000	FALSE	1.000	1.015	1214

deviance 0.000 0.000 0.000 0.000 0.000 FALSE 1.000 NaN 1

Successful convergence based on Rhat values (all < 1.1).
Rhat is the potential scale reduction factor (at convergence, Rhat=1).
For each parameter, n.eff is a crude measure of effective sample size.

overlap0 checks if 0 falls in the parameter's 95% credible interval.
f is the proportion of the posterior with the same sign as the mean;
i.e., our confidence that the parameter is positive or negative.

DIC info: (pD = var(deviance)/2)
pD = 0 and DIC = 0
DIC is an estimate of expected predictive error (lower is better).

(2) Infection ~ Host density

JAGS output for model 'model2.txt', generated by jagsUI.
Estimates based on 3 chains of 70000 iterations,
burn-in = 20000 iterations and thin rate = 50,
yielding 3000 total samples from the joint posterior.
MCMC ran in parallel for 35.828 minutes at time 2016-04-09 09:31:07.

	mean	sd	2.5%	50%	97.5%	overlap0	f	Rhat	n.eff
alpha.lamN	0.177	0.176	-0.158	0.172	0.534	TRUE	0.844	1.001	2977
alpha.lamI	1.086	0.142	0.822	1.081	1.378	FALSE	1.000	1.035	63
alpha_N	2.775	0.538	1.889	2.708	3.994	FALSE	1.000	1.004	555
alpha_I	2.972	0.435	2.289	2.915	3.990	FALSE	1.000	1.043	56
gammaN[1]	-2.263	1.194	-4.778	-2.030	-0.452	FALSE	0.999	1.007	289
gammaN[2]	-0.877	0.861	-3.632	-0.656	0.030	TRUE	0.965	1.008	1149
gammaI[1]	-2.705	1.387	-4.881	-2.787	-0.142	FALSE	0.985	1.055	46
gammaI[2]	0.032	0.878	-2.772	0.264	0.884	TRUE	0.686	1.092	48
alpha_IN	-1.627	0.988	-4.003	-1.453	-0.177	FALSE	0.992	1.000	3000
mu	-1.278	1.113	-3.761	-1.109	0.424	TRUE	0.888	1.001	3000
alpha_H	-0.933	0.991	-3.126	-0.844	0.781	TRUE	0.823	1.001	1869
alpha.pN[1]	-1.941	0.214	-2.370	-1.942	-1.541	FALSE	1.000	1.002	1029
alpha.pN[2]	-2.510	0.316	-3.132	-2.507	-1.887	FALSE	1.000	1.001	3000
alpha.pI[1]	-1.769	0.165	-2.095	-1.768	-1.458	FALSE	1.000	1.035	74
alpha.pI[2]	-1.858	0.254	-2.405	-1.836	-1.408	FALSE	1.000	1.062	40
beta.pN	0.481	0.146	0.193	0.481	0.763	FALSE	0.999	1.003	700
zzzfitN	295.308	13.963	270.333	294.238	324.580	FALSE	1.000	1.002	1160
zzzfitN.new	282.697	23.213	239.879	282.053	331.137	FALSE	1.000	1.000	3000
zzzfitI2	635.190	18.892	600.712	634.624	674.676	FALSE	1.000	1.030	79
zzzfitI2.new	663.292	36.508	597.599	661.416	741.909	FALSE	1.000	1.017	129
NT[1]	415.994	44.042	341.975	413.000	514.000	FALSE	1.000	1.031	73
NT[2]	307.160	59.751	215.000	297.000	454.025	FALSE	1.000	1.052	45
NT[3]	428.001	48.043	344.000	424.000	530.025	FALSE	1.000	1.020	118

```
NT[4]       321.180 59.521 229.000 311.000 462.000    FALSE 1.000 1.039    57
NNT[1]      119.800 18.593  91.000 117.000 165.000    FALSE 1.000 1.001  1162
NNT[2]       90.062 25.033  50.000  87.000 147.025    FALSE 1.000 1.002  3000
NNT[3]      121.193 22.386  86.000 118.000 172.025    FALSE 1.000 1.004  1163
NNT[4]       96.379 26.941  55.000  92.000 161.000    FALSE 1.000 1.003  2206
NIT[1]      296.194 39.420 233.000 291.000 382.025    FALSE 1.000 1.044    58
NIT[2]      217.097 52.262 145.000 206.000 349.025    FALSE 1.000 1.081    34
NIT[3]      306.807 41.507 237.000 302.000 397.000    FALSE 1.000 1.042    68
NIT[4]      224.801 50.761 153.000 215.000 353.050    FALSE 1.000 1.075    37
deviance      0.000  0.000   0.000   0.000   0.000    FALSE 1.000   NaN     1
```

Successful convergence based on Rhat values (all < 1.1).
Rhat is the potential scale reduction factor (at convergence, Rhat=1).
For each parameter, n.eff is a crude measure of effective sample size.

overlap0 checks if 0 falls in the parameter's 95% credible interval.
f is the proportion of the posterior with the same sign as the mean;
i.e., our confidence that the parameter is positive or negative.

DIC info: (pD = var(deviance)/2)
pD = 0 and DIC = 0
DIC is an estimate of expected predictive error (lower is better).

(3) Infection ~ infection intensity

JAGS output for model 'model2.txt', generated by jagsUI.
Estimates based on 3 chains of 1e+05 iterations,
burn-in = 30000 iterations and thin rate = 100,
yielding 2100 total samples from the joint posterior.
MCMC ran in parallel for 47.164 minutes at time 2016-04-09 15:17:35.

```
              mean     sd    2.5%     50%   97.5% overlap0     f  Rhat n.eff
alpha.lamN     0.193  0.179  -0.150   0.188   0.558     TRUE 0.863 1.011   269
alpha.lamI     1.073  0.138   0.822   1.072   1.358    FALSE 1.000 1.019   117
alpha_N        2.729  0.536   1.881   2.674   3.927    FALSE 1.000 1.023   168
alpha_I        2.896  0.390   2.249   2.853   3.813    FALSE 1.000 1.026   156
gammaN[1]     -2.378  1.228  -4.831  -2.194  -0.529    FALSE 1.000 1.005   405
gammaN[2]     -0.792  0.771  -3.046  -0.614   0.111     TRUE 0.947 1.021   242
gammaI[1]     -2.849  1.264  -4.893  -2.894  -0.561    FALSE 0.998 1.010   225
gammaI[2]      0.225  0.525  -1.075   0.319   0.936     TRUE 0.756 1.039    85
alpha_IN      -1.639  0.987  -3.907  -1.498  -0.161    FALSE 0.990 1.000  2100
mu            -1.633  1.023  -3.951  -1.517   0.028     TRUE 0.973 1.003   728
alpha_I2      -0.597  0.977  -2.732  -0.450   0.992     TRUE 0.694 1.001  1952
alpha.pN[1]   -1.967  0.229  -2.434  -1.960  -1.544    FALSE 1.000 1.005  2078
alpha.pN[2]   -2.492  0.319  -3.158  -2.487  -1.903    FALSE 1.000 1.014   247
alpha.pI[1]   -1.761  0.179  -2.121  -1.755  -1.424    FALSE 1.000 1.023   103
```

alpha.pI[2] -1.796 0.225 -2.285 -1.777 -1.398 FALSE 1.000 1.027 237
beta.pN 0.489 0.151 0.191 0.491 0.785 FALSE 1.000 1.006 286
zzzfitN 296.430 14.555 269.664 295.895 327.666 FALSE 1.000 1.011 229
zzzfitN.new 283.311 23.932 237.789 282.262 332.383 FALSE 1.000 1.001 2100
zzzfitI2 631.863 18.024 598.309 631.158 669.172 FALSE 1.000 1.015 184
zzzfitI2.new 659.297 34.964 597.606 656.875 732.834 FALSE 1.000 1.008 393
NT[1] 414.170 42.014 343.000 410.000 506.000 FALSE 1.000 1.027 95
NT[2] 293.380 48.343 215.000 288.000 406.525 FALSE 1.000 1.053 79
NT[3] 428.745 52.938 338.000 423.000 543.000 FALSE 1.000 1.012 207
NT[4] 308.802 51.219 226.000 303.000 425.000 FALSE 1.000 1.030 168
NNT[1] 121.742 19.527 92.000 119.000 168.050 FALSE 1.000 1.021 193
NNT[2] 88.602 25.403 49.000 86.000 150.000 FALSE 1.000 1.022 186
NNT[3] 123.565 24.685 84.475 121.000 181.000 FALSE 1.000 1.014 932
NNT[4] 95.201 27.418 55.000 91.000 163.525 FALSE 1.000 1.019 255
NIT[1] 292.429 36.887 232.000 289.000 376.000 FALSE 1.000 1.034 82
NIT[2] 204.778 42.973 143.475 197.000 311.000 FALSE 1.000 1.061 117
NIT[3] 305.180 44.295 232.000 300.000 405.000 FALSE 1.000 1.027 103
NIT[4] 213.601 44.176 150.000 206.000 324.525 FALSE 1.000 1.043 214
deviance 0.000 0.000 0.000 0.000 0.000 FALSE 1.000 NaN 1

Successful convergence based on Rhat values (all < 1.1).
Rhat is the potential scale reduction factor (at convergence, Rhat=1).
For each parameter, n.eff is a crude measure of effective sample size.

overlap0 checks if 0 falls in the parameter's 95% credible interval.
f is the proportion of the posterior with the same sign as the mean;
i.e., our confidence that the parameter is positive or negative.

DIC info: (pD = var(deviance)/2)
pD = 0 and DIC = 0
DIC is an estimate of expected predictive error (lower is better).

(4) Infection ~ Prevalence

JAGS output for model 'model2.txt', generated by jagsUI.
Estimates based on 3 chains of 5e+05 iterations,
burn-in = 20000 iterations and thin rate = 100,
yielding 14400 total samples from the joint posterior.
MCMC ran in parallel for 248.43 minutes at time 2016-04-09 17:38:36.

	mean	sd	2.5%	50%	97.5%	overlap0	f	Rhat	n.eff
alpha.lamN	0.185	0.181	-0.166	0.181	0.547	TRUE	0.847	1.000	8476
alpha.lamI	1.076	0.135	0.822	1.073	1.353	FALSE	1.000	1.010	220
alpha_N	2.753	0.524	1.871	2.696	3.951	FALSE	1.000	1.002	1425
alpha_I	2.907	0.382	2.271	2.870	3.760	FALSE	1.000	1.025	91
gammaN[1]	-2.194	1.236	-4.790	-1.937	-0.386	FALSE	0.999	1.003	789
gammaN[2]	-0.997	0.975	-4.098	-0.720	0.062	TRUE	0.960	1.010	324

```
gammaI[1]     -2.683  1.303  -4.868  -2.661  -0.317    FALSE 0.992 1.009   252
gammaI[2]      0.166  0.643  -1.437   0.289   0.909     TRUE 0.740 1.035   148
alpha_IN      -1.624  0.981  -3.933  -1.473  -0.146    FALSE 0.988 1.000 14400
mu            -0.906  1.339  -3.623  -0.856   1.472     TRUE 0.733 1.000 14400
alpha_P       -1.025  1.450  -3.838  -1.030   1.830     TRUE 0.761 1.000 14400
alpha.pN[1]   -1.946  0.224  -2.393  -1.942  -1.515    FALSE 1.000 1.001  1654
alpha.pN[2]   -2.527  0.317  -3.135  -2.529  -1.899    FALSE 1.000 1.004   595
alpha.pI[1]   -1.755  0.176  -2.115  -1.753  -1.420    FALSE 1.000 1.004   617
alpha.pI[2]   -1.823  0.225  -2.295  -1.814  -1.408    FALSE 1.000 1.045    53
beta.pN        0.478  0.150   0.179   0.478   0.773    FALSE 0.999 1.004   455
zzzfitN      296.241 14.316 269.283 295.896 325.414    FALSE 1.000 1.001  4452
zzzfitN.new  283.818 23.533 240.487 282.771 333.062    FALSE 1.000 1.000  6712
zzzfitI2     632.979 18.221 599.075 632.427 670.377    FALSE 1.000 1.015   145
zzzfitI2.new 660.628 34.799 596.891 659.231 732.100    FALSE 1.000 1.009   231
NT[1]        413.924 41.630 342.000 410.000 504.000    FALSE 1.000 1.012   207
NT[2]        301.076 49.638 219.000 296.000 410.000    FALSE 1.000 1.051    46
NT[3]        425.629 51.808 336.000 422.000 539.000    FALSE 1.000 1.005   599
NT[4]        315.114 51.881 232.000 309.000 432.000    FALSE 1.000 1.040    58
NNT[1]       121.060 19.306  91.000 119.000 166.000    FALSE 1.000 1.001  5551
NNT[2]        92.330 26.376  51.000  89.000 151.000    FALSE 1.000 1.007   367
NNT[3]       121.215 23.583  83.000 119.000 175.000    FALSE 1.000 1.001  2069
NNT[4]        97.676 27.327  56.000  94.000 162.000    FALSE 1.000 1.004   694
NIT[1]       292.864 36.309 233.000 289.000 374.000    FALSE 1.000 1.013   190
NIT[2]       208.747 41.999 144.000 203.000 307.000    FALSE 1.000 1.053    49
NIT[3]       304.415 43.791 232.000 300.000 403.000    FALSE 1.000 1.007   482
NIT[4]       217.438 43.791 152.000 211.000 321.025    FALSE 1.000 1.048    57
deviance       0.000  0.000   0.000   0.000   0.000    FALSE 1.000   NaN     1

Successful convergence based on Rhat values (all < 1.1).
Rhat is the potential scale reduction factor (at convergence, Rhat=1).
For each parameter, n.eff is a crude measure of effective sample size.

overlap0 checks if 0 falls in the parameter's 95% credible interval.
f is the proportion of the posterior with the same sign as the mean;
i.e., our confidence that the parameter is positive or negative.

DIC info: (pD = var(deviance)/2)
pD = 0 and DIC = 0
DIC is an estimate of expected predictive error (lower is better).
```

Bibliography

Alford, R. A., & Richards, S. J. (1999) Global amphibian declines: a problem in applied ecology. Annual Review of Ecology and Systematics, 30, 133–160.

Anderson, R. M., & May, R. M. (1978) Regulation and stability of host-parasite population interactions. Journal of Animal Ecology, 47, 219–247.

Anderson, M. J., Ellingsen, K. E., & McArdle, B. H. (2006) Multivariate dispersion as a measure of beta diversity. Ecology Letters, 9, 683–693.

Angeli, N. F., DiRenzo, G. V., Cunha, A., & Lips, K. R. (2015) Effects of density on spatial aggregation and habitat associations of the glass frog *Espadarana* (*Centrolene*) *prosoblepon*. Journal of Herpetology, 49, 388–394.

Banks-Leite, C., Pardini, R., Boscolo, D., Cassano, C. R., Püttker, T., Barros, C. S., & Barlow, J. (2014) Assessing the utility of statistical adjustments for imperfect detection in tropical conservation science. Journal of Applied Ecology, 51, 849–859.

Barbour, M. T., Gerritsen, J., Snyder, B. D., & Stribling J. B (1999) Rapid bioassessment protocols for use in wadeable streams and rivers: periphyton, benthic macroinvertebrates, and fish. United States Environmental Protection Agency, Office of Water, Washington DC.

Barinaga M. (1990) Where have all the froggies gone? Science 247, 1033–4.

Bell, S. C., Alford, R. A., Garland, S., Padilla, G., & Thomas, A. D. (2013) Screening bacterial metabolites for inhibitory effects against *Batrachochytrium dendrobatidis* using a spectrophotometric assay. Diseases of Aquatic

Organisms, 103, 77–85.

Belden, L. K., Hughey, M. C., Rebollar, E. A., Umile, T. P., Loftus, S. C., Burzynski, E. A., Minbiole, K. P. C., House, L. L., Jensen, R. V., Becker, M. H., Walke, J. B., Medina, D., Ibáñez, R., & Harris, R. N. (2015). Panamanian frog species host unique skin bacterial communities. Frontiers in Microbiology, 6, 1–21.

Benjamini, Y., & Y. Hochberg. (1995) Controlling the false discovery rate- a practical and powerful approach to multiple testing. Journal of the Royal Statistical Society Series B- Methological, 57, 289–300.

Best, A., White, A., & Boots, M. (2008) Maintenance of host variation in tolerance to pathogens and parasites. Proceedings of the National Academy of Sciences of the United States of America, 105, 20786–20791.

Blaustein, A. R., & Wake, D. B. (1990) Declining amphibian populations: a global phenomenon? Trends in Ecolology and Evolution, 7, 203–204.

Boyle, D., Boyle, D., Olsen, V., Morgan, J. & Hyatt, A. (2004) Rapid quantitative detection of chytridiomycosis (*Batrachochytrium dendrobatidis*) in amphibian samples using real-time Taqman PCR assay. Diseases of Aquatic Organisms, 60, 141–148.

Brem, F., & Lips, K. (2008) *Batrachochytrium dendrobatidis* infection patterns among Panamanian amphibian species, habitats and elevations during epizootic and enzootic stages. Diseases of Aquatic Organisms, 81, 189–202.

Briggs, C.J., Knapp, R.A. & Vredenburg, V.T. (2010) Enzootic and epizootic dynamics of the chytrid fungal pathogen of amphibians. Proceedings of the

National Academy of Sciences of the United State of America, 107, 9695-9700.

Brooks, S. P. & Gelman, A. (1998) General methods for monitoring convergence of iterative simulations. Journal of Computational and Graphical Statistics, 7, 434–455

Cashins, S. D., Grogan, L. F., McFadden, M., Hunter, D., Harlow, P. S., Berger, L., & Skerratt, L. F. (2013) Prior infection does not improve survival against the amphibian disease Chytridiomycosis. PloS One, 8, e56747.

Chase, J. M., & Leibold, M. A. (2003) Ecological niches: linking classical and contemporary approaches (interspecific interactions). The University of Chicago Press, Chicago, IL.

Cheng, T. L., S. M. Rovito, D. B. Wake, & V. T. Vredenburg. (2011) Coincident mass extirpation of neotropical amphibians with the emergence of the infectious fungal pathogen *Batrachochytrium dendrobatidis*. Proceedings of the National Academy of Sciences of the United States of America, 108, 9502–9507.

Chelgren, N. A. D., Adams, M. I. J., Bailey, L. A. L., & Bury, R. B. (2011) Using multilevel spatial models to understand salamander site occupancy patterns after wildfire. Ecology, 92, 408–421.

Chestnut, T., Anderson, C., Popa, R., Blaustein, A. R., Voytek, M., Olson, D. H., & Kirshtein, J. (2014) Heterogeneous occupancy and density estimates of the pathogenic fungus *Batrachochytrium dendrobatidis* in waters of North America. PloS One, 9, e106790.

Collier, B. A., Morrison, M. L., Farrell, S. L., Campomizzi, A. J., Butcher, J. A., Hays, K. B., MacKenzie, D. I., & Wilkins, R. N. (2010) Monitoring golden cheeked warblers on private lands in Texas. Journal of Wildlife Management, 74, 140–147.

Collins J. P., & Crump M. L. (2009) Extinction in our times: global amphibian decline. Oxford University Press, Oxford.

Colón-Gaud, C., Whiles, M. R., Lips, K. R., Pringle, C. M., Kilham, S. S., Connelly, S., Brenes, R., & Peterson, S. D. (2010) Stream invertebrate responses to a catastrophic decline in consumer diversity. Journal of the North American Benthological Society, 29, 1185–1198.

Coltherd, J. C., Morgan, C., Judge, J., Smith, L. A., & Hutchings, M. R. (2010) The effect of parasitism on recapture rates of wood mice (*Apodemus sylvaticus*). Wildlife Research, 37, 413–417.

Conn, P. B., & Cooch, E. G. (2009) Multistate capture-recapture analysis under imperfect state observation: an application to disease models. Journal of Applied Ecology, 46, 486–492.

Corey, S. J., & Waite, T. A. (2008) Phylogenetic autocorrelation of extinction threat in globally imperilled amphibians. Diversity and Distributions, 14, 614–629.

Crawford, A. J., Lips, K. R., & Bermingham, E. (2010) Epidemic disease decimates amphibian abundance, species diversity, and evolutionary history in the highlands of Central Panama. Proceedings of the National Academy of Sciences of the United States of America, 107, 13777–13782.

Crump, M. L. (1974) Reproductive strategies in a tropical anuran community. Miscellaneous Publications, University of Kansas Museum of Natural History. 61, 1–68.

Crump, M. L., Hensley, F. R., & Clark, K. L. (1992) Apparent decline of the Golden Toad: underground or extinct? Copeia, 1992, 413–420.

Dail, D., & Madsen, L. (2011) Models for estimating abundance from repeated counts of an open metapopulation. Biometrics, 67, 577–587.

DiRenzo, G. V, Langhammer, P. F., Zamudio, K. R., & Lips, K. R. (2014) Fungal infection intensity and zoospore output of *Atelopus zeteki*, a potential acute chytrid supershedder. PloS One, 9, e93356.

Dobson, A. (2000) Raccoon rabies in space and time. Proceedings of the National Academy of Sciences of the United States of America, 97, 14041–14043.

Duellman, W. E. (1999) Patterns of distribution of amphibians: a global perspective. Johns Hopkins University Press, Baltimore, MD.

Duellman, W. E., & Trued, L. (1986) The Biology of Amphibians. McGraw-Hill Books Company, New York, NY.

Ellison, A. R., Savage, A. E., DiRenzo, G. V., Langhammer, P., Lips, K. R., & Zamudio, K. R. (2014) Fighting a losing battle: vigorous immune response countered by pathogen suppression of host defenses in the chytridiomycosis-susceptible frog *Atelopus zeteki*. G3: Genes, Genomes, Genetics, 4, 1275–1289.

Ellison, A. R., Tunstall, T., DiRenzo, G. V., Hughey, M. C., Rebollar, E. A., Belden, L. K., Harris, R. N., Ibanez, R., Lips, K. R., & Zamudio, K. R. (2015) More

than skin deep: functional genomic basis for resistance to amphibian chytridiomycosis. Genome Biology and Evolution, 7, 286–98.

Ferraz, G., Nichols, J. D., Hines, J. E., Stouffer, P. C., Bierregaard, R. O. Jr & Lovejoy, T. E. (2007) A large-scale deforestation experiment: effects of patch area and isolation on Amazon birds. Science, 315, 238–241.

Fisher, M. C., Garner, T. W. J., & Walker, S. F. (2009) Global emergence of *Batrachochytrium dendrobatidis* and amphibian chytridiomycosis in space, time, and host. Annual Review of Microbiology, 63, 291–310.

Garmyn, A., Van Rooij, P., Pasmans, F., Hellebuyck, T., Van Den Broeck, W., Haesebrouck, F., & Martel, A. (2012) Waterfowl: Potential Environmental Reservoirs of the Chytrid Fungus *Batrachochytrium dendrobatidis*. PLoS ONE, 7, e35038.

Garner, T. W. J., Walker, S., Bosch, J., Leech, S., Marcus Rowcliffe, J., Cunningham, A. A., & Fisher, M. C. (2009) Life history tradeoffs influence mortality associated with the amphibian pathogen *Batrachochytrium dendrobatidis*. Oikos, 118, 783–791.

Gehring, C. A, Mueller, R. C., Haskins, K. E., Rubow, T. K., & Whitham, T. G. (2014) Convergence in mycorrhizal fungal communities due to drought, plant competition, parasitism, and susceptibility to herbivory: consequences for fungi and host plants. Frontiers in Microbiology, 5, 1–9.

Gelman, A., Carlin, J. B., Stern, H. S. & Rubin, D. B. (2004) Bayesian Data Analysis, 2nd edition. Chapman and Hall/CRC, New York, NY.

Gillies, C. S., Hebblewhite, M., Nielsen, S. E., Krawchuk, M. A., Aldridge, C. L., Frair, J. L., Saher, D. J., Stevens, C. E., & Jerde, C. L. (2006) Application of random effects to the study of resource selection by animals. Journal of Animal Ecology, 75, 887–898.

Gonzalez, A., & Chaneton, E. J. (2002) Heterotroph species extinction, abundance and biomass dynamics in an experimentally fragmented microecosystem. Journal of Animal Ecology, 71, 594–602.

Gonzalez, A., Ronce, O., Ferriere, R., & Hochberg, M. E. (2013) Evolutionary rescue: an emerging focus at the intersection between ecology and evolution. Philosophical Transactions of the Royal Society B: Biological Sciences, 368, 20120404.

Gu, T., Pung, H. K., Zhang, D. Q., Pung, H. K., & Zhang, D. Q. (2004) A bayesian approach for dealing with uncertain contexts.

Guillera-Arroita, G., Ridout, M. S., & Morgan, B. J. T. (2010) Design of occupancy studies with imperfect detection. Methods in Ecology and Evolution, 1, 131–139.

Guillera-Arroita, G. (2011) Impact of sampling with replacement in occupancy studies with spatial replication. Methods in Ecology and Evolution, 2, 401–406.

Harmon, L. J., Weir, J. T., Brock, C. D., Glor, R. E., & Challenger, W. (2008) GEIGER: investigating evolutionary radiations. Bioinformatics, 24, 129-131.

Heard, G. W., Robertson, P., & Scroggie, M. P. (2006) Assessing detection probabilities for the endangered growling grass frog (*Litoria raniformis*) in southern Victoria. Wildlife Research, 33, 557–564.

Heyer, W. R. (1976) Studies in larval amphibian habitat partitioning. Smithsonian Contributions in Zoology, 242, 1–27.

Heyer, W. R., Donnelly, M. A., McDiarmid, R. W., Hayek, L., & Foster, M. S. (1994) Measuring and monitoring biological diversity. Standard methods for amphibians. Smithsonian Institution Press, Washington, DC.

Hines, J. E., Nichols, J. D., Royle, J. A., MaKenzie, D. I., Gopalaswamy, A. M., & Kumar, N. S. (2010) Tigers on trails: occupancy modeling for cluster sampling. Ecological Applications, 20, 1456–1466.

Hyatt, A. D., Boyle, D. G., Olsen, V., Boyle, D. B., Berger, L., Obendorf, D., Dalton, A., Kriger, K., Hero, M., Hines, M., Phillott, R., Campbell, R., Marantelli, G., Gleason, F. & Colling, A. (2007) Diagnostic assays and sampling protocols for the detection of *Batrachochytrium dendrobatidis*. Diseases of Aquatic Organisms, 73, 175–192.

Inger, R. F., Voris, H. K., & Frogner, K. J. (1986) Organization of a community of tadpoles in rain forest streams in Borneo. Journal of Tropical Ecology, 2, 193–205.

James, T. Y., A. P. Litvintseva, R. Vilgalys, J. A. T. Morgan, J. W. Taylor, M. C. Fisher, Berger, L., Weldon, C., du Preez, L., & Longcore, J. E. (2009) Rapid expansion of an emerging fungal disease into declining and healthy amphibian populations. PLoS Pathogens, 5, e1000458.

James, T. Y., Toledo, L. F., Rödder D., da Silva, L. D., Belasen, A., Betancourt-Román, C. M., Jenkinson, T. S., Lambertini, C., Longo, A. V., Ruggeri J, Collins, J. P., Burrowes, P. A., Lips, K. R., Zamudio, K. R., & Longcore, J. E. (2015) Disentangling host, pathogen, and environmental determinants of a recently emerged wildlife disease: lessons from the first 15 years of amphibian chytridiomycosis research. Ecology and Evolution, doi: 10.1002/ece3.1672.

Johnson, M. L., & Speare, R. (2003) Survival of *Batrachochytrium dendrobatidis* in water: quarantine and disease control implications. Emerging Infectious Diseases, 9, 922–925.

Johnson, M. L., & Speare, R. (2005) Possible modes of dissemination of the amphibian chytrid *Batrachochytrium dendrobatidis* in the environment. Diseases of Aquatic Organisms, 65, 181–186.

Kellner, K. (2015) jagsUI: a wrapper around 'rjags' to streamline 'JAGS' analyses. R package version 1.3.7. http://CRAN.R-project.org/package=jagsUI

Kendall, W. L. (2009) One size does not fit all: adapting mark-recapture and occupancy models for state uncertainty. Environmental and Ecological Statistics, 3, 765–780.

Kéry, M. (2010) Introduction to WinBUGS for ecologists: Bayesian approach to regression, ANOVA, mixed models and related analyses. Academic Press, Burlington, MA.

Kéry, M., & Schaub, M. (2012) Bayesian population analysis using WinBUGS: a hierarchical perspective. Elsevier, Oxford, UK.

Kilburn, V., Ibáñez, R., & Green, D. (2011) Reptiles as potential vectors and hosts of the amphibian pathogen *Batrachochytrium dendrobatidis* in Panama. Diseases of Aquatic Organisms, 97, 127–134.

Kriger, K. M., & Hero, J. M. (2007) Large-scale seasonal variation in the prevalence and severity of chytridiomycosis. Journal of Zoology, 271, 352–359.

Kubicki, B., Bolaños, F., Chaves, G., Solís, F., Ibáñez, R., Coloma, L. A., Ron, S. R., Wild, E., Cisneros-Heredia, D.F. & Renjifo, J. 2010. *Espadarana prosoblepon*. The IUCN Red List of Threatened Species 2010: e.T54934A11228804. http://dx.doi.org/10.2305/IUCN.UK.2010-2.RLTS.T54934A11228804.en. Downloaded on 22 March 2016.

Küng, D., Bigler, L., Davis, L. R., Gratwicke, B., Griffith, E., & Woodhams, D. C. (2014) Stability of microbiota facilitated by host immune regulation: informing probiotic strategies to manage amphibian disease. PLoS ONE, 9, e87101.

Lachish, S., Gopalaswamy, A. M., Knowles, S. C. L., & Sheldon, B. C. (2012) Site-occupancy modelling as a novel framework for assessing test sensitivity and estimating wildlife disease prevalence from imperfect diagnostic tests. Methods in Ecology and Evolution, 3, 339–348.

Lampo, M., Celsa, S. J., Rodriguez-Contreras, A., Rojas-Runjaic, F., & Garcia, C. (2011) High turnover rates in remnant populations of the Harlequin Frog *Atelopus cruciger* (Bufonidae): low risk of extinction? Biotropica, 0, 1–7.

Langwig, K. E., Frick, W. F., Bried, J. T., Hicks, A. C., Kunz, T. H., & Kilpatrick, A. M. (2012) Sociality, density-dependence and microclimates determine the

persistence of populations suffering from a novel fungal disease, white-nose syndrome. Ecology Letters, 15, 1050–7.

Larsen, T. H., Williams, N. M., & Kremen, C. 2005. Extinction order and altered community structure rapidly disrupt ecosystem functioning. Ecology Letters, 8, 538–547.

Larsen, T. H., Lopera, A., & Forsyth, A. (2008) Understanding trait-dependent community disassembly: dung beetles, density functions, and forest fragmentation. Conservation Biology, 22, 1288–1298.

Lindo, Z., Whiteley, J., & Gonzalez, A. (2012) Traits explain community disassembly and trophic contraction following experimental environmental change. Global Change Biology, 18, 2448–2457.

Lips, K. R. (1998) Decline of tropical montane amphibian fauna. Conservation Biology, 12, 106–117.

Lips, K. R. (1999) Mass mortality and population declines of anurans at an upland site in western Panama. Conservation Biology, 13, 117–125.

Lips, K. R., Mendelson, J. R. III, Munoz-Alonso, A., Canseco-Marquez, L., & Mulcahy, D. G. (2004) Amphibian population declines in montane southern Mexico: resurveys of historical localities. Biological Conservation, 119, 555–564.

Lips, K. R., Diffendorfer, J., Mendelson, J. R. III, & Sears, M. W. (2008) Riding the wave: reconciling the roles of disease and climate change in amphibian declines. PLOS Biology 6:e72.

Lips, K. R., Brem, F., Brenes, R., Reeve, J. D., Alford, R. A., Voyles, J., Carey, C., Livo, L., Pessier, A. P., & Collins, J. P. (2006) Emerging infectious disease and the loss of biodiversity in a Neotropical amphibian community. Proceedings of the National Academy of Sciences of the United States of America, 103, 3165–3170.

Lips, K. R., Reeve, J. D., & Witters, L. R. (2003) Ecological traits predicting amphibian population declines in Central America. Conservation Biology, 17, 1078–1088.

Longcore, J. E., Pessier, A. P., & Nichols, D. K. (1999) *Batrachochytrium dendrobatidis* gen et sp nov, a chytridpathogenic to amphibians. Mycologia, 91, 219–227.

Longo, A. V., Lips, K. R., & Zamudio, K. R. (*in prep*) Highly competent hosts drive catastrophic diversity loss during disease emergence in a naïve amphibian community.

Longo, A. V., & Burrowes, P. A. (2010) Persistence with chytridiomycosis does not assure survival of direct-developing frogs. EcoHealth, 7, 185–195.

Longo, A. V., Burrowes, P. A., & Joglar, R. L. (2010) Seasonality of *Batrachochytrium dendrobatidis* infection in direct-developing frogs suggests a mechanism for persistence. Diseases of Aquatic Organisms, 92, 253–260.

Lunn, D., Jackson, C., Best, N., Thomas, A., & Spiegelhalter, D. (2012) The BUGS book: a practical introduction to Bayesian analysis. CRC Press, Boca Raton, FL.

Lynch, J. D., & Duellman, W. E. (1997) Frogs of genus *Eleutherodactylus* (Leptodactylidae) in Western Ecuador: systematics, ecology, and biogeography, Volume 23. pp. 1–235.

Mackenzie, D. I., & Royle, J. A. (2005) Designing occupancy studies: general advice and allocating survey effort. Journal of Applied Ecology, 42, 1105–1114.

MacKenzie, D. I., Nichols, J. D., Royle, J. A., Pollock, K. H., Bailey, L. L., & Hines, J. E. (2006) Occupancy estimation and modeling: inferring patterns and dynamics of species occurrence. Elsevier Academic Press, London, UK.

MacKenzie, D. I., Seamans, M. E., Gutierrez, R. J. & Nichols, J. D. (2011) Investigating the population dynamics of California spotted owls with-out marked individuals. Journal of Ornithology, 152, S597–S604.

Maslo, B., Valent, M., Gumbs, J. F., & Frick, W. F. (2015) Conservation implications of ameliorating survival of little brown bats with white-nose syndrome. Ecological Applications, 25, 1832–1840.

McCaffery, R., & Lips, K. R. (2013) Survival and abundance in males of the glass frog *Espadarana* (Centrolene) *prosoblepon* in Central Panama. Journal of Herpetology, 46, 213–220.

McCaffery R. M, Richards-Zawacki, C., & Lips, K. R. (2015) The demography of *Atelopus* decline: harlequin frog survival and abundance in Central Panama prior to and during a disease outbreak. Global Ecology and Conservation, 4, 232-242.

McCallum, H., Barlow, N., & Hone, J. (2001). How should pathogen transmission be modelled? *Trends in Ecology and Evolution*, *16*, 295–300.

McClanahan, T. R., & Rankin, P. (2016) Geography of conservation spending, biodiversity, and culture. Conservation Biology, 1, 153–157.

McDiarmid, R. W., & Altig, R. (1999) Tadpoles: the biology of the anuran larvae. The University of Chicago Press, Chicago, IL.

McMahon, T. A., Sears, B. F., Venesky, M. D., Bessler, S. M., Brown, J. M., Deutsch, K., Halstead, Neal T., Lentz, G., Tenouri, N., Young, S., Civitello, D. J., Ortega, N., Fites, J. S., Reinert, Laura, K., Rollins-Smith, L. A., Raffel, T. R., & Rohr, J R. (2014) Amphibians acquire resistance to live and dead fungus overcoming fungal immunosuppression. Nature, 511, 224–227.

Miller, D. A. W., Talley, B. L., Lips, K. R., & Campbell Grant, E. H. (2012) Estimating patterns and drivers of infection prevalence and intensity when detection is imperfect and sampling error occurs. Methods in Ecology and Evolution, 3, 850–859.

Mitchell, K. M., Churcher, T. S., Garner, T. W. J., & Fisher, M. C. (2008) Persistence of the emerging pathogen *Batrachochytrium dendrobatidis* outside the amphibian host greatly increases the probability of host extinction. Proceedings of The Royal Society B, 275, 329–34.

Murray, K. A, Skerratt, L. F., Speare, R., & McCallum, H. (2009) Impact and dynamics of disease in species threatened by the amphibian chytrid fungus, *Batrachochytrium dendrobatidis*. Conservation Biology, 23, 1242–1252.

Muths, E., Scherer, R. D., & Pilliod, D. S. (2011) Compensatory effects of recruitment and survival when amphibian populations are perturbed by disease. Journal of Applied Ecology 48, 873-879.

Oksanen, J., Blanchet, F. G., Kindt, R., Legendre, P., Minchin, P. R., O'Hara, R. B., Simpson, G. L., Solymos, P., Henry, M., Stevens, H., & Wagner, H. (2011) vegan: Community Ecology Package. R package version 2.0-1. http://CRAN.R-project.org/package=vegan.

Ostfeld, R. S, & LoGiudice, K. (2003) Community disassembly, biodiversity loss, and the erosion of an ecosystem service. Ecology, 84, 1421–1427.

Parris, M. J., & Cornelius T. O. (2004) Fungal pathogen causes competitive and developmental stress in larval amphibian communities. Ecology, 85, 3385–3395.

Pasmans, F., P. Zwart, & Hyatt A. D. (2004) Chytridiomycosis in the Central American Bolitoglossa salamander (*Bolitoglossa dofleini*). The Veterinary Record, 154, 153.

Pessier, A. P., Nichols, D. K., Longcore, J. E., & Fuller, M. S. (1999) Cutaneous chytridiomycosis in poison dart frogs (*Dendrobates spp.*) and White's tree frogs (*Litoria caerulea*). Journal of Veterinary Diagnostic Investigation 11, 194–199.

Phillott, A. D., Grogan, L. F., Cashins, S. D., McDonald, K. R., Berger, L., & Skerratt, L. F. (2013) Chytridiomycosis and seasonal mortality of tropical stream-associated frogs 15 Years after introduction of *Batrachochytrium dendrobatidis*. Conservation Biology: The Journal of the Society for Conservation Biology, 00, 1–11.

Pilliod, D. S., Muths, E., Scherer, R. D., Bartelt, P. E., Corn, P. S., Hossack, B. R., Lambert, B. A., McCaffery R., & Gaughan, C. (2010) Effects of amphibian

chytrid fungus on individual survival probability in wild boreal toads. Conservation Biology: The Journal of the Society for Conservation Biology, 24, 1259–67.

Piotrowski, J. S., Annis, S. L., & Longcore, J. E. (2004). Physiology of *Batrachochytrium dendrobatidis*, a chytrid pathogen of amphibians. Mycologia, 96, 9–15.

Plummer, M. (2015). rjags: Bayesian graphical models using MCMC. R package version 3-15. http://CRAN.R-project.org/package=rjags

R Core Team (2015). R: a language and environment for statistical computing. R Foundation for Statistical Computing, Vienna, Austria. URL http://www.R-project.org/.

Rabinowitz, D. (1981) Seven forms of rarity. In: Synge, H. (Ed.), The Biological Aspects of Rare Plant Conservation. John Wiley & Sons Ltd., NJ, pp. 205–217.

Rachowicz, L. J., & Briggs, C. J. (2007) Quantifying the disease transmission function: effects of density on *Batrachochytrium dendrobatidis* transmission in the mountain yellow-legged frog *Rana muscosa.* The Journal of Animal Ecology, 76, 711–21.

Rader, R., Bartomeus, I., Tylianakis, J. M., & Laliberté, E. (2014) The winners and losers of land use intensification: pollinator community disassembly is non-random and alters functional diversity. Diversity and Distributions, 20, 908–917.

Ranvestel, A. W., Lips, K. R., Pringle, C. M., Whiles, M. R., & Bixby, R. J. (2004) Neotropical tadpoles influence stream benthos: evidence for the ecological consequences of decline in amphibian populations. Freshwater Biology, 49, 274–285.

Reeder, N. M. M., Pessier, A. P., & Vredenburg, V. T. (2012) A reservoir species for the emerging amphibian pathogen *Batrachochytrium dendrobatidis* thrives in a landscape decimated by disease. PLoS ONE, 7, e33567.

Reshi, Z., Rashid, I., Khuroo, A. A., & Wafai, B. A. (2008) Effect of invasion by *Centaurea iberica* on community assembly of a mountain grassland of Kashmir Himalaya, India. Tropical Ecology, 49, 147–156.

Retallick, R. W. R., McCallum, H., & Speare, R. (2004). Endemic infection of the amphibian chytrid fungus in a frog community post-decline. PLoS Biology, 2, e351.

Robertson, J. M., Lips, K. R., & Heist, E. J. (2008) Fine scale gene flow and individual movements among subpopulations of *Centrolene prosoblepon* (Anura: Centrolenidae). Revista de Biología Tropical, 56, 13–26.

Rodriguez, D., Becker, C. G., Pupin, N. C., Haddad, C. F. B., & Zamudio, K. R. (2014) Long-term endemism of two highly divergent lineages of the amphibian-killing fungus in the Atlantic Forest of Brazil. Molecular Ecology, 23, 774–787.

Rosenblum, E. B., Fisher, M. C., James, T. Y., Stajich, J. E., Longcore, J. E., Gentry, L. R., & Poorten, T. J. (2010) A molecular perspective: biology of the

emerging pathogen *Bactrachochytrium dendrobatidis*. Diseases of Aquatic Organisms, 92, 131–147.

Rowley, J., & Alford, R.A. (2007). Behaviour of Australian rainforest stream frogs may affect the transmission of chytridiomycosis. Diseases of Aquatic Organisms, 77, 1–9.

Rowley J., & Alford R.A. (2013) Hot bodies protect amphibians against chytrid infection in nature. Scientific Reports, 3, 1515.

Roy, B. A., & Kirchner, J. W. (2000) Evolutionary dynamics of pathogen resistence and tolerance. Evolution, 54, 51–63.

Royle, J. A. (2004) N-Mixture Models for estimating population size from spatially replicated counts. Biometrics, 60, 108–115.

Ruiz-Gutiérrez, V., Zipkin, E. F., & Dhondt, A. (2010) Occupancy dynamics in a tropical bird community: unexpectedly high forest use by birds classified as non-forest species. Journal of Applied Ecology, 47, 621–630.

Ryan, M. J., Lips, K. R., & Eichholz, M. W. (2008) Decline and extirpation of an endangered Panamanian stream frog population (*Craugastor punctariolus*) due to an outbreak of chytridiomycosis. Biological Conservation, 141, 1636–1647.

Sapsford, S. J., Voordouw, M. J., Alford, R. A, & Schwarzkopf, L. (2015) Infection dynamics in frog populations with different histories of decline caused by a deadly disease. Oecologia, 179, 1099–1110.

Sanders, N. J., Gotelli, N. J., Heller, N .E., & Gordon, D. M. (2003) Community disassembly by an invasive species. Proceedings of the National Academy of Sciences of the United States of America, 100, 2474–2477.

Savage, J. M. 2002. The amphibians and reptiles of Costa Rica: a herpetofauna between two continents, between two seas. University of Chicago Press, USA.

Savage, A. E., & Zamudio, K. R. (2011) MHC genotypes associate with resistance to a frog-killing fungus. Proceedings of the National Academy of Sciences of the United States of America, 108, 16705–10.

Semlitsch R. D., Scott D. E. & Pechmann J. H. K. (1996) Structure and dynamics of an amphibian community: evidence from a 16-year study of a natural pond. In: Long-Term Studies of Vertebrate, Academic Press, NewYork, NY.

Schneider, D. S., & Ayres, J. S. (2008) Two ways to survive infections: what resisteance and tolerance can teach us about treating infectious diseases. Nature, 8, 889–895.

Sheldon, K. S., Yang, S., & Tewksbury, J. J. (2011) Climate change and community disassembly: impacts of warming on tropical and temperate montane community structure. Ecology Letters, 14, 1191–1200.

Smith, K. G., Lips, K. R., & Chase, J. M. (2009) Selecting for extinction: nonrandom disease-associated extinction homogenizes amphibian biotas. Ecology Letters, 12, 1069–1078.

Smith, M. J., Schreiber, E. S. G., Scroggie, M. P., Kohout, M., Ough, K., Potts, J., Lennie R., Turnbull, D., Jin, C., & Clancy, T. (2007) Associations between

anuran tadpoles and salinity in a landscape mosaic of wetlands impacted by secondary salinisation. Freshwater Biology, 52, 75–84.

Stevenson, L. A, Alford, R. a, Bell, S. C., Roznik, E. A, Berger, L., & Pike, D. A. (2013) Variation in thermal performance of a widespread pathogen, the amphibian chytrid fungus *Batrachochytrium dendrobatidis*. PloS One, 8, e73830.

Su, Y. S., Yajima, M., & Su, M. Y. S. (2014) Package 'R2jags'.

Schwarz, C. (2011) Sampling, Regression, Experimental Design and Analysis for Environmental Scientists, Biologists, and Resource Managers. Burnaby: Simon Fraser University.

Tarvin, R. D., Pena, P., Ron, S. R. (2014) Changes in population size and survival in *Atelopus spumarius* (Anura: Bufonidae) are not correlated with chytrid prevalence. Journal of Herpetology, 48, 291– 297.

Thompson, K. G. (2007) Use of site occupancy models to estimate prevalence of Myxobolus cerebralis infection in trout. Journal of Aquatic Animal Health, 19, 8–13.

Titman, A. C., & Sharples, L. D. (2010) Model diagnostics for multi-state models. Statistical Methods in Medical Research, 19, 621–51.

Tobler, U., Borgula, A., & Schmidt, B. R. (2012) Populations of a susceptible amphibian species can grow despite the presence of a pathogenic chytrid fungus. PLoS ONE, 7, 1–8.

Tunstall, T. S., DiRenzo, G. V., Longo, A. V., Zamudio, K. R., & Lips, K. R. (*in prep*) Multi-host pathogen causes simultaneous peaks in prevalence and

infection intensity among several amphibian species during a chytridiomycosis outbreak.

Vander Wal, E., Sherbrooke, U. De, & Biologie, D. D. (2013) Evolutionary rescue in vertebrate conservation: evidence, applications, and uncertainty. Philosophical Transactions of the Royal Society B: Biological Sciences, 368, 20120090.

Voyles, J., Young, S., Berger, L., Campbell, C., Voyles, W. F., Dinudom, A., Cook, D., Webb, R., Alford, R. A., Skerratt, L. F., & Speare, R. (2009) Pathogenesis of chytridiomycosis, a cause of catastrophic amphibian declines. Science, 326, 582–585.

Vredenburg, V. T., Knapp, R. A., Tunstall, T. S., & Briggs, C. J. (2010) Dynamics of an emerging disease drive large-scale amphibian population extinctions. Proceedings of the National Academy of Sciences of the United States of America, 107, 9689–94.

Warwick, R. M., Clarke, K. R., & Suharsono. (1990) A statistical analysis of coral community responses to the 1982– 1983 El Nino in the Thousand Islands, Indonesia. Coral Reefs, 8, 171–179.

Whitfield, S. M., Lips, K. R., & Donnelly, M. A. (*in press*) Amphibian decline and conservation in Central America. Copeia, 104.

Woodhams, D. C., Voyles, J., Lips, K. R., Carey, C., & Rollins-Smith, L. A. (2006) Predicted disease susceptibility in a Panamanian amphibian assemblage based on skin peptide defenses. Journal of Wildlife Diseases, 42, 207–18.

Wright, D. H., Gonzalez, A., & Coleman, D. C. (2007) Changes in nestedness in experimental communities of soil fauna undergoing extinction. Pedobiologia, 50, 497–503.

Zavaleta, E., Pasari, J., Moore, J., Hernández, D., Suttle, K. B., & Wilmers, C. C. (2009) Ecosystem responses to community disassembly. Annals of the New York Academy of Sciences, 1162, 311–333.

Zipkin, E. F., DeWan, A., & Royle, J. A. (2009) Impacts of forest fragmentation on species richness: a hierarchical approach to community modeling. Journal of Applied Ecology, 46, 815–822

Zipkin, E. F., Jennelle, C. S., & Cooch, E. G. (2010). A primer on the application of Markov chains to the study of wildlife disease dynamics. Methods in Ecology and Evolution, 1, 192–198.

Zipkin, E. F., Sillett, T. S., Grant, E. H. C., Chandler, R. B., & Royle, J. A. (2014) Inferences about population dynamics from count data using multistate models: a comparison to capture-recapture approaches. Ecology and Evolution, 4, 417–426.

Zipkin, E. F., Thorson, J. T., See, K., Lynch, H. L., Grant, E. H. C., Kanno, Y., Chandler, R. B., Letcher, B. H., & Royle, J. A. (2014) Modeling structured population dynamics using data from unmarked individuals. Ecology, 95, 22–29.